Engineering the Keratinocyte Microenvironment: Harnessing Topography to Direct Cellular Function

WPI

A Dissertation
Submitted to the Faculty
of the
WORCESTER POLYTECHNIC INSTITUTE

in partial fulfillment of the requirements for the
Degree of Doctor of Philosophy in
Biomedical Engineering

November 2014

By

Amanda Lynn Clement

Approved by:

George D. Pins, PhD, Advisor
Associate Professor
Biomedical Engineering
Worcester Polytechnic Institute

Anjana Jain, PhD
Assistant Professor
Biomedical Engineering
Worcester Polytechnic Institute

Tanja Dominko, DVM, PhD
Associate Professor
Biology and Biotechnology
Worcester Polytechnic Institute

Joseph B. Duffy
Associate Professor and Department Head
Biology and Biotechnology
Worcester Polytechnic Institute

Stelios T. Andreadis, PhD
Professor and Department Chair
Chemical and Biological Engineering
SUNY at Buffalo

Acknowledgements

I would like to thank my advisor, George Pins, for his support and encouragement throughout my time at WPI. He has always pushed scientifically and intellectually and I am a better researcher because of it.

I would also like to thank my committee members, Anjana Jain, Tanka Dominko, Joseph Duffy and Stelios Andreadis. Their guidance has been invaluable and I came away from every committee meeting with new ideas and a fresh perspective.

I'd also like to thank the many students who contributed to this research over the years through independent studies, REUs, and lab volunteer work. This thesis would not have been possible without your hard work and it was a pleasure working with you all. I would especially like to acknowledge Tom Moutinho, Kevin Ackerman, Katie Cabral and MacKenzie Brandes for their direct contributions to this work.

I also thank all of my fellow graduate students for their support over the years both in and out of the lab. I am grateful for both the scientific colleagues and the friends that I've made here. I would especially like to thank Jon Grasman and Jen Molignano. The Pins lab would not have been the same without you!

Finally, I would like to thank my family and friends for all of their support. Before, during and after this process, you have always been there for me and I know that you always will be.

Abstract

Skin wound healing presents a challenging and expensive clinical problem with nearly 20 million wounds requiring intervention leading to an annual cost of more than $8 million. Tissue engineered skin substitutes are valuable not only as a clinical therapy for chronic wounds and severe traumas, but also as *in vitro* 3D model systems to investigate wound healing and skin pathogenesis. However, these substitutes are limited by a lack of topography at the dermal-epidermal junction (DEJ). In contrast, the native DEJ is characterized by a series of dermal papillae which project upward into the epidermal layer and create physical topographic microniches that support keratinocyte stem cell clustering. In this thesis, we created novel 3D skin model systems to investigate the role of microtopography in regulating keratinocyte function and cell fate using scaffolds containing precisely engineered topographic features. We hypothesized that the microtopography of the DEJ creates distinct keratinocyte microniches that promote epidermal morphogenesis and modulate keratinocyte stem cell clustering which can be harnessed to create a more robust skin substitute that expedites wound closure. Using photolithographic techniques, we created micropatterned DEJ analogs and micropatterned dermal-epidermal regeneration matrices (μDERM) which couple a dermal support matrix to a micropatterned DEJ analog. We found that the incorporation of microtopography into our *in vitro* skin model resulted in a thicker, more robust epidermal layer. Additionally, we identified three distinct functional keratinocyte niches: the proliferative niche in narrow channels, the synthetic niche in wide channels and the keratinocyte stem cell niche in narrow channels and corner topographies. Ultimately, incorporation of both narrow and wide channels on a single construct allowed us to recreate native keratinocyte stem cell patterning *in vitro*. These model systems will allow us to investigate the role of cellular microniches in regulating cellular function and epidermal disease pathogenesis as well as to identify topographic cues that enhance the rate of wound healing.

Table of Contents

Table of Figures

Chapter 1: Overview

1.1 Introduction

Each year, an estimated 80 skin grafts are performed per 100,000 population (Milenkovic *et al.*, 2007). Worldwide, there are over 49 million reported wounds per year, including more than 14 million venous and diabetic ulcers and 5.2 million pressure sores (MedMarket, 2007). Since these chronic wounds are most prevalent in individuals over sixty years of age, as the population ages these numbers are expected to rise. The treatment of chronic wounds presents a challenging and expensive clinical problem, with the annual cost of treatment exceeding $8 billion USD. One method of treatment for chronic non-healing wounds is skin grafting; between 1998 and 1999 approximately 163,000 grafting procedures were performed on Medicare patients (Shaffer *et al.*, 2005). Additionally, in the US, approximately 40,000 burns require hospitalization annually, resulting in over 10,000 grafts per year (American Burn Association, 2007; Milenkovic, Russo and Elixhauser, 2007). While the current gold standard is a split-thickness autograft, donor site morbidity and limited availability present significant drawbacks (Sheridan and Tompkins, 1999). In patients with compromised wound healing, these disadvantages are even more pronounced. Several tissue engineered skin substitutes have been developed and commercialized to address this need. Although promising, they exhibit limited mechanical stability, sub-optimal wound healing, and prolonged healing times (Bar-Meir *et al.*, 2006; Metcalfe and Ferguson, 2007; Priya *et al.*, 2008).

A common limitation of current therapeutic strategies is the failure to recreate the native topography of skin. In native skin, the epidermis conforms to the topography of the dermal grooves and papillae. This complex interdigitated topography not only promotes mechanical integrity between the dermis and the epidermis, but also creates microniches with dimensions

ranging from 50 to 400 μm in width and 50 to 200 μm in depth (Fawcett and Jensh, 1997; Odland, 1950). These microtopographic niches create cellular micro environments that promote keratinocyte clustering and differentially drive keratinocyte functions (Butler and Orgill, 2005; Jones *et al.*, 1995; Lavker and Sun, 1982a, 1983; Odland, 1950; Vracko, 1974). Additionally, $\beta_1^{bri}p63^+$ keratinocytes have been shown to localize to the deep rete ridges and the tips of the dermal papillae of the dermal-epidermal junction (Jensen *et al.*, 1999; Jones and Watt, 1993; Jones, Harper and Watt, 1995; Kai-Hong *et al.*, 2007; Lavker and Sun, 1983; Lavker and Sun, 1982b). Keratinocytes that express high levels of β_1 integrin and the nuclear transcription factor p63 have demonstrated the highest colony forming efficiency and have been identified as putative stem cells (Barrandon and Green, 1987; Hotchin *et al.*, 1995; Hotchin and Watt, 1992; Jones and Watt, 1993; Jones, Harper and Watt, 1995; Kai-Hong, Jun, Kai-Meng, Ying and Hou-Qi, 2007; Pellegrini *et al.*, 2001; Van Rossum *et al.*, 2004; Yang *et al.*, 1999). In native skin, β_1^{bri} keratinocytes have been shown to cluster in specific topographical locations at the dermal-epidermal junction based on the location of the skin. In skin from foreskin and scalp, β_1^{bri} keratinocytes cluster in the tips of the dermal papillae, whereas in skin from the palm, β_1^{bri} cells cluster in the bottoms of the rete ridges (Hotchin, Gandarillas and Watt, 1995; Jones, Harper and Watt, 1995). Ultimately, recreating stem cell patterning in 3D *in vitro* models will provide a more accurate model of epidermal morphogenesis for the study of disease pathologies. Further, incorporating native stem cell clustering in therapeutic skin substitutes may provide a more stable graft to help reduce wound healing times and increase graft persistence.

In addition to promoting stem cell localization, the microtopography of the dermal-epidermal junction (DEJ) may play a role in directing keratinocyte proliferation, differentiation, and migration. *In vitro* studies have shown that culture substrate can drive keratinocyte shape, differentiation and proliferation (Bush and Pins, 2010; Fujisaki *et al.*, 2008; Fujisaki and Hattori, 2002). In particular, it has been suggested that microtopography may direct keratinocyte proliferation and differentiation in addition to influencing clustering of keratinocytes with the highest colony forming efficiency. Recently we showed that epidermal stratification on micropatterned dermal-epidermal regeneration matrices (μDERM) was increased in deep

microchannels compared to shallow channels and flat regions and that β_1^{bri} keratinocytes cluster in microchannels (Bush and Pins, 2012). Additionally, we have shown that the rate of keratinocyte differentiation may be increased in narrower versus wider channels, based on thickness analysis of the involucrin positive layer, suggesting that microtopography may direct keratinocyte differentiation (Downing *et al.*, 2005). By incorporating these topographic cues, the next generation "smart" skin substitutes can differentially control these keratinocyte functions thereby enhancing the rate of engraftment and re-epithelialization. Further, these future grafts can be precisely tailored to deliver specific topography to best address the underlying pathology necessitating grafting.

Our earlier μDERM model provides a platform for the systematic evaluation of these cues. However, the current model is not without limitations. Most significantly, it utilizes a keratinocyte monoculture. Previous work has shown the importance of fibroblast signaling for epidermal morphogenesis and maintaining keratinocyte function (El-Ghalbzouri *et al.*, 2002; El Ghalbzouri *et al.*, 2004; El Ghalbzouri *et al.*, 2002; Smola *et al.*, 1993). Therefore, to fully evaluate the keratinocyte response to microtopographic cues, studies should be performed in co-culture with fibroblasts. Additionally, the thickness of the collagen gel layer in the first generation μDERM may limit diffusion. By reducing the thickness of this layer, diffusion of keratinocyte-fibroblast paracrine signals can be enhanced, improving the usability of the μDERM model system. Therefore, this project will first modify the existing model system and then use the improved μDERM model to investigate the role of microtopographic cues in regulating cell fate and function.

1.2 Overall Goal and Hypothesis

The ultimate goal of this project is to gain a greater understanding of how microtopographic cues influence cell fate and function and to use this knowledge to advance the current state of the art wound treatment by creating a more robust and highly physiologically relevant skin substitute.

We *hypothesize that the microtopography of the dermal-epidermal junction creates distinct keratinocyte microniches that promote epidermal morphogenesis and modulate keratinocyte*

stem cell clustering which can be harnessed to create a more robust skin substitute that expedites wound closure.

Epidermal morphogenesis includes overall tissue morphology including keratinocyte shape and stratification, epidermal thickness, keratinocyte proliferation, differentiation and basement membrane protein deposition. Putative keratinocyte stem cells will be identified as $\beta_1^{bri}p63^+$ keratinocytes. The expected outcome of these studies is the development of an implantable full-thickness skin substitute which includes both fibroblasts and keratinocytes and that incorporates microtopographic features designed to enhance *in vitro* graft formation and ultimately graft integration *in vivo.*

To systematically test this hypothesis, this thesis was separated into three parts with a total of four objectives.

1.3 Part 1: Identification of microchannel niche dimensions that regulate cell function on bilayered skin analogs containing fibroblast paracrine signaling cues.

1.3.1 Objective 1: Incorporate fibroblasts into the Micropatterned Dermal-Epidermal Regeneration Matrix (µDERM) model and determine the effect of fibroblast signaling on epidermal morphology and epidermal thickness.

Previously, we developed a bi-layered skin substitute (µDERM) with a DEJ comprised of a series of microchannels (50-400 µm wide, 200µm deep) (Bush and Pins, 2012). This design allows for high throughput immunohistochemical analysis of multiple channel dimensions on each µDERM. However, the original model lacks critical fibroblast paracrine signals which have been shown to enhance epidermal morphogenesis by stimulating keratinocyte proliferation and promoting epidermal stratification (El-Ghalbzouri, Gibbs, Lamme, Van Blitterswijk and Ponec, 2002; El Ghalbzouri, Hensbergen, Gibbs, Kempenaar, van der Schors and Ponec, 2004; El Ghalbzouri, Lamme and Ponec, 2002; Smola, Thiekotter and Fusenig, 1993). Because culture in the absence of fibroblast paracrine signals may result in a more quiescent phenotype, Chapter 3 discusses the incorporation of fibroblasts into our µDERM model and evaluates the effect of fibroblast signaling, specifically keratinocyte growth factor (KGF) on epidermal thickness and overall graft

morphology. Fibroblasts were statically seeded into the dermal sponge component 48 hours prior to keratinocyte seeding and µDERMs were subsequently cultured at the air-liquid interface for 7 days. Quantitative histological evaluation demonstrated that in the presence of fibroblasts, keratinocytes on µDERMs formed thicker, better organized epidermal layers. Immunohistochemistry for keratinocyte growth factor (KGF) suggested that KGF secretion by fibroblasts may be partially responsible for the observed changes in epidermal morphogenesis. The incorporation of fibroblasts into µDERMs will allow us to more explicitly probe the ability of microtopography to create distinct keratinocyte niches. Additionally, since inclusion of fibroblasts in skin implants has been shown to enhance vascularization and reduce graft contraction *in vivo*, their addition to the µDERM model is critical for successful implantation studies. *Clement AL, Moutinho T, Pins GD (2013) Micropatterned Dermal-Epidermal Regeneration Matrices Create Functional Niches that Enhance Epidermal Morphogenesis. Acta Biomaterialia 9:9474-84.*

1.3.2 Objective 2: Evaluate keratinocyte response to microtopography and identify topographic dimensions that increase: (i) epidermal morphology, (ii) epidermal thickness, (iii) keratinocyte proliferation, (iv) keratinocyte differentiation, (v) laminin 332 deposition, and (vi) keratinocyte stem cell localization.

We previously demonstrated a relationship between keratinocyte function and microtopographic features on the surfaces of bioengineered skin substitutes with µDERMs lacking fibroblasts (Bush and Pins, 2012). Since fibroblast signaling plays an important role in the regulation of keratinocyte function, Chapter 4 uses µDERMs that contain fibroblasts to systematically analyze the relationship between microtopographic dimensions and epidermal morphology, epidermal thickness, keratinocyte proliferation, keratinocyte differentiation, basement membrane deposition (laminin 332) and keratinocyte stem cell clustering. Inclusion of microtopography was found to enhance overall epidermal morphology while quantitative morphometric analysis demonstrated that microtopographic features are capable of modulating epidermal thickness, with the thickest epidermal layers found in regions with narrow microchannels. Subsequent immunohistochemistry showed increased expression of the differentiation marker involucrin in these thicker epidermal layers. Using quantitative immunohistochemistry, we identified three possible functional keratinocyte niches: the

proliferative niche (narrow geometries), the basement membrane protein synthesis niche (wide geometries), and the putative keratinocyte stem cell niche (narrow geometries and corners). These findings will allow us to identify cellular microniche dimensions that best support epidermal morphogenesis in bioengineered skin substitutes *in vitro* and will be used to design topographies for Parts 2 and 3. *Clement AL, Moutinho T, Pins GD (2013) Micropatterned Dermal-Epidermal Regeneration Matrices Create Functional Niches that Enhance Epidermal Morphogenesis. Acta Biomaterialia 9:9474-84.*

1.4 Part 2: Evaluation of keratinocyte attachment and stem cell localization on dermal papillae analogs.

1.4.1 Objective 3: Create multi-scale dermal papillae analogs and develop methods for evaluating attachment and stem cell localization in whole mount.

Native skin is characterized by a series of dermal papillae and rete ridges at the DEJ (Fawcett and Jensh, 1997). In Chapters 3 and 4, we used μDERMs with channel topographies to identify topographic dimensions that promote stem cell localization and regulate different cellular functions including proliferation and laminin 332 deposition. However, this grooved topography does not fully replicate the complex papillae structures of the DEJ. In Chapter 5, we create multi-scale dermal papillae analogs. Based on the results from Part 1, these analogs feature hexagonal posts (papillae) separated by both wide and narrow channels (rete ridges) that recreate the geometries found in native skin to improve epidermal morphology and increase the rate of epidermal stratification. Recreating the native microtopography at the dermal-epidermal interface of skin grafts increases the relative surface area of the interface, which enhances dermal-epidermal adhesion, and creates microniches. The multi-scale DEJ analogs result in a 118% increase in surface area, although alternative patterning strategies may allow for a nearly 2000% increase in surface area. Using confocal microscopy, we found that keratinocytes form a monolayer 24 hours post seeding. Additionally, using whole mount immunofluorescent staining (β_1 integrin and p63), we demonstrated keratinocyte stem cell clustering at the bases of the dermal papillae. These results are consistent with our observations in Aim 1 and support our hypothesis that microtopography can be used to control keratinocyte clustering.

1.5 Part 3: Assessment of µDERM graft integration *in vivo*

1.5.1 Objective 3: Implant µDERMs into an athymic mouse model to assess graft integration and determine if µDERMs can create functional keratinocyte niches *in vivo*.

Although current bioengineered skin substitutes have had some clinical success, they are not without their limitations. These limitations, which include a lack of mechanical and structural stability, poor regenerative capacity, lengthy wound closure times, and epidermal de-lamination, often necessitate multiple applications and can lead to graft failure (Boyce and Warden, 2002; Parenteau *et al.*, 1996; Sheridan and Tompkins, 1999). A common limitation of current tissue engineering strategies is a lack of topography at the interface between the dermal and epidermal components. µDERMs recreate this complex topography and create microniches that drive keratinocyte function. In Chapter 6, we investigate the implantation of µDERMs *in vivo* to test the hypothesis that incorporation of microtopographic features at the dermal-epidermal junction of skin grafts will promote healing and yield a more robust skin substitute. µDERMs with microchannel topography (Chapters 3 and 4) were implanted into full thickness wounds on the dorsum of athymic nude (*Foxn1^{nu})* mice. Our preliminary results suggested that the high degree of cross-linking of µDERM inhibits graft integration. Implantation of a less cross-linked µDERM better supported graft integration and prevented wound contraction after 7 days, although these grafts did not maintain their topography. These results suggest that further development of the µDERMs skin graft to reduce the amount of crosslinking required to maintain topographic cues while allowing for improved graft integration is necessary for optimal clinical outcomes.

1.6 References

American Burn Association (2007) Burn Incidence and Treatment in the U.S.: 2007 Fact Sheet.

Bar-Meir E, Mendes D and Winkler E (2006) Skin Substitutes. *IMAJ* 8:188-91.

Barrandon Y and Green H (1987) Three Clonal Types of Keratinocyte with Different Capacities for Multiplication. *Proc Nati Acad Sci USA* 84:2302-06.

Boyce ST and Warden GD (2002) Principles and Practices for Treatment of Cutaneous Wounds with Cultured Skin Substitutes. *Am J Surg* 183:445-56.

Bush K and Pins G (2010) Carbodiimide Conjugation of Fibronectin on Collagen Basal Lamina Analogs Enhances Cellular Binding Domains and Epithelialization. *Tissue Eng Part A* 16:829-38.

Bush K and Pins G (2012) Development of Microfabricated Dermal Epidermal Regenerative Matrices to Evaluate the Role of Cellular Microenvironments on Epidermal Morphogenesis. *Tissue Eng Part A* 18:2343-53.

Butler CE and Orgill DP (2005) Simultaneous in Vivo Regeneration of Neodermis, Epidermis, and Basement Membrane. *Adv Biochem Eng Biotechnol* 94:23-41.

Downing BR, Cornwell K, Toner M and Pins GD (2005) The Influence of Microtextured Basal Lamina Analog Topography on Keratinocyte Function and Epidermal Organization. *J Biomed Mater Res A* 72:47-56.

El-Ghalbzouri A, Gibbs S, Lamme E, Van Blitterswijk CA and Ponec M (2002) Effect of Fibroblasts on Epidermal Regeneration. *Br J Dermatol* 147:230-43.

El Ghalbzouri A, Hensbergen P, Gibbs S, Kempenaar J, van der Schors R and Ponec M (2004) Fibroblasts Facilitate Re-Epithelialization in Wounded Human Skin Equivalents. *Lab Invest* 84:102-12.

El Ghalbzouri A, Lamme E and Ponec M (2002) Crucial Role of Fibroblasts in Regulating Epidermal Morphogenesis. *Cell Tissue Res* 310:189-99.

Fawcett DW and Jensh RP (1997) *Bloom & Fawcett: Concise Histology*. Chapman and Hall: New York.

Fujisaki H, Adachi E and Hattori S (2008) Keratinocyte Differentiation and Proliferation Are Regulated by Adhesion to the Three-Dimensional Meshwork Structure of Type Iv Collagen. *Connect Tissue Res* 49:426-36.

Fujisaki H and Hattori S (2002) Keratinocyte Apoptosis on Type I Collagen Gel Caused by Lack of Laminin 5/10/11 Deposition and Akt Signaling. *Exp Cell Res* 280:255-69.

Hotchin N, Gandarillas A and Watt F (1995) Regulation of Cell Surface Beta 1 Integrin Levels During Keratinocyte Terminal Differentiation. *J Cell Biol* 128:1209-19.

Hotchin N and Watt F (1992) Transcriptional and Post-Translational Regulation of Beta 1 Integrin Expression During Keratinocyte Terminal Differentiation. *J Biol Chem* 267:14852-8.

Jensen UB, Lowell S and Watt FM (1999) The Spatial Relationship between Stem Cells and Their Progeny in the Basal Layer of Human Epidermis: A New View Based on Whole-Mount Labelling and Lineage Analysis. *Development* 126:2409-18.

Jones P and Watt F (1993) Separation of Human Epidermal Stem Cells from Transit Amplifying Cells on the Basis of Differences in Integrin Function and Expression. *Cell* 73:713-24.

Jones PH, Harper S and Watt FM (1995) Stem Cell Patterning and Fate in Human Epidermis. *Cell* 80:83-93.

Kai-Hong J, Jun X, Kai-Meng H, Ying W and Hou-Qi L (2007) P63 Expression Pattern During Rat Epidermis Morphogenesis and the Role of P63 as a Marker for Epidermal Stem Cells. *J Cutan Pathol* 34:154-9.

Lavker R and Sun T (1982a) Heterogeneity in Epidermal Basal Keratinocytes: Morphological and Functional Correlations. *Science* 215:1239-41.

Lavker R and Sun T (1983) Epidermal Stem Cells. *J Invest Dermatol* 81:121s-7s.

Lavker RM and Sun TT (1982b) Heterogeneity in Epidermal Basal Keratinocytes: Morphological and Functional Correlations. *Science* 215:1239-41.

MedMarket (2007) Worldwide Wound Management, 2007-2016. Report no. #S245.

Metcalfe AD and Ferguson MW (2007) Tissue Engineering of Replacement Skin: The Crossroads of Biomaterials, Wound Healing, Embryonic Development, Stem Cells and Regeneration. *J R Soc Interface* 4:413-37.

Milenkovic M, Russo CA and Elixhauser A (2007) Hospital Stays for Burns, 2004. Hcup Statistical Brief #25. *Agency for Healthcare Research and Quality, Rockville, MD*:http://www.hcup-us.ahrq.gov/reports/statbriefs/sb25.pdf.

Odland G (1950) The Morphology of the Attachment between the Dermis and the Epidermis. *Anat Record* 108:399-413.

Parenteau N, Sabolinski M, Prosky S, Nolte C, Oleson M, Kriwet K and Bilbo P (1996) Biological and Physical Factors Influencing the Successful Engraftment of a Cultured Human Skin Substitute. *Biotechnol Bioeng* 52:3-14.

Pellegrini G, Dellambra E, Golisano O, Martinelli E, Fantozzi I, Bondanza S, Ponzin D, McKeon F and De Luca M (2001) P63 Identifies Keratinocyte Stem Cells. *Proc Natl Acad Sci U S A* 98:3156-61.

Priya SG, Jungvid H and Kumar A (2008) Skin Tissue Engineering for Tissue Repair and Regeneration. *Tissue Eng Pt B* 114:105-18.

Shaffer CL, Feldman SR, Fleischer AB, Huether MJ and Chen J (2005) The Cutaneous Surgery Experience of Multiple Specialties in the Medicare Population *J Am Acad Dermatol* 52:1045-48.

Sheridan RL and Tompkins RG (1999) Skin Substitutes in Burns. *Burns* 25:97-103.

Smola H, Thiekotter G and Fusenig NE (1993) Mutual Induction of Growth Factor Gene Expression by Epidermal-Dermal Cell Interaction. *J Cell Biol* 122:417-29.

Van Rossum MM, Framssem MEJ, Cloin WAH, Van de Bosch GJM, Boezmman JBM, Schalkwijk J, Van de Kerkhof PCM and Van Erp PEJ (2004) Functional Characterization of Beta1-Integrin-Positive Epidermal Cell Populations. *Acta Derm Venereol* 84:265-70.

Vracko R (1974) Basal Lamina Scaffold-Anatomy and Significance for Maintenance of Orderly Tissue Structure. *Am J Pathol* 77:314-46.

Yang A, Schweitzer R, Sun D, Kaghad M, Walker N, Bronson R, Tabin C, Sharpe A, Caput D, Crum C and McKeon F (1999) P63 Is Essential for Regenerative Proliferation in Limb, Craniofacial and Epithelial Development. *Nature* 398:714-18.

Chapter 2: Background

2.1 Project Scope and Significance

Skin wound healing and dermatology therapeutics are multibillion dollar markets. Annually there are over 49 million wounds worldwide including both traumas such as burns (450,000) and chronic wounds such as venous and diabetic ulcers (14 million) and pressure sores (5.2 million) that require treatment (American Burn Association, 2013; MedMarket, 2007). In 2010, burn injuries resulted in over 24,000 hospitalizations. Although small area burns have a relatively low mortality rate (0.6% for burns with a total body surface area burns of less than 10%), mortality rates increase with burn size and reach 50% for burns with a total body surface area of 70%. Along with excisional debridement, skin grafting is one of the most frequent procedures performed on burn inpatients (American Burn Association and National Burn Repository, 2012).

Chronic wounds present an even larger problem. Sometimes chronic ulcers can remain open for months even with treatment and when wound closure cannot be attained, non-healing wounds can sometimes lead to in amputation. Annually in the United States nearly 80,000 lower limb amputations are performed as a result of complications from diabetes (4.3 per 1000 diabetics) (Margolis *et al.*, 2011). Due to the prevalence of chronic wounds among elderly patients, it is expected that incidence rates will continue to rise as the population ages. In fact, by 2030 it is estimated that 360 million people (5% of the population) will have diabetes (Margolis, Malay, Hoffstad, Leonard, MaCurdy, de Nava, Tan, Molina and Siegel, 2011). Accordingly, the development of advanced wound healing techniques for chronic and large area wounds is of paramount importance.

2.1.1 Clinical Need for Bioengineered Skin Substitutes

Although minor skin wounds will heal without significant intervention, large area or chronic wounds require the rapid restoration of the skin barrier to prevent serious complications such as infection and desiccation which can lead to scarring, amputation and death. Worldwide, there are over 49 million wounds per year, including more than 14 million venous and diabetic ulcers and 5.2 million pressure sores (MedMarket, 2007). Since these chronic wounds are most prevalent in individuals over sixty years of age, as the population ages these numbers are expected to rise. The treatment of chronic wounds presents a challenging and expensive clinical problem, with the annual cost of treatment exceeding $8billion USD. One method of treatment for chronic non-healing wounds is skin grafting; between 1998 and 1999 approximately 163,000 grafting procedures were performed on Medicare patients (Shaffer *et al.*, 2005). Additionally, in the US, approximately 40,000 burns require hospitalization annually, resulting in over 10,000 grafts per year (American Burn Association, 2007; Milenkovic *et al.*, 2007). In total, an estimated 80 skin grafts are performed per 100,000 people in the United States each year (Milenkovic, Russo and Elixhauser, 2007). While autografts are considered the current "gold standard" treatment, donor site morbidity and limited availability present significant drawbacks (Barret *et al.*, 2000; Sheridan and Tompkins, 1999). In patients with compromised wound healing, including diabetics and the elderly, these disadvantages are even more pronounced. Tissue engineered skin substitutes represent a promising alternative therapy, and several substitutes have been developed and commercialized to address this need. In 2013, tissue engineered skin substitutes made up nearly 3% of the multi-billion dollar global wound healing market (MedMarket Diligence, 2013). Although these skin substitutes have exhibited some clinical success, they exhibit limited mechanical stability, sub-optimal wound healing, and prolonged healing times (Bar-Meir *et al.*, 2006; Metcalfe and Ferguson, 2007; Priya *et al.*, 2008). These drawback highlight a critical need for more advanced off-the-shelf tissue engineered skin substitutes that can rapidly and robustly restore the skin barrier.

2.1.3 Need for Relevant *In Vitro* Skin Research Models

In addition to their use as therapeutics, skin substitutes provide a platform for *in vitro* investigation of skin pathologies including epidermal cancers. Skin disease has a high incidence, with one in three Americans suffering from some form of skin disease (Bickers *et al.*, 2006). This number includes 3.5 million new cases of skin cancer diagnosed annually (Rogers *et al.*, 2010). For over 100 years, *in vitro* cell culture has allowed researchers to investigate the physical and biochemical signals that affect cell fate and function and has provided model systems for investigating disease pathogenesis and wound healing as well as for testing toxicity and carcinogenicity (Mather and Roberts, 1998). Most cell culture is carried out in 2 dimensions (2D) on treated glass or plastic substrates; however, this over-simplified environment fails to recreate the physiological conditions in native tissues. This has led to the development of 3D organotypic models of skin in order to better investigate the cellular and molecular mechanisms involved in epidermal morphogenesis, wound healing, and disease progression (Bellas *et al.*, 2012; Gautrot *et al.*, 2012; Groeber *et al.*, 2011; Huang *et al.*, 2010; Ojeh and Navsaria, 2013; Powell *et al.*, 2010; Waugh and Sherratt, 2007). These models can also be used for drug and cosmetics screening. Although no model fully recreates the complexity of native skin, several groups have developed on methods to incorporate skin appendages into *in vitro* models in order to create a more physiologically relevant model (Atac *et al.*, 2013; Huang, Xu, Wu, Sha and Fu, 2010).

2.2 Structure and Function of Skin

Skin, a complex multi-layered organ, creates a physical barrier between the body and the external environment. In addition to providing protection from pathogens, UV damage and chemical exposure, it is also responsible for sensory detection and maintaining tissue homeostasis (Madison, 2003; Rook and Burns, 2010).

2.2.1 Epidermis

The outer most layer of skin, the epidermis, provides a protective barrier to the external environment. The epidermis is avascular and is comprised primarily of keratinocytes which are responsible for creating the semi-permeable barrier. To create the complex structure of the

epidermis, keratinocytes cycle through four epidermal strata: the stratum basale, stratum spinosum, stratum granulosum, and the stratum corneum. This constant cycling makes the epidermis highly regenerative, with a complete turnover time of approximately 28 days.

The innermost epidermal layer, the stratum basale, consists of a single layer of small, cuboidal keratinocytes and contains both slow-cycling keratinocyte stem cells and highly proliferative transit amplifying (TA) cells. The keratinocyte stem cells are responsible for the regenerative potential of skin. As they divide, keratinocyte stem cells give rise to daughter TA cells which rapidly divide to produce the terminally differentiated cells that comprise the other three epidermal strata. Terminal differentiation is characterized by down-regulation of integrin expression which results in keratinocyte detachment from the underlying basal lamina and initiates their upward migration. The keratinocytes in the next layer – the stratum spinosum – are larger and begin synthesizing the keratin that will eventually comprise the stratum corneum. As the keratinocytes continue to differentiate, they migrate upwards into the stratum granulosum where they begin to flatten. The keratinocytes of the stratum granulosum contain both keratohyalin granules composed of profillagrin (the precursor to fillagrin) and involucrin and lamellar granules comprised of lipids and polysaccharides. The stratum granulosum is the last layer comprised of viable cells. As cells transition from the stratum granulosum to the stratum corneum, they enucleate and release the granule contents. The flattened, keratinized cells of the stratum corneum provide the semi-permeable barrier of skin.

2.2.2 Dermis

The dermis is a supporting matrix comprised of predominantly collagen, elastin and glycosaminoglycans. Collagen is the primary extracellular matrix component of the dermis and the crosslinked collagen fibers are responsible for the tensile strength of skin. The interwoven elastic fibers, composed of elastin and elastin-associated microfibrils, provide skin its resilience and elasticity. Interspersed between the collagen and elastic fibers, glycosaminoglycans and proteoglycan macromolecules help maintain tissue hydration (Rook and Burns, 2010). In addition to structural support, the vascularized dermis provides nutrient support for the avascular

epidermal layer. The dermis itself can be divided into two layers: the uppermost papillary layer and the innermost reticular layer. The papillary dermis is characterized by dermal papillae, fingerlike projections that extend upward into the epidermis and contain capillaries which sustain the epidermis. The papillary dermis is highly porous and densely populated by fibroblasts. In contrast, the reticular dermis is characterized by larger, more densely packed collagen fibers and is the principal location of elastic fibers (Chang *et al.*, 2002; Janson *et al.*, 2012; Tajima and Pinnell, 1981). Re-vascularization of the dermis is a critical component of the skin wound healing process (Tonnesen *et al.*, 2000).

2.2.3 Dermal-Epidermal Junction

The dermal-epidermal junction (DEJ) is the dynamic basement membrane interface between the stratified epidermis and the dermis. The DEJ not only regulates transport of molecules between the dermis in the epidermis, but also regulates keratinocyte behavior by modulating cellular functions including proliferation, migration, and differentiation (Burgeson and Christiano, 1997).

2.2.3.1 Topography of the DEJ and its Role in Stem Cell Localization

In native skin, the DEJ is not flat, but rather conforms to the topography of the dermal papillae. This interdigitated topography increases the surface area between the dermis and the epidermis which enhances the resistance to mechanical shearing and promotes dermal-epidermal adhesion resulting in increased structural and mechanical integrity. The increased surface area afforded by the topography of the DEJ also promotes nutrient diffusion from the vasculature of the dermis to the epidermis. Additionally, the dermal projections define microniches with dimensions ranging from 50-400 µm width and 50-200 µm depths (Fawcett and Jensh, 1997; Odland, 1950). These keratinocyte microniches serve a critical role in directing epidermal morphogenesis and regulating epidermal wound healing (Jones *et al.*, 1995b; Lavker and Sun, 1982b, 1983b). Additionally, microtopographic niches create distinct cellular microenvironments that differentially direct keratinocyte phenotype and cellular function.

Notably, there is a high degree of variation in DEJ topography based on anatomical location. Areas exposed to more friction including the palms and soles have longer are characterized by

longer, more densely packed papillae compared to areas of less friction such as the back and abdomen (Odland, 1950). Additionally, some skin pathologies involve changes to the DEJ topography. For example, the dermal papillae are lengthened in psoriasis and flattened in aged skin (Montagna and Carlisle, 1979; Murphy *et al.*, 2007).

2.2.3.2 Basal Lamina

Conforming to the topography of the DEJ is a thin (30-50nm), ECM dense layer called the basal lamina (Briggaman, 1982; Briggaman and Wheeler, 1975). The basal lamina is comprised of collagen (types I, III, IV, VII, XVII), fibronectin, and laminin (Alberts, 2002). The basal lamina functions as a physical barrier between the fibroblasts of dermis and the epidermis and provides biochemical cues which direct keratinocyte proliferation and differentiation.

2.3 Keratinocyte Stem Cells

Due to their proliferative capacity and differentiation potential, keratinocyte stem cells represent a promising tool for regenerative medicine research as both building blocks for novel tissue engineered therapies and as a research platform for studying wound healing and disease pathogenesis. In order to advance the development of both clinical and *in vitro* model applications, it is critical to identify the different types of keratinocyte stem cells and to understand how the cellular microenvironment regulates stem cell fate and function.

The study of keratinocyte stem cells remains a controversial area of research. In particular, there is significant debate surrounding the specific locations of stem cell in the epidermis as well as the identification of markers for epidermal stem cells. There is also no single accepted model for the study of epidermal stem cells. The confusion in part originates from the heterogeneous nature of the epidermal stem cell population. In fact, there are several distinct keratinocyte stem cell populations located within the epidermis, including interfollicular (IF) stem cells, hair follicle stem cells and sebaceous gland stem cells (Pincelli and Marconi, 2013). These physical microniches, or keratinocyte stem cell niches, contain multiple distinct keratinocyte sub-populations in addition to the keratinocyte stem cells, including both rapidly proliferating basal cells and terminally committed keratinocytes. Each of these stem cell niches supports different aspects of tissue

regeneration and epidermal maintenance. For example, cell tracking studies suggest that hair follicle stem cells are the cells primarily responsible for epidermal wound healing while IF stem cells are responsible for homeostatic maintenance (Blanpain and Fuchs, 2009; Senoo, 2013). Interestingly, recent studies suggest that there is some degree of plasticity in these populations. For example, Silva-Vargas *et al* demonstrated that high levels of β-catenin induced hair follicle formation from IFE stem cells without recruitment of bulge stem cells (Silva-Vargas *et al.*, 2005). Additionally, the bulge stem cells are well established multipotent cells capable of differentiating into IFE, sebaceous glands and hair follicles in response to appropriate signals (Sun *et al.*, 2013). Importantly, while many early studies on epidermal stem cells were conducted in mouse models, there are significant differences between the murine stem cell niche and the human stem cell niche. This review focuses on the latter.

2.3.1 Keratinocyte Heterogeneity in the Interfollicular Epidermis and the Stem Cell Microenvironment

Once considered a homogenous population, it is now generally accepted that basal keratinocytes represent a heterogeneous cell reservoir. Along the basal lamina, keratinocytes cluster into patches of phenotypically similar keratinocytes. In the early 1980s, Lavker and Sun identified two spatially segregated keratinocyte subpopulations: nonserrated, slow-cycling keratinocytes located at the base of deep rete ridges and serrated keratinocytes located in shallow rete ridges (Lavker and Sun, 1982b, 1983b). The slow-cycling keratinocytes were later identified as keratinocyte stem cells. Watt *et al.* examined this phenomenon of stem cell patterning in the IF epidermis by correlating the regional variation in integrin expression levels in human skin with the colony forming efficiency of keratinocytes (Jones, Harper and Watt, 1995b; Watt, 1998, 2001, 2002). Additionally, a recent study of keratinocytes seeded on a microfabricated dermal papilla template showed differential gene expression on micropatterned membranes compared to flat controls suggesting a role for topography in defining keratinocyte functional niches (Lammers *et al.*, 2012). In fact, we have previously demonstrated increased keratinocyte stratification in deep, narrow channels compared to wide channels and flats (Downing *et al.*, 2005). We have also

shown that *in vivo* topographic clustering of keratinocytes expressing high levels of β_1 integrin can be recreated *in vitro* using a micropatterned substrate (Bush and Pins, 2012).

2.3.2 Keratinocyte Stem Cell Markers

Ultimately, keratinocyte stem cells are defined by their self-renewal ability. However, due to the challenges inherent to functional identification, it is useful to identify biochemical markers which characterize the keratinocyte stem cell. Many different markers have been proposed to identify keratinocyte stem cells. Identifying the stem cells of the intrafollicular region has proven to be particularly difficult because studies have shown a different organization in murine compared to human epidermis. This limits the utility of the standard label-retaining studies for the identification of slow cycling stem cells (Abbas and Mahalingam, 2009). Therefore, the majority of human IF keratinocyte research has been conducted using *in* vitro culture models. A summary of currently identified human IF keratinocyte stem cell markers can be found in Table 2.1.

Using flow cytometry and clonal analysis, Jones and Watt found that cells with high levels of surface β_1 integrin expression (β_1^{bti} cells) had the highest colony forming efficiency (CFE) (Jones and Watt, 1993). They would go on to demonstrate clustering of these β_1^{bri} keratinocytes in the basal layer of the epidermis (Jones *et al.*, 1995a). However, while these studies found that approximately 40% of basal keratinocytes were β_1^{bri}, previous *in vivo* studies suggest that keratinocyte stem cells make up only 1 to 10% of the basal cell population (Li *et al.*, 1998; Morris *et al.*, 1985; Morris and Potten, 1994). These findings establish the importance of using multiple markers to positively identify keratinocyte stem cells. In addition to the β_1 integrin subunit, the α_6 integrin subunit is upregulated in keratinocytes with high CFE, these cells also have low transferrin receptor CD71 expression, leading to the identification of the $\alpha_6^{bri}CD71^{dim}$ phenotype as a putative stem cell (Li, Simmons and Kaur, 1998). However, the use of the α_6 integrin and CD71 surface markers still relies on the classification of bright and dim cells.

Cytokeratins have also been used to distinguish keratinocyte stem cells from committed terminally differentiating cells. Notably, cytokeratins 5 and 14 (K5 and K14) are upregulated in basal stem cells while K1 and K10 are markers of differentiation that are found in the upper

epidermal strata (Alam *et al.*, 2011). Additionally, increased keratin 15 (K15) expression has been noted in the slow-cycling basal cells of the upper rete ridges and along with increased expression of integrin α_6 identifies keratinocytes with a high clonogenic potential (Schluter *et al.*, 2011).

Here we identify $\beta_1^{bri}p63^+$ keratinocytes as probable keratinocyte stem cells. Previously, keratinocytes that express both high levels of β_1 integrin and the nuclear transcription factor p63 have demonstrated the highest colony forming efficiency and have been identified as putative stem cells by multiple labs (Barrandon and Green, 1987; Hotchin *et al.*, 1995; Hotchin and Watt, 1992; Jones and Watt, 1993; Jones, Harper and Watt, 1995b; Kai-Hong *et al.*, 2007; Pellegrini *et al.*, 2001; Van Rossum *et al.*, 2004; Yang *et al.*, 1999). By using two separate markers, we reduce the likelihood of false positive identification.

Table 2.1 Markers of human keratinocyte stem cells in the interfollicular epidermis

Marker	Expression Level	Reference
α6 integrin	High	Li et al 1998
β1 integrin	High	Jones et al 1995
Desmogelin-3 (DSG3)	Low	Wan et al 2003
Keratin 14	High	Alam et al 2011
Keratin 15	High	Schlüter et al 2011
Keratin 5	High	Alam et al 2011
Leu-rich repeats and immunoglobulin-like domains 1 (LRIG1)	High	Jensen and Watt 2006
Melanoma-associated chondroitin sulphate proteoglycan (MCSP)	High	Legg et al 2003
Notch ligand delta like-1 (DLL1)	High	Lowell et al 2000
p63	High	Pellegrini et al 2001
Transferrin receptor (CD71)	Low	Kaur et al 2004

2.4 Current Skin Grafting Strategies

A variety of treatment strategies have been employed to address the large and growing number of chronic and traumatic cutaneous wounds. Since the primary concern with skin wounds is the rapid restoration of barrier function the most fundamental approach for their treatment is cleaning and dressing the wound. In fact, bandages and wound dressings account for over 50% of the wound healing market (MedMarket Diligence, 2013). However, while wound dressing may prevent desiccation and promote skin regeneration, in large area and chronic wounds, dressings alone are insufficient for preventing wound contraction and restoring the epidermal barrier. Furthermore, choosing a dressing can be difficult because each wound situation is unique. In order to rapidly restore skin functionality in these large and non-healing wounds, skin grafts are being investigated (Powers *et al.*, 2013). While autografting remains the preferred treatment, recent advances in bioengineered skin substitutes have created several promising new treatment strategies.

2.4.1 Autografts

Autografting is considered the "gold standard" treatment for the rapid closure of large skin wounds. The procedure involves the removal of healthy, undamaged skin from one area of the patient's body and subsequent transplantation into the wound bed. Currently, the most common autograft treatment for skin wounds is the split-thickness autograft, in which the harvested skin consists of the epidermis and the uppermost layer of the dermis. This treatment strategy allows for a more structurally robust graft, while somewhat limiting the donor site trauma. However, because it involves a secondary surgery site, autografting is often not an option for the treatment of large area burns and skin traumas due to the lack of available donor sites. Additionally, autografting may not be feasible in patients with compromised wound healing, such as diabetics. Further, autograft harvest results in donor site morbidity (Sheridan and Tompkins, 1999). As such, there is a need for an off-the-shelf skin substitute that provides immediate and permanent coverage to skin traumas and chronic wounds.

2.4.2 Bioengineered Skin Substitutes

The ideal bioengineered skin substitute would allow for rapid restoration of barrier integrity while supporting the re-establishment of normal anatomy and physiology of skin in the healing wound. Specifically, it should create a semi-permeable barrier that serves to prevent infection while maintaining tissue homeostasis with respect to temperature and hydration, integrate efficiently into the host tissue with minimal impact on cosmesis, promote angiogenesis and prevent wound contraction. Additionally, it should be cost efficient, easy to handle, and approximate native skin mechanically and anatomically (Metcalfe and Ferguson, 2007). There are three primary strategies for bioengineered skin grafts: dermal only substitutes, epidermal only substitutes and composite dermal-epidermal substitutes.

2.4.2.1 Dermal Skin Substitutes

Wound contraction is a major concern in the healing of large area skin traumas. The ability of a dermal substitute to prevent wound contraction in full-thickness wounds is well established (Singer and Clark, 1999). Dermal substitute strategies are primarily acellular, which can make them more cost effective and simpler to regulate than epidermal and composite strategies. However, because dermal substitutes alone do not provide barrier function, they are often used in conjunction with epidermal substitutes or temporary synthetic barrier layers.

2.4.2.1.1 Alloderm

Alloderm is a scaffold created by decellularizing human cadaver dermal matrix. The proprietary lyophilization process preserves the extracellular matrix and basement membrane structure while eliminating the immunogenicity associated with allogeneic skin transplant (Wainwright, 1995; Woo *et al.*, 2007). Since Alloderm does not provide an epidermal barrier, it is often used in conjunction with a meshed split-thickness autograft. Although the autografting procedure still requires a secondary surgery, the use of a dermal support substitute improves cosmesis of the meshed graft and minimizes the amount of autologous skin required for grafting (Wainwright, 1995). In addition to requiring an autograft or epidermal substitute, Alloderm is also limited by inconsistent re-vascularization and the availability of donor skin (Shakespeare, 2005; Shevchenko *et al.*, 2010).

2.4.2.1.2 Integra

Integra DRT, developed based on the work of Yannas *et al.,* is a collagen-glycosaminoglycan (GAG) sponge with a temporary silicone rubber epidermal barrier (Dagalakis *et al.*, 1980; Shastri, 2006; Stern *et al.*, 1990; Yannas and Burke, 1980). The sponge is gradually infiltrated by the patient's own cells and revascularized over a period of 2-3 weeks. Following the integration of the dermal component, the silicone barrier layer is removed and replaced with a meshed split-thickness autograft. Integra has several advantages including ease of handling and a long shelf life. It has had widespread success as a dermal substitute for preventing wound contraction in full thickness burns and chronic ulcers. Despite its success, Integra DRT requires a second procedure to replace the epidermis, and does not completely eliminate the need for autografting (Shastri, 2006; Supp and Boyce, 2005).

2.4.2.1.3 Dermagraft

Dermagraft is a dermal substitute that is primarily used for the treatment of chronic diabetic foot ulcers. It is composed of a polyglactin mesh that is cryopreserved following seeding with neonatal fibroblasts (Marston *et al.*, 2003; Shevchenko, James and James, 2010). As the scaffold degrades in the wound bed, growth factors and ECM components synthesized by the fibroblasts are released promoting dermal regeneration and keratinocyte re-epithelialization. A major disadvantage of Dermagraft is its high cost compared with other dermal substitutes due to the incorporation of fibroblasts. Additionally, it requires multiple applications.

2.4.2.2 Epidermal Skin Substitutes

Since prompt restoration of barrier function is essential for positive healing outcomes, one strategy is the use of a cellular epidermal layer to provide immediate barrier protection. Currently there are many varied strategies for the development of bioengineered epidermal skin substitutes. In general the approaches differ in three aspects: cell source and cell culture techniques, cell differentiation state and level of epidermal organization, and delivery method. Most commonly, autologous cells are harvested from a small biopsy taken from the patient at the time of wound debridement and expanded *in vitro*. Both submerged and air-liquid culture techniques have been explored for the generation of these epidermal substitutes. Variation in

culture conditions can alter the overall state of the cell population. The presence of keratinocyte stem cells is essential for both optimal *in vitro* expansion and long term graft survival *in vivo.* Thus strategies focused on creating permanent epidermal substitutes utilize cell populations that include a large number of undifferentiated keratinocyte stem cells. These cells can be grown into confluent, stratifying sheets or maintained in sub-confluent cultures. Finally, several different delivery methods have been explored ranging from transplantation of confluent stratified epidermal sheets to aerosolized delivery of keratinocytes in suspension.

Although epidermal only substitutes have enjoyed some clinical success, the lack of an underlying dermal support matrix leads to poor graft stability and sub-par wound healing (Atiyeh and Costagliola, 2007; Compton *et al.*, 1993). In particular, the need for a composite dermal-epidermal graft for effective treatment of full-thickness wounds is well established. Accordingly, epidermal only substitutes are sometimes used in conjunction with dermal substitutes. Some commercially available epidermal skin substitutes are described below.

2.4.2.2.1 Epicel

The technology behind Cultured Epithelial Autografts (CEAs), human keratinocytes cultured *in vitro* into sheets suitable for grafting into a wound bed, was first pioneered in the late 1970s by James Rheinwald, Ph.D. and Howard Green, M.D (Gallico and O'Connor, 1985; Gallico *et al.*, 1984; Green *et al.*, 1979; O'Connor *et al.*, 1981; Shevchenko, James and James, 2010). Epicel is made by expanding and culturing autologous keratinocytes to confluence over a period of 2-3 weeks. The keratinocytes are then enzymatically detached from the culture substrate as a contiguous sheet. This sheet can then be transplanted to the wound. CEAs provide wound covering and begin to promote the regeneration of the DEJ within weeks, although full maturation requires over a year (Compton *et al.*, 1989). However, despite early reports of clinical success, the clinical excitement for CEAs faded due in large part to the lengthy culture times required for CEA application and the highly variable rates of graft take (Atiyeh and Costagliola, 2007; Carsin *et al.*, 2000; Williamson *et al.*, 1995). Notably, CEAs perform best when used on wounds that retain

some dermal appendages or in conjunction with a dermal substitute (Atiyeh and Costagliola, 2007).

2.4.2.2.2 MySkin

Although not FDA approved for use in the US, MySkin is approved for use in the UK for the treatment of burns and chronic wounds. MySkin consists of a temporary silicone substrate which is used to deliver sub-confluent autologous keratinocytes to the wound bed. In contrast to Epicel, MySkin does not require enzymatic detachment of the keratinocytes from the culture substrate. Instead, the keratinocytes are cultured on the polymer substrate which is then used to transfer a sub-confluent population of un-differentiated keratinocytes to the wound bed (Haddow *et al.*, 2003). The silicone layer is then kept in place for four days as a dressing before being replaced with an absorbent dressing (Hernon *et al.*, 2006). Multiple weekly applications are required for wound closure. MySkin offers several advantages over traditional CEAs. Not only is the required culture time following biopsy shorter (approximately 10 days compared to 14 for CEAs), but if the treatment needs to be rescheduled for any reason such as infection in the wound bed the keratinocytes can be harvested from the MySkin substrate, replated and be ready for transplant in two days. This flexibility increases the chance of a positive treatment outcome. Additionally, the enzymatic keratinocyte detachment required for the generation of CEAs may negatively impact the ability of the basal keratinocytes to reattach and engraft in the wound bed, whereas MySkin does not require dissociation of the cells from the substrate. Instead, the substrate itself aids in graft transfer and enhances mechanical stability. However, MySkin still requires multiple applications and lacks an underlying dermal support (Shevchenko, James and James, 2010).

2.4.2.2.2 ReCell

ReCell Spray-On Skin is an autologous cell harvest and delivery system that does not require culture time. Instead a small, split-thickness biopsy is obtained during surgery and digested with trypsin. The epidermis is then separated from the dermis and the cells were disassociated and resuspended in Lactate solution resulting in a cell suspension consisting of predominantly keratinocytes (>60%), but also containing fibroblasts and melanocytes (Wood *et al.*, 2012). The

cell suspension is then applied to the prepared wound bed within an hour of isolation (Gravante *et al.*, 2007). ReCell can be applied directly to the wound or used in conjunction with a split-thickness autograft or a dermal skin substitute. ReCell has been shown to enhance re-epithelialization and promote improved cosmetic outcomes. However, some authors have reported poor healing outcomes when used alone without a split-thickness autograft. Additionally, as with other autografts the ReCell technique can result in donor site morbidity (Tenenhaus and Rennekampff, 2012).

2.4.2.3 Composite Skin Substitutes

The most advanced skin substitutes are dermal-epidermal composite grafts designed to replace both layers of skin with a single treatment. Because they provide both dermal support to prevent wound contraction and an epidermal layer to re-establish barrier function, these substitutes are also the most expensive. Due to their complexity and required culture time, most composite skin substitutes utilize allogeneic keratinocytes.

2.4.2.3.1 Apligraf®

One of the first composite skin grafts was developed by Eugene Bell. The graft utilized neonatal allogenic cells and consisted of keratinocytes cultured on the surface of a flat, pre-contracted fibroblast populated type I bovine collagen matrix. The keratinocytes formed a stratified epidermis that resembles native epidermal strata. This technology was later commercialized by Organogenesis as Apligraf® as a treatment for non-healing ulcers. Apligraf® has had demonstrated clinical success for the treatment of diabetic ulcers. Compared to compression therapy alone, Apligraf® has been shown to expedite wound closure and has been used to promote healing of wounds that failed to respond to conventional therapy (Sams *et al.*, 2002; Sheridan and Tompkins, 1999; Shevchenko, James and James, 2010; Veves *et al.*, 2001). However, its high cost of \$28/cm^2, short 5 days shelf life and instability in the wound bed remain significant limitations.

2.4.2.3.2 OrCel

OrCel is a tissue-engineered skin construct similar to Apligraf®. OrCel is fabricated by seeding neonatal allogenic fibroblasts into type I bovine collagen sponge with a non-porous collagen-gel coating. Keratinocytes are seeded on the non-porous coating and cultured to form a confluent layer. OrCel is used in the treatment of dystrophic epidermolysis bullosa, a blistering skin disease, as well as to promote healing at the autograft donor site in burn patients. Like Apligraf®, OrCel does not function like a permanent skin substitute, but rather as a temporary (7-14 days) bioactive dressing. As the grafts are broken down in the wound bed they release important ECM proteins and growth factors that stimulate the wound healing cascade (Shevchenko, James and James, 2010). Compared with an acellular bioactive dressing, Orcel treatment resulted in shorter healing times (Still *et al.*, 2003).

2.4.4 Limitations of Current Strategies

A common feature of current strategies is the failure to recreate the native topography of skin, whereas in native skin, the epidermis conforms to the topography of the dermal grooves and papillae. Since these microtopographic niches create cellular micro environments that promote keratinocyte clustering and differentially drive keratinocyte functions such as proliferation, differentiation and migration (Butler and Orgill, 2005; Jones, Harper and Watt, 1995b; Lavker and Sun, 1982a, 1983a; Odland, 1950; Vracko, 1974), we hypothesize that the incorporation of these critical microniches into the next generation of tissue engineered skin substitutes will advance the current state of the art wound treatment by creating a more robust and highly physiologically relevant skin substitute.

2.5 Micropatterned Dermal-Epidermal Regeneration Matrices

Several *in vitro* models have been developed to characterize the effects of the cellular microenvironment on keratinocyte function (Charest *et al.*, 2009; Gilbert and Blau, 2011; Gobaa *et al.*, 2011; Trappmann *et al.*, 2012). Charest *et al* seeded keratinocytes on microprinted surfaces designed to either allow or prevent cell-cell contact. They found that cell-cell contact promoted keratinocyte differentiation, independent of cell geometry (Charest, Jennings, King, Kowalczyk

and Garcia, 2009). In order to study the micro-environment of multi-cellular constructs, Gautrot *et al* developed micro-epidermis, small (<10 cells) stratified tissues grown on 100 μm diameter collagen coated discs and rings (40 μm inner diameter). They found that changing the shape of the micropatterned collagen coating (disc to ring) led to changes in epidermal organization (Gautrot, Wang, Liu, Goldie, Trappmann, Huck and Watt, 2012). These models provide important information about the role of the microenvironment in regulating cell function. However, the focus of these studies is using 2D surface ECM cues to drive keratinocyte fate, and therefore they do not attempt to study the native 3D microenvironment. Chandrasekaran *et al* incorporate 3D topography in their study of the keratinocyte microenvironment. In order to investigate how epithelial cells interact with their microenvironment and regulate themselves, they seeded HaCaT cells (immortalized keratinocytes) into microfabricated, spherical microbubble PDMS wells with diameters ranging from 100-300μm. Due to the geometries of the microwells, the microbubbles promote autocrine signaling. Although cells seeded on both flat PDMS and in wells formed spheroids, they found that only HaCaT cells cultured in microbubbles underwent a transition from spheroid to sheeting morphology similar to the epidermal to mesenchymal transition observed in cancer metastasis (Chandrasekaran *et al.*, 2011). This study provides an important platform for examining the soluble factor cues of the cellular microenvironment, however because PDMS is non-adherent, it does not allow for the evaluation of cell-matrix or cell topographic interactions. Taken together, these results demonstrate the importance of the microenvironment in driving cellular processes. However, there remains a need for an *in vitro* model system to study the specific role of DEJ topographic cues in regulating cell fate and function which will provides a better understanding of the keratinocyte microniche and its role in epidermal morphogenesis.

We developed micropatterned dermal-epidermal regeneration matrices (μDERMs) – a 3D *in vitro* model system that allows for the study of topographic cues alongside biochemical and cellular cues (Bush and Pins, 2012; Clement *et al.*, 2013). Determining how these cues interact to direct keratinocyte proliferation and cellular function will improve our understanding of epidermal morphogenesis and provide insight into skin wound healing. Specifically, we investigated the

role of topographic geometries of varying dimensions in directing keratinocyte stem cell clustering and epidermal morphogenesis including the effect of topography on keratinocyte proliferation, differentiation, and laminin 332 deposition. Briefly, μDERMs are a bilayered template that allows for the co-culture of dermal fibroblasts in a collagen-GAG sponge with keratinocytes on the surface of a micropatterned collagen gel. These tissue constructs can be cultured at the air-liquid interface to create full thickness skin substitutes *in vitro* (Clement, Moutinho and Pins, 2013).

2.6 Conclusions

Tissue engineered skin substitutes not only provide a clinical therapy for chronic wounds and large area skin trauma, but also provide a powerful *in vitro* model platform for the investigation of wound healing and skin pathogenesis. However, while native skin is characterized by the complex interdigitated topography of the dermal-epidermal junction, current organotypic models used to investigate cell-cell, cell-soluble factor and cell-matrix interactions do not enable the investigation of the role of topography in the regulation of cell function. The topography of the DEJ physically defines keratinocyte microenvironments. As such elucidating microtopographic cues is critical for understanding the keratinocyte stem cell niche, epidermal morphogenesis and wound healing. Further, a better understanding of the significance of microtopography in epidermal tissue engineering will provide key design parameters for the next generation clinical skin substitutes. Recently, we demonstrated that physical topographical features and cellular microniches on micropatterned dermal-epidermal matrices (μDERMs) could be used to sequester keratinocyte stem cells and control keratinocyte functions such as proliferation and basement membrane synthesis. This suggests that an understanding of how keratinocytes respond to their topographic 3D microenvironment is critical to the development of the next generation skin substitutes and *in vitro* model systems.

2.7 References

Abbas O and Mahalingam M (2009) Epidermal Stem Cells: Practical Perspectives and Potential Uses. *Br J Dermatol* 161:228-36.

Alam H, Sehgal L, Kundu ST, Dalal SN and Vaidya MM (2011) Novel Function of Keratins 5 and 14 in Proliferation and Differentiation of Stratified Epithelial Cells. *Mol Biol Cell* 22:4068-78.

Alberts ea (2002) *Molecular Biology of the Cell*, vol. 4th Edition. Garland Science: New York.

American Burn Association (2007) Burn Incidence and Treatment in the U.S.: 2007 Fact Sheet.

American Burn Association (2013) Burn Incidence and Treatment in the United States: 2013 Fact Sheet.

American Burn Association and National Burn Repository (2012) National Burn Repository Report of Data from 2002-2011.

Atac B, Wagner I, Horland R, Lauster R, Marx U, Tonevitsky AG, Azar RP and Lindner G (2013) Skin and Hair on-a-Chip: In Vitro Skin Models Versus Ex Vivo Tissue Maintenance with Dynamic Perfusion. *Lab Chip* 13:3555-61.

Atiyeh BS and Costagliola M (2007) Cultured Epithelial Autograft (CEA) in Burn Treatment: Three Decades Later. *Burns* 33:405-13.

Bar-Meir E, Mendes D and Winkler E (2006) Skin Substitutes. *IMAJ* 8:188-91.

Barrandon Y and Green H (1987) Three Clonal Types of Keratinocyte with Different Capacities for Multiplication. *Proc Nati Acad Sci USA* 84:2302-06.

Barret JP, Wolf SE, Desai MH and Herndon DN (2000) Cost-Efficacy of Cultured Epidermal Autografts in Massive Pediatric Burns. *Ann Surg* 231:869-76.

Bellas E, Seiberg M, Garlick J and Kaplan DL (2012) In Vitro 3d Full-Thickness Skin-Equivalent Tissue Model Using Silk and Collagen Biomaterials. *Macromol Biosci* 12:1627-36.

Bickers DR, Lim HW, Margolis D, Weinstock MA, Goodman C, Faulkner E, Gould C, Gemmen E and Dall T (2006) The Burden of Skin Diseases: 2004 a Joint Project of the American Academy of Dermatology Association and the Society for Investigative Dermatology. *J Am Acad Dermatol* 55:490-500.

Blanpain C and Fuchs E (2009) Epidermal Homeostasis: A Balancing Act of Stem Cells in the Skin. *Nat Rev Mol Cell Biol* 10:207-17.

Briggaman RA (1982) Biochemical Composition of the Epidermal-Dermal Junction and Other Basement Membrane. *J Invest Dermatol* 78:1-6.

Briggaman RA and Wheeler CE, Jr. (1975) The Epidermal-Dermal Junction. *J Invest Dermatol* 65:71-84.

Burgeson RE and Christiano AM (1997) The Dermal-Epidermal Junction. *Curr Opin Cell Biol* 9:651-8.

Bush K and Pins G (2012) Development of Microfabricated Dermal Epidermal Regenerative Matrices to Evaluate the Role of Cellular Microenvironments on Epidermal Morphogenesis. *Tissue Eng Part A* 18:2343-53.

Butler CE and Orgill DP (2005) Simultaneous in Vivo Regeneration of Neodermis, Epidermis, and Basement Membrane. *Adv Biochem Eng Biotechnol* 94:23-41.

Carsin H, Ainaud P, Le Bever H, Rives J, Lakhel A, Stephanazzi J, Lambert F and Perrot J (2000) Cultured Epithelial Autografts in Extensive Burn Coverage of Severely Traumatized Patients: A Five Year Single-Center Experience with 30 Patients. *Burns* 26:379-87.

Chandrasekaran S, Giang UB, King MR and DeLouise LA (2011) Microenvironment Induced Spheroid to Sheeting Transition of Immortalized Human Keratinocytes (Hacat) Cultured in Microbubbles Formed in Polydimethylsiloxane. *Biomaterials* 32:7159-68.

Chang HY, Chi JT, Dudoit S, Bondre C, van de Rijn M, Botstein D and Brown PO (2002) Diversity, Topographic Differentiation, and Positional Memory in Human Fibroblasts. *Proc Natl Acad Sci U S A* 99:12877-82.

Charest JL, Jennings JM, King WP, Kowalczyk AP and Garcia AJ (2009) Cadherin-Mediated Cell-Cell Contact Regulates Keratinocyte Differentiation. *J Invest Dermatol* 129:564-72.

Clement AL, Moutinho T and Pins GD (2013) Micropatterned Dermal-Epidermal Regeneration Matrices Create Functional Niches That Enhance Epidermal Morphogenesis. *Acta Biomater* 9:9474-84.

Compton CC, Gill JM, Bradford DA, Regauer S, Gallico GG and O'Connor NE (1989) Skin Regenerated from Cultured Epithelial Autografts on Full-Thickness Burn Wounds from 6 Days to 5 Years after Grafting. A Light, Electron Microscopic and Immunohistochemical Study. *Lab Invest* 60:600-12.

Compton CC, Hickerson W, Nadire K and Press W (1993) Acceleration of Skin Regeneration from Cultured Epithelial Autografts by Transplantation to Homograft Dermis. *J Burn Care Rehabil* 14:653-62.

Dagalakis N, Flink J, Stasikelis P, Burke JF and Yannas IV (1980) Design of an Artificial Skin. Part Iii. Control of Pore Structure. *J Biomed Mater Res* 14:511-28.

Downing BR, Cornwell K, Toner M and Pins GD (2005) The Influence of Microtextured Basal Lamina Analog Topography on Keratinocyte Function and Epidermal Organization. *J Biomed Mater Res A* 72:47-56.

Fawcett DW and Jensh RP (1997) *Concise Histology*. Chapman and Hall: New York, NY.

Gallico GG, 3rd and O'Connor NE (1985) Cultured Epithelium as a Skin Substitute. *Clin Plast Surg* 12:149-57.

Gallico GG, 3rd, O'Connor NE, Compton CC, Kehinde O and Green H (1984) Permanent Coverage of Large Burn Wounds with Autologous Cultured Human Epithelium. *N Engl J Med* 311:448-51.

Gautrot JE, Wang C, Liu X, Goldie SJ, Trappmann B, Huck WT and Watt FM (2012) Mimicking Normal Tissue Architecture and Perturbation in Cancer with Engineered Micro-Epidermis. *Biomaterials* 33:5221-9.

Gilbert PM and Blau HM (2011) Engineering a Stem Cell House into a Home. *Stem Cell Res Ther* 2:3.

Gobaa S, Hoehnel S, Roccio M, Negro A, Kobel S and Lutolf MP (2011) Artificial Niche Microarrays for Probing Single Stem Cell Fate in High Throughput. *Nat Methods* 8:949-55.

Gravante G, Di Fede MC, Araco A, Grimaldi M, De Angelis B, Arpino A, Cervelli V and Montone A (2007) A Randomized Trial Comparing Recell System of Epidermal Cells Delivery Versus Classic Skin Grafts for the Treatment of Deep Partial Thickness Burns. *Burns* 33:966-72.

Green H, Kehinde O and Thomas J (1979) Growth of Cultured Human Epidermal Cells into Multiple Epithelia Suitable for Grafting. *Proc Natl Acad Sci U S A* 76:5665-8.

Groeber F, Holeiter M, Hampel M, Hinderer S and Schenke-Layland K (2011) Skin Tissue Engineering--in Vivo and in Vitro Applications. *Adv Drug Deliver Rev* 63:352-66.

Haddow DB, Steele DA, Short RD, Dawson RA and Macneil S (2003) Plasma-Polymerized Surfaces for Culture of Human Keratinocytes and Transfer of Cells to an in Vitro Wound-Bed Model. *J Biomed Mater Res A* 64:80-7.

Hernon CA, Dawson RA, Freedlander E, Short R, Haddow DB, Brotherston M and MacNeil S (2006) Clinical Experience Using Cultured Epithelial Autografts Leads to an Alternative Methodology for Transferring Skin Cells from the Laboratory to the Patient. *Regen Med* 1:809-21.

Hotchin N, Gandarillas A and Watt F (1995) Regulation of Cell Surface Beta 1 Integrin Levels During Keratinocyte Terminal Differentiation. *J Cell Biol* 128:1209-19.

Hotchin N and Watt F (1992) Transcriptional and Post-Translational Regulation of Beta 1 Integrin Expression During Keratinocyte Terminal Differentiation. *J Biol Chem* 267:14852-8.

Huang S, Xu Y, Wu C, Sha D and Fu X (2010) In Vitro Constitution and in Vivo Implantation of Engineered Skin Constructs with Sweat Glands. *Biomaterials* 31:5520-5.

Janson DG, Saintigny G, van Adrichem A, Mahe C and El Ghalbzouri A (2012) Different Gene Expression Patterns in Human Papillary and Reticular Fibroblasts. *J Invest Dermatol* 132:2565-72.

Jones P and Watt F (1993) Separation of Human Epidermal Stem Cells from Transit Amplifying Cells on the Basis of Differences in Integrin Function and Expression. *Cell* 73:713-24.

Jones PH, Harper S and Watt FM (1995a) Stem Cell Patterning and Fate in Human Epidermis. *Cell* 80:83-93.

Jones PH, Harper S and Watt FM (1995b) Stem Cell Patterning and Fate in Human Epidermis. *Cell* 80:83-93.

Kai-Hong J, Jun X, Kai-Meng H, Ying W and Hou-Qi L (2007) P63 Expression Pattern During Rat Epidermis Morphogenesis and the Role of P63 as a Marker for Epidermal Stem Cells. *J Cutan Pathol* 34:154-9.

Kaur P, Li A, Redvers R and Bertoncello I (2004) Keratinocyte Stem Cell Assays: An Evolving Science. *J Invest Dermatol* 9:238-47.

Lammers G, Roth G, Heck M, Zengerle R, Tjabringa GS, Versteeg EM, Hafmans T, Wismans R, Reinhardt DP, Verwiel ET, Zeeuwen PL, Schalkwijk J, Brock R, Daamen WF and van Kuppevelt TH (2012) Construction of a Microstructured Collagen Membrane Mimicking the Papillary Dermis Architecture and Guiding Keratinocyte Morphology and Gene Expression. *Macromol Biosci* 12:675-91.

Lavker R and Sun T (1982a) Heterogeneity in Epidermal Basal Keratinocytes: Morphological and Functional Correlations. *Science* 215:1239-41.

Lavker R and Sun T (1983a) Epidermal Stem Cells. *J Invest Dermatol* 81:121s-7s.

Lavker RM and Sun TT (1982b) Heterogeneity in Epidermal Basal Keratinocytes: Morphological and Functional Correlations. *Science* 215:1239-41.

Lavker RM and Sun TT (1983b) Epidermal Stem Cells. *J Invest Dermatol* 81:121s-7s.

Legg J, Jensen UB, Broad S, Leigh I and Watt FM (2003) Role of Melanoma Chondroitin Sulphate Proteoglycan in Patterning Stem Cells in Human Interfollicular Epidermis. *Development* 130:6049-63.

Li A, Simmons PJ and Kaur P (1998) Identification and Isolation of Candidate Human Keratinocyte Stem Cells Based on Cell Surface Phenotype. *Proc Natl Acad Sci U S A* 95:3902-7.

Lowell S, Jones P, Le Roux I, Dunne J and Watt FM (2000) Stimulation of Human Epidermal Differentiation by Delta-Notch Signalling at the Boundaries of Stem-Cell Clusters. *Curr Biol* 10:491-500.

Madison KC (2003) Barrier Function of the Skin: "La Raison D'etre" of the Epidermis. *J Invest Dermatol* 121:231-41.

Margolis DJ, Malay DS, Hoffstad OJ, Leonard CE, MaCurdy T, de Nava KL, Tan Y, Molina T and Siegel KL (2011) Incidence of Diabetic Foot Ulcer and Lower Extremity Amputation among Medicare Beneficiaries, 2006 to 2008: Data Points #2. In: *Data Points Publication Series* (Rockville (MD).

Marston WA, Hanft J, Norwood P and Pollak R (2003) The Efficacy and Safety of Dermagraft in Improving the Healing of Chronic Diabetic Foot Ulcers: Results of a Prospective Randomized Trial. *Diabetes Care* 26:1701-5.

Mather JP and Roberts PE (1998) *Introduction to Cell and Tissue Culture : Theory and Technique*. Plenum Press: New York, xv, 241 p.

MedMarket (2007) Worldwide Wound Management, 2007-2016. Report no. #S245.

MedMarket Diligence (2013) Worldwide Wound Management, Forecast to 2021: Established and Emerging Products, Technologies and Markets in the Americas, Europe, Asia/Pacific and Rest of World.

Metcalfe AD and Ferguson MW (2007) Tissue Engineering of Replacement Skin: The Crossroads of Biomaterials, Wound Healing, Embryonic Development, Stem Cells and Regeneration. *J R Soc Interface* 4:413-37.

Milenkovic M, Russo CA and Elixhauser A (2007) Hospital Stays for Burns, 2004. Hcup Statistical Brief #25. *Agency for Healthcare Research and Quality, Rockville, MD*:http://www.hcup-us.ahrq.gov/reports/statbriefs/sb25.pdf.

Montagna W and Carlisle K (1979) Structural Changes in Aging Human Skin. *J Invest Dermatol* 73:47-53.

Morris RJ, Fischer SM and Slaga TJ (1985) Evidence That the Centrally and Peripherally Located Cells in the Murine Epidermal Proliferative Unit Are Two Distinct Cell Populations. *J Invest Dermatol* 84:277-81.

Morris RJ and Potten CS (1994) Slowly Cycling (Label-Retaining) Epidermal Cells Behave Like Clonogenic Stem Cells in Vitro. *Cell Prolif* 27:279-89.

Murphy M, Kerr P and Grant-Kels JM (2007) The Histopathologic Spectrum of Psoriasis. *Clin Dermatol* 25:524-8.

O'Connor NE, Mulliken JB, Banks-Schlegel S, Kehinde O and Green H (1981) Grafting of Burns with Cultured Epithelium Prepared from Autologous Epidermal Cells. *Lancet* 1:75-8.

Odland G (1950) The Morphology of the Attachment between the Dermis and the Epidermis. *Anat Record* 108:399-413.

Ojeh NO and Navsaria HA (2013) An in Vitro Skin Model to Study the Effect of Mesenchymal Stem Cells in Wound Healing and Epidermal Regeneration. *J Biomed Mater Res A*.

Pellegrini G, Dellambra E, Golisano O, Martinelli E, Fantozzi I, Bondanza S, Ponzin D, McKeon F and De Luca M (2001) P63 Identifies Keratinocyte Stem Cells. *Proc Natl Acad Sci U S A* 98:3156-61.

Pincelli C and Marconi A (2013) Keratinocyte Stem Cells: Biology and Clinical Applications. In: *Regenerative Medicine and Cell Therapy* (Baharvand H, Aghdami N, eds): Humana Press, 57-64.

Powell HM, McFarland KL, Butler DL, Supp DM and Boyce ST (2010) Uniaxial Strain Regulates Morphogenesis, Gene Expression, and Tissue Strength in Engineered Skin. *Tissue Eng Part A* 16:1083-92.

Powers JG, Morton LM and Phillips TJ (2013) Dressings for Chronic Wounds. *Dermatol Ther* 26:197-206.

Priya SG, Jungvid H and Kumar A (2008) Skin Tissue Engineering for Tissue Repair and Regeneration. *Tissue Eng Pt B* 114:105-18.

Rogers HW, Weinstock MA, Harris AR, Hinckley MR, Feldman SR, Fleischer AB and Coldiron BM (2010) Incidence Estimate of Nonmelanoma Skin Cancer in the United States, 2006. *Arch Dermatol* 146:283-7.

Rook A and Burns T (2010) Rook's Textbook of Dermatology. (Wiley-Blackwell: Chichester, West Sussex, UK ; Hoboken, NJ.

Sams HH, Chen J and King LE (2002) Graftskin Treatment of Difficult to Heal Diabetic Foot Ulcers: One Center's Experience. *Dermatol Surg* 28:698-703.

Schluter H, Paquet-Fifield S, Gangatirkar P, Li J and Kaur P (2011) Functional Characterization of Quiescent Keratinocyte Stem Cells and Their Progeny Reveals a Hierarchical Organization in Human Skin Epidermis. *Stem Cells* 29:1256-68.

Senoo M (2013) Epidermal Stem Cells in Homeostasis and Wound Repair of the Skin. *Adv Wound Care* 2:273-82.

Shaffer CL, Feldman SR, Fleischer AB, Huether MJ and Chen J (2005) The Cutaneous Surgery Experience of Multiple Specialties in the Medicare Population *J Am Acad Dermatol* 52:1045-48.

Shakespeare PG (2005) The Role of Skin Substitutes in the Treatment of Burn Injuries. *Clin Dermatol* 23:413-8.

Shastri VP (2006) Future of Regenerative Medicine: Challenges and Hurdles. *Artif Organs* 30:828-34.

Sheridan RL and Tompkins RG (1999) Skin Substitutes in Burns. *Burns* 25:97-103.

Shevchenko RV, James SL and James SE (2010) A Review of Tissue-Engineered Skin Bioconstructs Available for Skin Reconstruction. *J R Soc Interface* 7:229-58.

Silva-Vargas V, Lo Celso C, Giangreco A, Ofstad T, Prowse DM, Braun KM and Watt FM (2005) Beta-Catenin and Hedgehog Signal Strength Can Specify Number and Location of Hair Follicles in Adult Epidermis without Recruitment of Bulge Stem Cells. *Dev Cell* 9:121-31.

Singer AJ and Clark RA (1999) Cutaneous Wound Healing. *N Engl J Med* 341:738-46.

Stern R, McPherson M and Longaker M (1990) Histological Study of Artificial Skin Used in the Treatment of Full-Thickness Thermal Injury. *J Burn Care Rehabil* 11:7-13.

Still J, Glat P, Silverstein P, Griswold J and Mozingo D (2003) The Use of a Collagen Sponge/Living Cell Composite Material to Treat Donor Sites in Burn Patients. *Burns* 29:837-41.

Sun X, Fu X, Han W, Zhao M and Chalmers L (2013) Epidermal Stem Cells: An Update on Their Potential in Regenerative Medicine. *Expert Opin Biol Th* 13:901-10.

Supp D and Boyce S (2005) Engineered Skin Substitutes: Practices and Potentials *Clin Dermatol* 23:403-12.

Tajima S and Pinnell SR (1981) Collagen Synthesis by Human Skin Fibroblasts in Culture: Studies of Fibroblasts Explanted from Papillary and Reticular Dermis. *J Invest Dermatol* 77:410-2.

Tenenhaus M and Rennekampff HO (2012) Surgical Advances in Burn and Reconstructive Plastic Surgery: New and Emerging Technologies. *Clin Plast Surg* 39:435-43.

Tonnesen MG, Feng X and Clark RA (2000) Angiogenesis in Wound Healing. *J Invest Dermatol* 5:40-6.

Trappmann B, Gautrot JE, Connelly JT, Strange DG, Li Y, Oyen ML, Cohen Stuart MA, Boehm H, Li B, Vogel V, Spatz JP, Watt FM and Huck WT (2012) Extracellular-Matrix Tethering Regulates Stem-Cell Fate. *Nat Mater* 11:642-9.

Van Rossum MM, Framssem MEJ, Cloin WAH, Van de Bosch GJM, Boezmman JBM, Schalkwijk J, Van de Kerkhof PCM and Van Erp PEJ (2004) Functional Characterization of Beta1-Integrin-Positive Epidermal Cell Populations. *Acta Derm Venereol* 84:265-70.

Veves A, Falanga V, Armstrong DG and Sabolinski ML (2001) Graftskin, a Human Skin Equivalent, Is Effective in the Management of Noninfected Neuropathic Diabetic Foot Ulcers: A Prospective Randomized Multicenter Clinical Trial. *Diabetes Care* 24:290-5.

Vracko R (1974) Basal Lamina Scaffold-Anatomy and Significance for Maintenance of Orderly Tissue Structure. *Am J Pathol* 77:314-46.

Wainwright DJ (1995) Use of an Acellular Allograft Dermal Matrix (Alloderm) in the Management of Full-Thickness Burns. *Burns* 21:243-8.

Wan H, Stone MG, Simpson C, Reynolds LE, Marshall JF, Hart IR, Hodivala-Dilke KM and Eady RA (2003) Desmosomal Proteins, Including Desmoglein 3, Serve as Novel Negative Markers for Epidermal Stem Cell-Containing Population of Keratinocytes. *J Cell Sci* 116:4239-48.

Watt FM (1998) Epidermal Stem Cells: Markers, Patterning and the Control of Stem Cell Fate. *Philos Trans R Soc Lond B Biol Sci* 353:831-7.

Watt FM (2001) Stem Cell Fate and Patterning in Mammalian Epidermis. *Curr Opin Genet Dev* 11:410-7.

Watt FM (2002) The Stem Cell Compartment in Human Interfollicular Epidermis. *J Dermatol Sci* 28:173-80.

Waugh HV and Sherratt JA (2007) Modeling the Effects of Treating Diabetic Wounds with Engineered Skin Substitutes. *Wound Repair Regen* 15:556-65.

Williamson JS, Snelling CF, Clugston P, Macdonald IB and Germann E (1995) Cultured Epithelial Autograft: Five Years of Clinical Experience with Twenty-Eight Patients. *J Traum* 39:309-19.

Woo K, Ayello EA and Sibbald RG (2007) The Edge Effect: Current Therapeutic Options to Advance the Wound Edge. *Adv Skin Wound Care* 20:99-117.

Wood FM, Giles N, Stevenson A, Rea S and Fear M (2012) Characterisation of the Cell Suspension Harvested from the Dermal Epidermal Junction Using a Recell(R) Kit. *Burns* 38:44-51.

Yang A, Schweitzer R, Sun D, Kaghad M, Walker N, Bronson R, Tabin C, Sharpe A, Caput D, Crum C and McKeon F (1999) P63 Is Essential for Regenerative Proliferation in Limb, Craniofacial and Epithelial Development. *Nature* 398:714-18.

Yannas IV and Burke JF (1980) Design of an Artificial Skin. I. Basic Design Principles. *J Biomed Mater Res* 14:65-81.

Young B, Burkitt HG, Heath JW and Wheater PR *Wheater's Functional Histology*.

Chapter 3: Fibroblasts Enhance the Epidermal Morphology of Cultured µDERM

3.1 Introduction

Tissue engineered skin substitutes represent both a promising clinical therapy for large area and chronic wounds and a powerful model system for *in vitro* study of skin pathologies and drug screening. However, current tissue engineered skin substitutes fail to replicate the complex topographic microenvironment of the dermal-epidermal junction (DEJ). The absence of DEJ topography may contribute to mechanically induced graft failure and may have unknown effects on studies performed in *in vitro* models.

To investigate the role of DEJ architecture in epidermal morphogenesis, we created a fully implantable, bi-layered skin substitute that incorporates both topographical and ECM cues (Bush and Pins, 2012). This study found that the rate of epithelialization was increased in deep, narrow channels and promoted *in vitro* clustering of β_1^{bri} keratinocytes. These micropatterned dermal-epidermal regeneration matrices (µDERM) provide an *in vitro* platform for studying epidermal morphogenesis, wound healing, and skin disease pathogenesis. Additionally, they represent the next evolutionary step in the development of the "smart" bioengineered skin substitutes for the treatment of severe burns and non-healing wounds such as diabetic ulcers and pressure sores. However, the first generation µDERM lacked paracrine signaling necessary to create a complete model system. In particular, the lack of fibroblasts signaling limits the keratinocyte proliferation potential.

Many studies have demonstrated the importance of fibroblast-keratinocyte paracrine signaling in epidermal morphogenesis (El Ghalbzouri *et al.*, 2004; Erdag and Sheridan, 2004; Krejci *et al.*, 1991). Fibroblast incorporation into *in vitro* skin models has been shown to upregulate keratinocyte proliferation and promote differentiation within the stratum granulosum (El-Ghalbzouri *et al.*, 2002; El Ghalbzouri, Hensbergen, Gibbs, Kempenaar, van der Schors and Ponec,

2004; El Ghalbzouri *et al.*, 2002; Smola *et al.*, 1993). Specifically, the appropriate localization of basement membrane protein at the dermal-epidermal junction depends on fibroblast signaling (El Ghalbzouri *et al.*, 2005; Marionnet *et al.*, 2006).

Fibroblasts facilitate keratinocyte growth and differentiation via a double paracrine mechanism (Maas-Szabowski *et al.*, 1999a; Szabowski *et al.*, 2000; Werner and Smola, 2001), as well as enhance re-epithelialization and improve the performance of skin substitutes (El Ghalbzouri, Hensbergen, Gibbs, Kempenaar, van der Schors and Ponec, 2004; Erdag and Sheridan, 2004; Krejci, Cuono, Langdon and McGuire, 1991). Specifically, this research demonstrated that keratinocyte proliferation and differentiation was enhanced within the stratum granulosum. Since barrier function is dependent in part on a well-organized stratum granulosum, evaluation of epidermal morphogenesis in the presence of fibroblasts is of significant interest.

In addition to fibroblasts, signaling from other cell types has been shown to enhance epidermal wound healing. For example, bone marrow derived mesenchymal stem cells (BM-MSCs) have been used to accelerate wound closure *in vivo* (Wu et al., 2007). In that study, BM-MSCs were shown to accelerate wound closure and contribute to appendage formation. While some of the engrafted BM-MSCs expressed epithelial markers, other studies have shown that BM-MSC conditioned media promotes keratinocyte proliferation *in vitro*, suggesting that both stem cell differentiation and paracrine signaling are responsible for the enhanced re-epithelialization (Wu *et al.*, 2010). In fact, BM-MSCs have been shown to secrete many of the same keratinocyte regulating cytokines as fibroblasts including keratinocyte growth factor (Wu, Zhao and Tredget, 2010).

Keratinocyte growth factor (KGF; also fibroblast growth factor 7) is a critical signaling molecule in the fibroblast-keratinocyte signaling loop (Werner *et al.*, 2007). KGF, a potent keratinocyte mitogen, is released by fibroblasts in the dermis in response to signals from the epidermis and is critical for epidermal morphogenesis and wound healing. Although its primary function is the regulation of keratinocyte proliferation, KGF has also been shown to induce laminin 332 and laminin 511/521 expression (El Ghalbzouri, Jonkman, Dijkman and Ponec, 2005). Both IL-1α and

IL-1β are secreted by the keratinocytes in response to skin wounding. Although IL-1 has no direct effect on the rate of keratinocyte proliferation, both IL-1 variants induce KGF expression in dermal fibroblasts. In this way, keratinocytes can indirectly regulate their own proliferation (Barreca *et al.*, 1992; Maas-Szabowski, Shimotoyodome and Fusenig, 1999a). Since KGF is not directly secreted by keratinocytes, it is a useful marker of fibroblast signaling in keratinocyte-fibroblast co-culture.

Because culture in the absence of fibroblast paracrine signals may result in a more quiescent phenotype, we hypothesize that incorporation of fibroblasts into µDERMs will increase epidermal thickness, improve epidermal morphology and ultimately allow us to more explicitly probe the ability of microtopography to create distinct keratinocyte niches. For example, in our previous studies we demonstrated a decrease in proliferating keratinocytes in the epidermal layer of µDERMs following initial seeding. This phenotypic switch makes elucidating differences in proliferation due to channel topographies difficult. Additionally, inclusion of fibroblasts in skin implants has been shown to enhance vascularization and reduce graft contraction *in vivo*. Therefore, in this chapter we will investigate the effect of fibroblast incorporation on epidermal morphology and epidermal thickness on µDERMs. Additionally, to elucidate whether paracrine signaling may be responsible for changes in epidermal thickness, we will use immunohistochemistry to compare KGF expression in µDERMs cultured with and without fibroblasts.

3.2 Materials and Methods

3.2.1 Cell Culture and Media Formulations

Neonatal primary human foreskin keratinocytes (NHKs) and primary human foreskin fibroblasts (NHFs) were isolated from foreskins, obtained as non-identifiable discard tissue from the University of Massachusetts Memorial Medical Center (Worcester, MA), and were approved with exempt status from the New England Institutional Review Board, using previously described methods (Bush *et al.*, 2007; Cornwell *et al.*, 2004). Prior to seeding on µDERMs, keratinocytes were cultured on a feeder layer of mitomycin C treated J2s (generously donated by Dr. Stelios

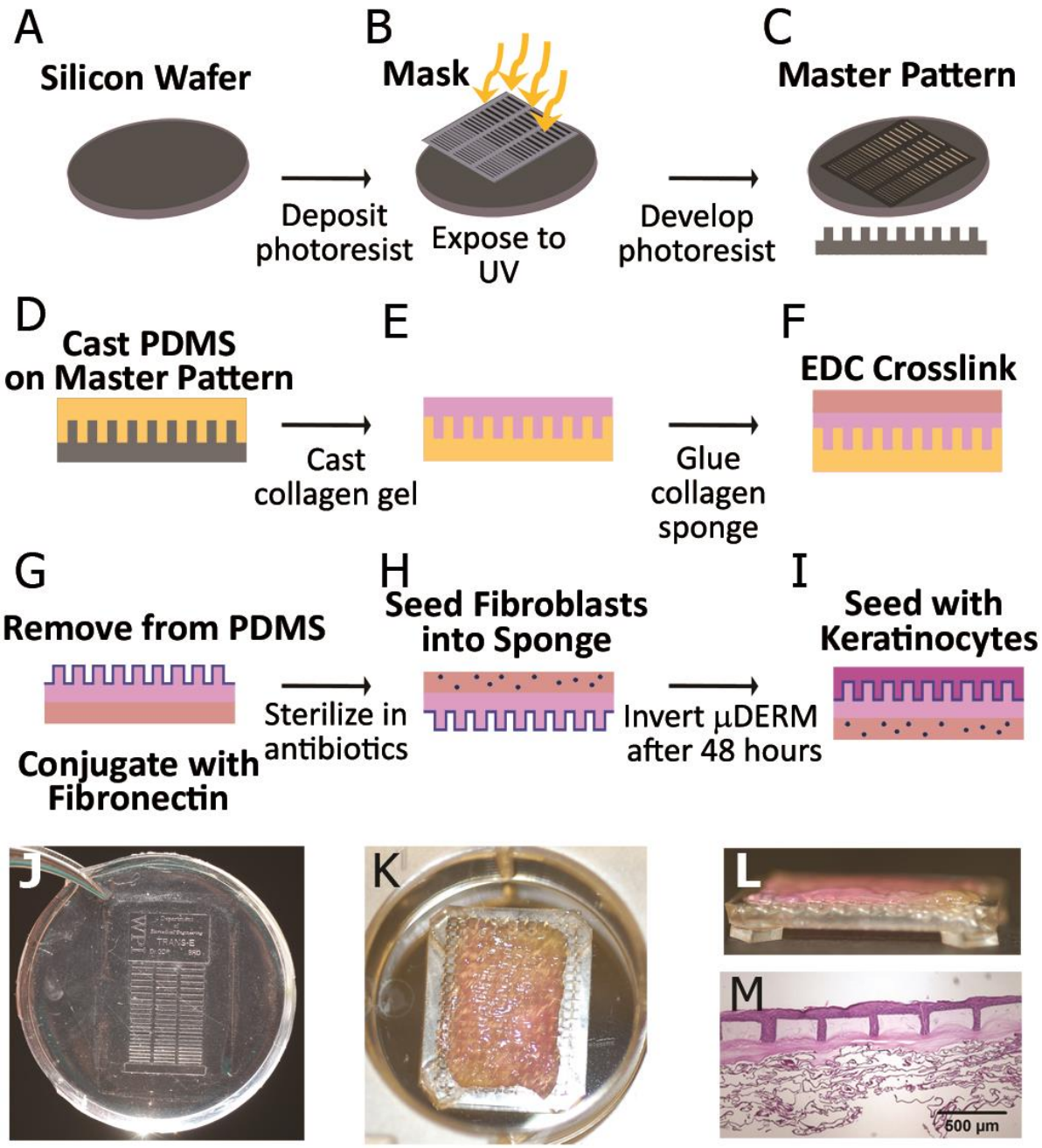

Figure 3.1 Production of µDERMs and 3D skin model system. Photolithography was used to create a silicon wafer with microtopographic features resembling the DEJ (A-C). Polydimethylsiloxane silicone elastomer (PDMS, 10:1 base to curing agent; Sylgard184; Dow Corning) was cured on the wafer's surface creating a negative mold (D). Type I collagen was self-assembled on the micropatterned molds (E) and a collagen-GAG sponge was laminated to the collagen matrix, and crosslinked to form the µDERM (F). µDERMs were conjugated with fibronectin (FN, 32 µg/cm2; BD Biosciences) and sterilized (G). The dermal side was seeded with fibroblasts and for 48 hours (H) then the micropatterned epidermal surface was seeded with keratinocytes (I). After 48 hours, µDERMs were cultured at the air-liquid interface. (J) Photograph of PDMS pattern used to create µDERMs. The collagen gel was cast over the entire area of the patterns, which were designed to fit into 6 well plates. (K) µDERM (collagen gel side up) on cell seeding screen in a 6 well plate. After removal from patterns, µDERMs were trimmed to 1.25cm x 2.0 cm and placed on cell-seeding screens. (L) Side view of µDERM on cell-seeding screen. Screens enable air-liquid interface culture. (M) Low magnification image of µDERM after 7 days of air-liquid culture.

Andreadis, State University of New York at Buffalo, Buffalo, NY). NHF medium consisted of Dulbecco's modified Eagle's medium (DMEM) with 10% fetal bovine serum (FBS) and 1% penicillin-streptomycin. NHK medium was comprised of a 3:1 blend of high glucose DMEM and Ham's F12 with 10% fetal bovine serum and 1% penicillin-streptomycin supplemented with adenine (1.8 x 10^{-14} M), cholera toxin (10^{-10} M), hydrocortisone (0.4 μg/ml), insulin (5 μg/ml), transferring (5 μg/ml), and triiodo-L-thyronine (2x10^{-9} M). The day after initial NHK plating, medium was replaced with NHK medium containing 10 ng/ml epidermal growth factor (EGF). Seeding medium for μDERM culture consisted of a 3:1 blend of high glucose DMEM and Ham's F12 with 1% fetal bovine serum and 1% penicillin-streptomycin supplemented with cholera toxin (10^{-10} M), hydrocortisone (0.2 μg/ml), insulin (5 μg/ml) and ascorbic acid (50 μg/ml). Priming medium consisted of seeding medium supplemented with 24 μM BSA, 25 μM oleic acid, 15 μM linoleic acid, 7 μM arachidonic acid, 25 μM palmitic acid, 10 μM L-carnitine, and 10 mM L-serine). Air-liquid interface (A/L) medium was serum-free priming medium supplemented with 1 ng/ml EGF.

3.2.2 μDERM Fabrication

μDERM fabrication was modified from a previous method (Bush and Pins, 2012) by incorporating fibroblasts into the dermal sponge and decreasing the thickness of the collagen gel-matrix (Figure 3.1). Specifically, a pattern was designed with a series of 200μm deep channels with varying widths (50μm, 100μm, 200μm, 400μm) (Bush and Pins, 2012; Downing *et al.*, 2005). Type I acid-soluble collagen (10 mg/ml in 5 mM HCl) was purified from rat tail tendons (Cornwell, Downing and Pins, 2004; Elsdale and Bard, 1972) and 0.3 ml of this collagen solution was self-assembled on the micropatterned molds using 5x DMEM (Invitrogen) with 0.22 M $NaHCO_3$ and 0.1 M NaOH (Sigma) for 18 hours at 37˚C and 10% CO_2. To construct a dermal analog, a collagen-GAG sponge was fabricated as previously described by lyophilizing a suspension of 5mg/ml SEMED-S collagen (Kensey Nash) and 0.18 mg/ml chondroitin sulfate (Sigma-Aldrich) in acetic acid (Bush and Pins, 2012). Following polymerization of the self-assembled collagen, the collagen-GAG sponge was laminated to the back of the micropatterned gel using an additional 0.3 ml of self-assembled collagen and then crosslinked with EDC (60 mM EDC in 50 mM MES buffer for 4 hours). Following

crosslinking, µDERMs were removed from the PDMS patterns and conjugated with fibronectin overnight (FN, 32 µg/cm^2; BD Biosciences). µDERMs were sterilized in an antibiotic cocktail (100 IU/ml-100µg/ml penicillin-streptomycin, 2.5µg/ml amphotericin B, 10pg/ml ciprofloxacin, 100µg/ml gentamycin) for a minimum of 24 hours at room temperature and rinsed with DMEM.

3.2.3 Fibroblast and Keratinocyte Seeding and *in vitro* Culture of µDERMs

For cell seeding, µDERMs were placed on custom-designed cell seeding screens (Figure 3.1K,L). Medical grade 316 stainless steel screens were embedded in PDMS platforms, leaving the center of the screen open. These PDMS platforms elevated the screens to allow for culture at the air-liquid interface. Initially, 8x10^4 NHFs/cm^2 in 100µl of NHF medium were seeded on the dermal side of the scaffold and incubated for 2 hours. Following incubation, additional fibroblast medium was added, and µDERMs were cultured for 48 hours (37˚C, 10%CO_2) with daily medium changes (Figure 3.1H). µDERMs were inverted onto A/L screens, NHKs were seeded on the micropatterned side at a density of 5x10^5 cells/cm^2 in 100µl seeding medium for 2 hours then µDERMs were submerged in seeding medium (Figure 3.1I). As a control, de-epidermized dermis (DED) was seeded with keratinocytes and cultured alongside µDERMs, as previously described (Bush and Pins, 2012). After 24 hours, seeding medium was replaced with priming medium for 48 hours. Finally, priming medium was replaced with A/L interface medium and µDERMs were cultured for 3 or 7 days at the A/L interface (Figure 3.1M).

3.2.4 Epidermal Thickness Measurements on Cultured µDERMs

µDERMs were fixed in neutral buffered formalin, embedded in Paraplast (McCormick Scientific) and sectioned perpendicular to the microchannel topography. Slides were stained with hematoxylin and eosin (Richard Allen Scientific). Channel depth, channel width, epidermal thickness in the channel and epidermal thickness on the neighboring plateaus were measured for each channel using Spot software (Figure 3.2A). For each well, channel depth and epidermal thickness were measured in 3 locations (center and each side) and then averaged to determine channel depth and epidermal thickness. Channel width was measured in 3 places (bottom, top and center) and then averaged to determine channel width. To account for variations in µDERM

dimensions, the average epidermal thickness was normalized to the average channel depth of the corresponding well. Plateau thickness was measured immediately adjacent to either side of each channel and then averaged to determine the adjacent plateau thickness (Figure 3.2B). Each µDERM section contained up to 4 replicates of each channel geometry. For each geometry, channels were analyzed on at least 3 separate µDERMs. Sample sizes for normalized epidermal thickness measurements were n= 19, 19, 19, and 21, for µDERMs cultured with fibroblasts (50µm, 100µm, 200µm and 400µm channel widths, respectively) and n = 4, 5, 3, and 8, for µDERMs cultured without fibroblasts (50µm, 100µm, 200µm and 400µm channel widths, respectively). Sample sizes for plateau thickness measurements were n= 21, 40, 38, 38, 40, for µDERMs cultured with fibroblasts (flats, 50µm, 100µm, 200µm and 400µm channel widths, respectively) and n = 9, 6, 10, 6, 16, for µDERMs cultured without fibroblasts (flats, 50µm, 100µm, 200µm and 400µm channel widths, respectively). Epidermal thickness of DED and native foreskin tissue was also measured. Finally, individual channels with mean geometries that deviated from the population mean values by more than two standard deviations were excluded from analysis.

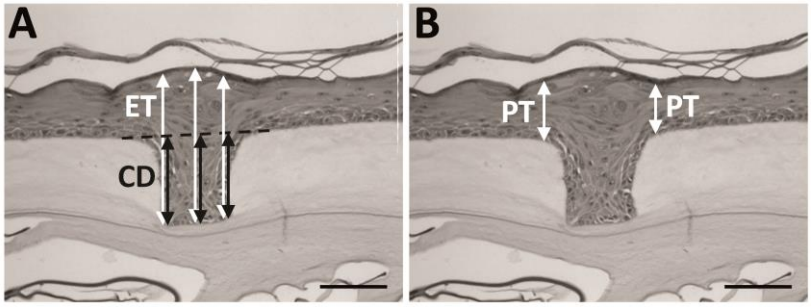

Figure 3.2 Method for measuring epidermal thickness on µDERM. (A) Normalized epidermal thickness was calculated by dividing epidermal thickness (ET) by channel depth (CD). (B) Plateau thickness (PT) was measured immediately adjacent to each channel topography (B) and in the center of control flats.

3.2.5 Immunohistochemical Analysis of Keratinocyte Growth Factor (KGF)

Following deparaffinization with xylene and rehydration through graded alcohols, antigen retrieval was performed as previously described (Bush and Pins, 2012). Briefly, slides were placed in boiling 0.01 M citrate buffer and boiled in a 6 quart pressure cooker for 15 minutes. Sections were blocked in 10% horse serum for 10 minutes and then incubated with goat-anti-human KGF antibody (FGF-7; 1:50; C-19, Santa Cruz) overnight at 4˚C. Subsequently, sections were incubated with AlexaFluor568 donkey-anti-goat secondary antibody (1:100; Invitrogen) for 1 hour at room

temperature and then nuclei were then stained with Hoechst 33342 (33.3 µg/ml) for 15 minutes. Negative control samples were incubated with blocking buffer, in lieu of primary antibody. Foreskin and panniculectomy discard tissues (obtained as non-identifiable tissue from the University of Massachusetts Medical School, Worcester, MA) were used as positive immunohistochemistry controls. The slides were then imaged with a Nikon Eclipse E400 microscope using an RT Color SPOT Camera. Negative control samples were used to set the exposure times to eliminate detection of autofluorescence. To visualize areas of increased KGF expression, false colorization was applied by modifying the image look up table (LUT) after background subtraction (blue = top 1/3 intensity, green = mid 1/3 intensity and red = lowest 1/3 intensity).

3.2.6 Statistical Analysis

Statistical differences were evaluated using SigmaPlot Version 11.0 (Systat Software, Inc.). Students t-tests were performed between fibroblast co-culture and keratinocyte only culture conditions for each geometry. Additionally, a 2-Way ANOVA on RANKS with Holm-Sidak post hoc analysis was performed to determine the contribution of fibroblasts independent of geometry. For all comparisons, a significant difference between groups was indicated by a p value < 0.05.

3.3 Results

3.3.1 Fibroblasts Enhance Epidermal Morphology on Cultured µDERM

To assess the effect of fibroblast paracrine signaling on µDERM culture and establish keratinocyte responses that more closely mimicked the native tissue micro-environments, dermal fibroblasts were incorporated into the 3D *in vitro* µDERM culture model. Although keratinocytes stratified on all µDERMs, those co-cultured with fibroblasts (Figure 3.3 B, D, F) exhibited increased epidermal thickness and enhanced epidermal morphology, including a more robust basal layer, compared to µDERMs cultured without fibroblasts (Figure 3.3 A, C, E). On µDERMs lacking fibroblasts, the viable cell layer was only a few cells thick and in places consisted solely of the basal layer (Figure 3.3 A, C, E). Overall, even in the thicker cell layers seen in microchannels of

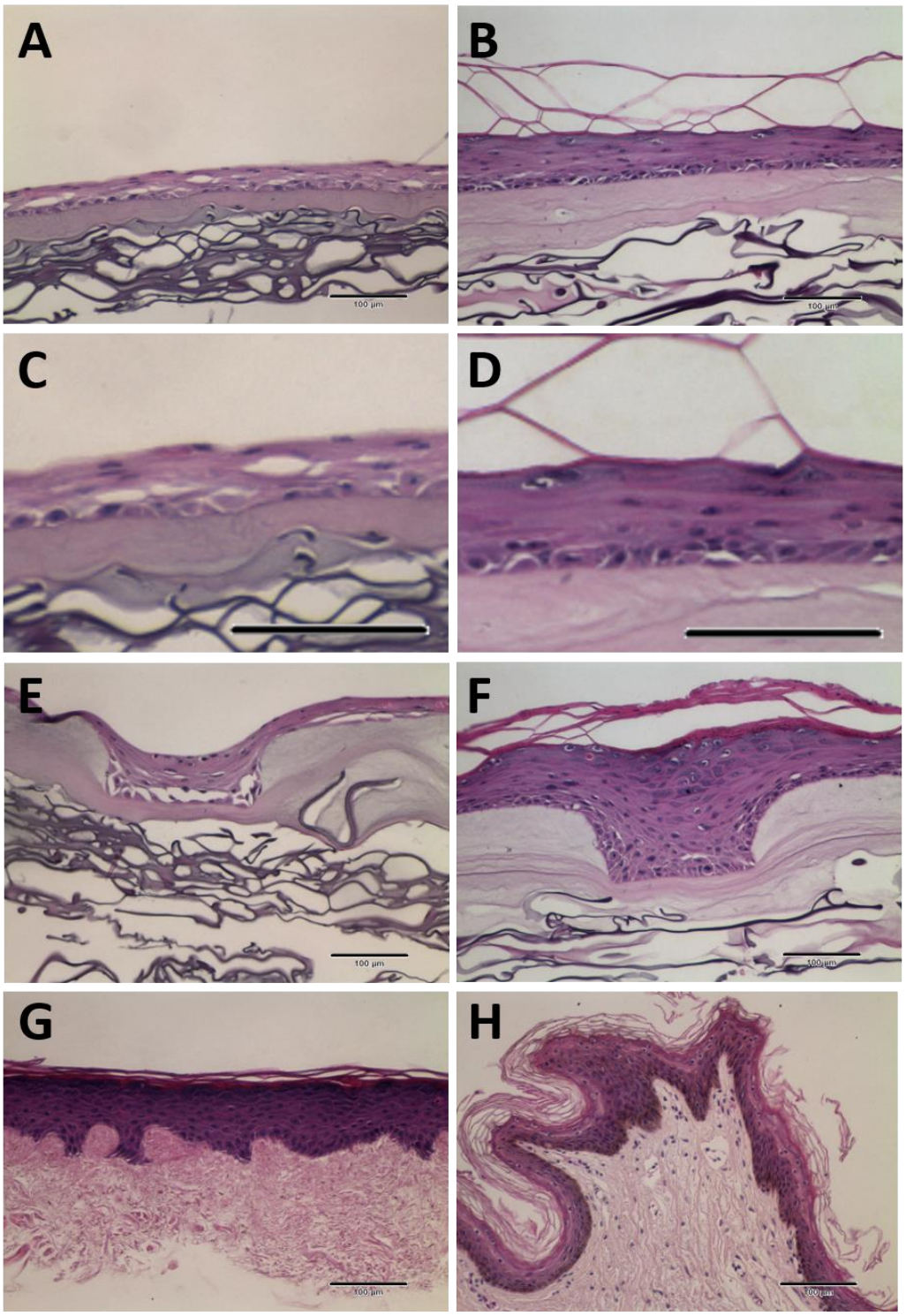

Figure 3.3 Epidermal stratification on µDERM cultured for 7 days at the A/L interface with and without fibroblasts. Hematoxylin and eosin stain of keratinocytes cultured on µDERM lacking fibroblasts (A, low magnification and C, high magnification of flats, E, low magnification of 100 µm channel) form thin strata without defined stratum granulosum or stratum spinosum layers. Keratinocytes cultured on µDERM containing fibroblasts (B, low magnification and D, high magnification of flats, F, low magnification of 100 µm channel) form thicker epidermal layers with evidence of a granular layer that more closely resembles keratinocytes cultured on DED (G) and native skin (H).

µDERMs lacking fibroblasts, the epidermis is poorly organized and lacks the distinct stratum spinosum and stratum granulosum seen in native skin. In contrast, the basal keratinocytes in the robust basal layer of grafts containing fibroblasts (Figure 3.3 B, D, F) are cuboidal, smaller and more tightly packed than on grafts lacking fibroblasts.

3.3.2 Fibroblasts Increase Epidermal Thickness on Cultured µDERMs

Measuring epidermal thickness on cultured µDERM allows for quantitative assessment of the influence of fibroblast-keratinocyte co-culture on epidermal morphogenesis. To analyze the effect of fibroblasts on epidermal thickness, we compared the normalized epidermal thickness in channels of µDERMs cultured without fibroblasts to the normalized epidermal thickness in channels of corresponding dimensions on µDERMS cultured with fibroblasts pre-seeded into the dermal collagen-GAG sponge (Figure 3.4A). In general, channels on grafts containing fibroblasts had a thicker normalized epidermal thickness, except in the 50µm channels.

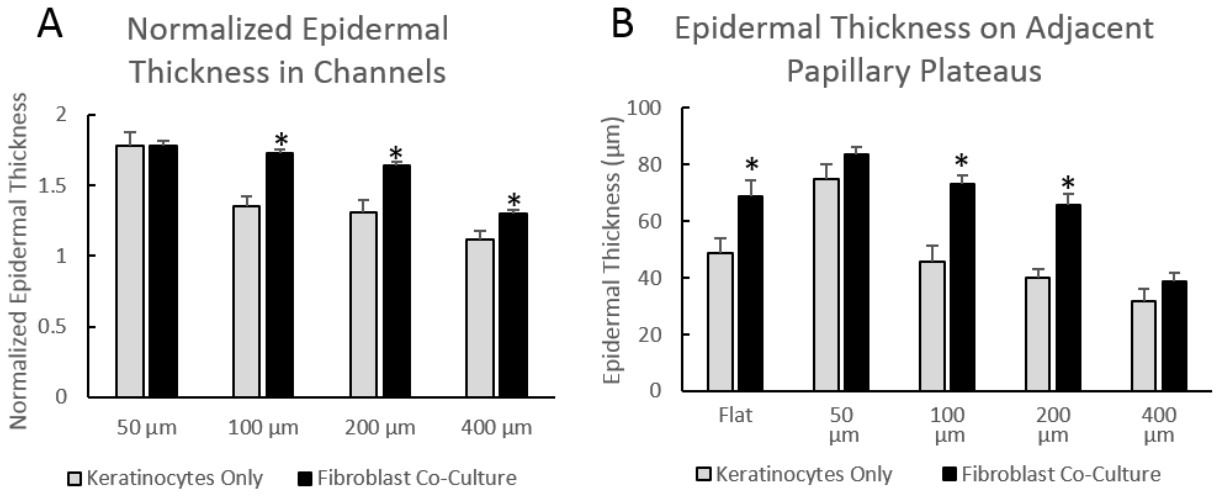

Figure 3.4 Epidermal thickness on µDERM cultured with and without fibroblast. Epidermal thickness is increased on µDERM containing fibroblasts. Normalized epidermal thickness (A) is increased by the inclusion of fibroblasts in 100, 200 and 400 µm channels. Epidermal thickness on papillary plateaus (B) is increased on flat controls, 100 and 200 µm channels in the presence of fibroblasts. *Indicates statistically significant difference from keratinocyte only culture of the same geometry ($p<0.05$ using students T-Test)

Additionally, we compared the epidermal thickness on papillary plateaus (both flat regions and regions adjacent to channel geometries) on μDERMs lacking fibroblasts to matching regions on μDERMs containing fibroblasts (Figure 3.4B). Again, epidermal thickness was increased on μDERM containing fibroblasts compared to μDERM cultured with keratinocytes only. This trend was more pronounced on flat regions and in 100 and 200 μm channels where epidermal thickness on papillary plateaus (Figure 3.4B) increased by 41%, 60% and 22% respectively. In addition to comparing between matched geometries, a 2-way ANOVA on RANKS was performed to determine if the effect of fibroblast inclusion was dependent on channel dimension. We found that there was not a statistically significant interaction between the effects of geometry and fibroblast inclusion (P=0.124). This suggests that the inclusion of fibroblasts increases epidermal thickness independent of substrate geometry.

3.3.3 Fibroblasts Secrete KGF in Cultured μDERM

To assess the role of paracrine signaling in epidermal morphogenesis on μDERM containing fibroblasts, we analyzed histological sections for KGF (FGF-7) using immunohistochemistry (Figure 3.5 A-F). We observed increased KGF signal in the collagen gel layer of μDERMs containing fibroblasts compared to μDERMs cultured with keratinocytes only. This is especially apparent when images are thresholded and color mapped to indicate regions of increased KGF expression (Figure 3.5 G-L). Interestingly, there was no apparent difference in the level of KGF staining in the collagen-GAG sponges of μDERMs cultured with and without fibroblasts (high magnification of collagen-GAG sponges shown in Figure 3.6). Additionally, we observed positive KGF expression in the keratinocyte layer which may indicate non-specific primary antibody binding.

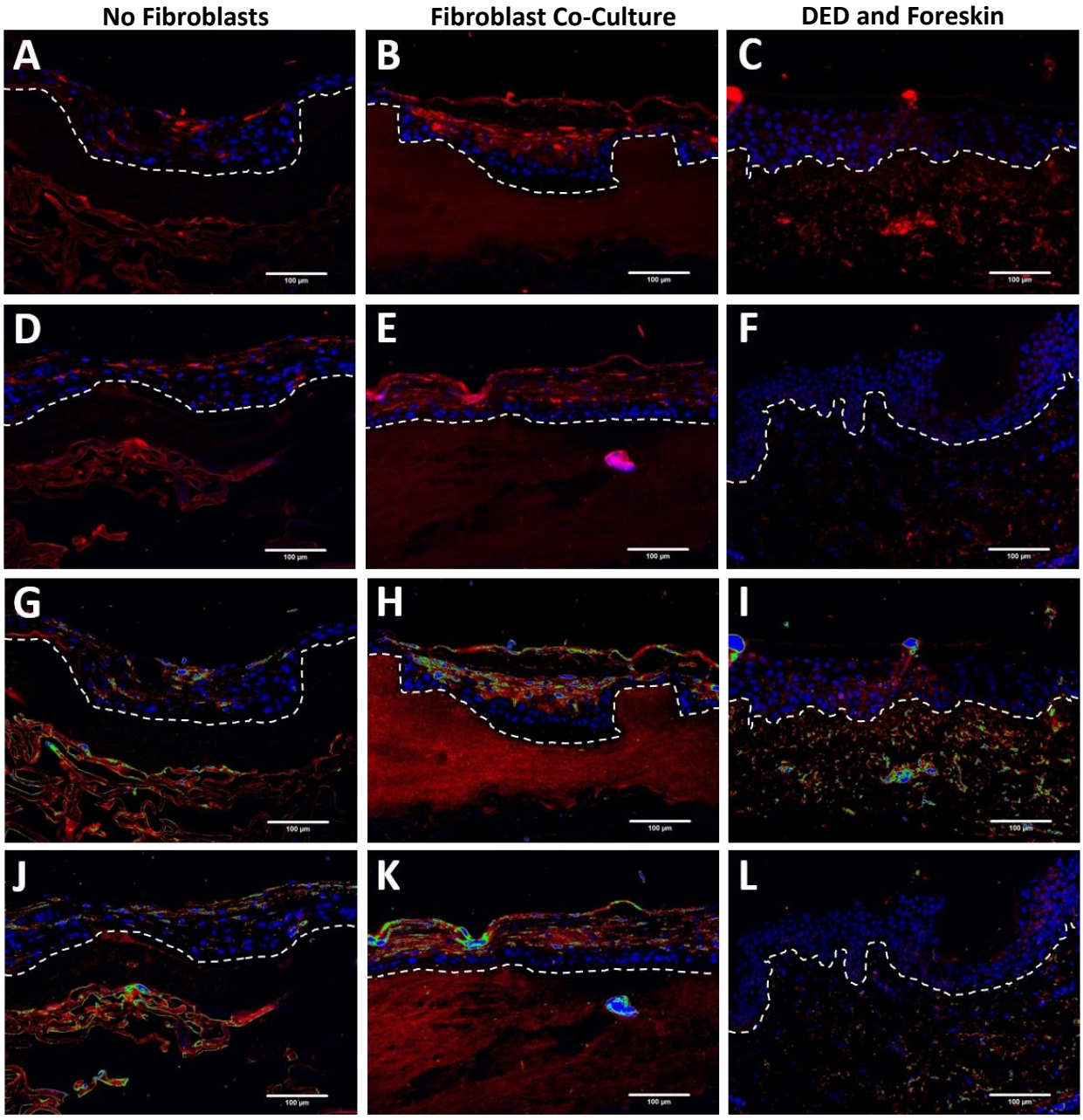

Figure 3.5 KGF Expression in µDERM with and without Fibroblasts. Representative images of KGF expression (Alexafluor568) on cultured µDERMs cultured with keratinocytes only (A,D, G, J) or with both keratinocytes and fibroblasts (B,E, H, K) and on DED (C, I) and native foreskin tissue (F,L). Original images (A-F). LUT false colorization of KGF expression (G-L); blue = highest 1/3 KGF expression, green = mid 1/3 KGF expression, red = lowest 1/3 KGF expression. Dotted line indicates DEJ boundary between the collagen gel and the keratinocyte layer. Note that due to variation in the collagen gel thickness, the dermal sponge is not visible in all panels. Scale bar = 100 µm

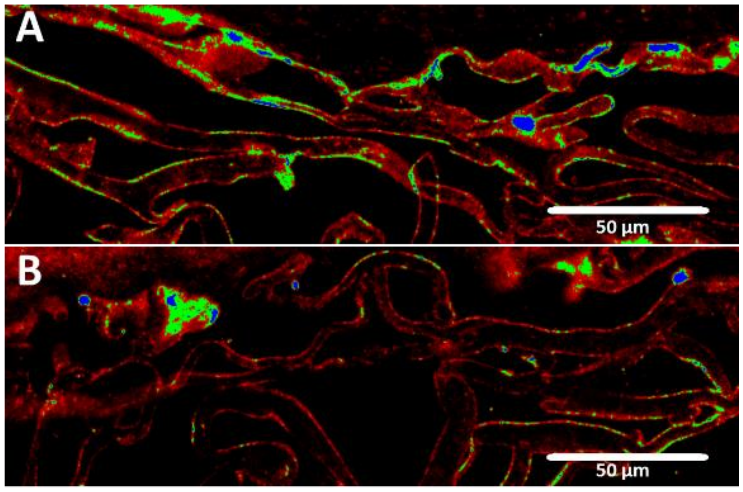

Figure 3.6 KGF Expression in dermal collagen-GAG sponge of cultured µDERM.
KGF staining is present in the dermal sponge of µDERMs cultured with and without fibroblasts. False LUT colorization of KGF expression in sponges of µDERM lacking fibroblasts (A) and containing fibroblasts (B). blue = highest 1/3 KGF expression, green = mid 1/3 KGF expression, red = lowest 1/3 KGF expression. Scale bar = 50µm

3.4 Discussion

By incorporating fibroblasts into the dermal layer of our µDERM model, we have increased epidermal thickness and enhanced overall epidermal morphology. We observed a more robust epidermal layer on µDERMs co-cultured with fibroblasts were compared to µDERMs cultured without fibroblast. Significantly, µDERMs containing fibroblasts exhibited a defined granular layer absent in keratinocyte only cultures, consistent with previous findings that fibroblasts stimulate keratinocyte proliferation and differentiation within the stratum granulosum (El-Ghalbzouri, Gibbs, Lamme, Van Blitterswijk and Ponec, 2002; El Ghalbzouri, Hensbergen, Gibbs, Kempenaar, van der Schors and Ponec, 2004; El Ghalbzouri, Lamme and Ponec, 2002; Smola, Thiekotter and Fusenig, 1993). The stratum granulosum is necessary for full barrier function and for proper formation of the cornified layer.

We also observed better keratinocyte adhesion to the DEJ in µDERM containing fibroblasts. In grafts without fibroblasts, the basal cell layer is detached in several locations and the basal cells are larger and less tightly packed. The epidermal morphology of µDERM containing fibroblasts resembled that of keratinocytes cultured cells on DED. A key advantage of µDERMs compared to DED is that µDERMs lack the complex BM protein organization of native skin. This allows µDERMs to be used to assess basement membrane protein deposition, organization and resultant functional outcomes. Previous findings have demonstrated the importance of fibroblast-

keratinocyte paracrine signaling in BM protein synthesis and organization (El Ghalbzouri, Jonkman, Dijkman and Ponec, 2005; Marionnet, Pierrard, Vioux-Chagnoleau, Sok, Asselineau and Bernerd, 2006). We hypothesize that incorporating fibroblasts into µDERMs results in an increase in basement membrane protein deposition resulting in enhanced DEJ adhesion.

In addition to enhanced morphology, µDERMs containing fibroblasts supported the formation of a thicker epidermal layer after 7 days of A/L culture. This finding can be explained by the observation that the fibroblasts seeded into the dermal analog secret KGF, which is known to stimulate keratinocyte proliferation. Interestingly, KGF is also known to upregulate laminin-332 deposition (Maas-Szabowski *et al.*, 1999b). KGF-induced upregulation of laminin 332 deposition may explain the better formed basal layers observed in µDERMs with fibroblasts. Importantly, these findings validate the diffusion of soluble paracrine signals through the collagen sponge and micropatterned collagen gel matrix of µDERM. Interestingly, we observe low levels of KGF in µDERMs without fibroblasts. Although true keratinocyte monocultures will have no KGF expression, minor fibroblast contamination, common in primary keratinocyte cultures can mimic co-culture effect (Maas-Szabowski, Shimotoyodome and Fusenig, 1999a). In native skin, KGF expression is found exclusively in the dermis (Werner *et al.*, 1993). However, we note aberrant KGF expression in the epidermal layers of µDERM. Although this staining pattern may suggest non-specific antibody interactions, the increased KGF staining in conjunction with the increased epidermal thickness observed in µDERMs containing fibroblasts provide strong evidence for the existence of paracrine signaling cues in the µDERM co-culture. In future studies, KGF expression can be confirmed using a different primary antibody. We hypothesize that incorporation of these fibroblast signaling cues will support both proliferative and synthetic keratinocyte phenotypes within the µDERM model and we will investigate the role of topography in regulating these phenotypes in Chapter 4.

Interestingly, although there is not a statistically significant interaction between fibroblast incorporation and epidermal thickness as a function of µDERM geometry. The effect of fibroblast signaling on epidermal thickness appears to be more pronounced on flat µDERM and adjacent to

wider channels. In fact, no statistical difference in epidermal thickness was noted in or near 50µm channels. One explanation for this observation is that changes in epidermal thickness are modulated in part by a space filling mechanism. Previous studies in µDERM cultured without fibroblasts suggested that there was no statistically significant difference in the density of ki67+ keratinocytes in channels of different dimensions versus flats on µDERM cultured at the A/L interface for 7 days, despite the increase in epidermal thickness observed in narrower channels, providing evidence for a space filing mechanism in keratinocyte monocultures (Bush and Pins, 2012). It is believed that upon seeding the keratinocytes form a monolayer conforming to the topography of the micropattern. Since narrower wells have a smaller volume than wider wells, the initial number of cells/volume is increased in narrow channels. Therefore, if proliferation is unchanged, the keratinocytes in the narrow wells would require fewer doublings to fill the channels, resulting in a thicker epidermis. Since fibroblast signaling is essential for maintaining keratinocytes in a proliferative state (El-Ghalbzouri, Gibbs, Lamme, Van Blitterswijk and Ponec, 2002; El Ghalbzouri, Hensbergen, Gibbs, Kempenaar, van der Schors and Ponec, 2004; Maas-Szabowski, Shimotoyodome and Fusenig, 1999a; Werner, Krieg and Smola, 2007) and the absence of fibroblast signaling in the prior model may have resulted in an overall quiescent keratinocyte phenotype by the 7 day time point. When fibroblasts are incorporated, the proliferative state is maintained and the thickness of the epidermis is increased overall. However, in native skin the epidermal layer is not continuously thickening. Rather, it reaches a steady state where the cornified outer layers slough off as the basal layer continues to proliferate. This results in an epidermis with a consistent thickness. Following 7 days of A/L culture, epidermal thickness adjacent to 50µm channels approaches the epidermal thickness of native skin in µDERM cultured without fibroblasts. Since the epidermal stratification has already reached the critical thickness of native skin, the addition of fibroblasts does not affect epidermal thickness in these channels. In contrast, the epidermal thickness adjacent to 100µm, 200µm, and 400µm channels and on flats is significantly less than native skin, so the addition of fibroblasts to the dermal sponge leads to an increase in epidermal thickness due to the maintenance of proliferative phenotype. To further investigate the proposed space filling and proliferative mechanisms, we will investigate

the initial keratinocyte seeding pattern (Chapter 5) and the effect of topography on keratinocyte proliferation in µDERM containing fibroblasts (Chapter 4).

Although we have preliminarily demonstrated an increase in epidermal thickness and corresponding enhancement of epidermal morphology on µDERMs containing fibroblasts, previous studies have shown that there is a dose-dependent response to the inclusion of fibroblasts and that at high fibroblast densities keratinocytes do not differentiate appropriately (Erdag and Sheridan, 2004). Although our fibroblast density was selected based on those previous results, future studies performing a dose-response analysis would allow us to determine the optimal fibroblast density for our model system. Additionally, we have established that the dermal sponge analog can be used to facilitate a co-culture system that allows for paracrine signaling but prevents cell-cell contact.

In the future, we can also use this model to investigate keratinocyte responses to other mesenchymal cells such as BM-MSCs, dermal papillae cells or genetically modified fibroblasts. Additionally, by changing the cell source for the dermal sponge we can use the co-culture system to establish disease models. For example, co-culture with psoriatic fibroblasts has been shown to induce a hyperproliferative psoriatic phenotype in previously normal keratinocytes (Saiag *et al.*, 1985). Loading µDERMs with psoriatic fibroblasts would create an *in vitro* psoriasis model which we could use to better study the role in DEJ topography in regulating keratinocyte hyperproliferation in psoriasis.

Importantly, previous work shows an upregulation of KGF production by dermal fibroblasts following wound healing (Werner *et al.*, 1992). This increased KGF expression has been shown to promote re-epithelialization, enhance epidermal morphology, support angiogenesis and accelerate wound closure (Geer *et al.*, 2005; Peng *et al.*, 2011; Werner *et al.*, 1994b). Additionally, KGF production by dermal fibroblasts is reduced in diabetic wounds compared with normal wounds (Werner *et al.*, 1994a). Together these findings establish the importance of including fibroblast signaling in future µDERM wound healing and disease models. However, overexpression of KGF can result in keratinocyte hyperproliferation, dysregulation of epidermal

differentiation and dermal fibrosis (Andreadis *et al.*, 2001; Canady *et al.*, 2013). This further supports the importance of determining the optimal fibroblast seeding density for the µDERM co-culture model.

By incorporating fibroblasts into our µDERM model we have enhanced our *in vitro* model system to enable the evaluation of the effect of microtopography on cellular functions, such as keratinocyte proliferation and basement membrane protein synthesis, which require appropriate fibroblast signaling Fibroblast-keratinocyte signaling is essential for proper epidermal morphogenesis. By incorporating fibroblasts into the dermal collagen-GAG sponge analog of µDERMs, we created a more complete organotypic model of skin. Critically, we are minimizing potential changes in keratinocyte phenotype upon removal from the J2 co-culture method used for *in vitro* expansion and maintenance. Ultimately, this model system provides a more physiologic model to study the effect of microtopography on epidermal morphology and keratinocyte function. In Chapter 4 of this thesis, we will use this new model to investigate the effect of microtopography on keratinocyte function in the presence of fibroblast paracrine signals.

3.5 Acknowledgments

This research was funded by the NIH (EB-005645). Special thanks to Dr. Mehmet Toner and Octavio Hurtado at the BioMicroElectroMechanical Systems (BioMEMS) Resource Center, Massachusetts General Hospital, Boston, MA (NIH Grant: P41 EB02503 [MT]), for their assistance with the microfabrication processes. I would like to thank my advisor, Professor George Pins, for his scientific contribution to the work. I would also like to thank Jen Molignano and Tom Moutinho for technical assistance, the Department of Obstetrics and Gynecology at UMMS (Worcester, MA) for providing us with neonatal foreskins for keratinocyte isolations and Russell Kronengold, Ph.D., at the Kensey Nash Corporation (Exton, PA), for his generous donations of SEMED-S collagen.

3.6 References

Andreadis ST, Hamoen KE, Yarmush ML and Morgan JR (2001) Keratinocyte Growth Factor Induces Hyperproliferation and Delays Differentiation in a Skin Equivalent Model System. *FASEB* 15:898-906.

Barreca A, De Luca M, Del Monte P, Bondanza S, Damonte G, Cariola G, Di Marco E, Giordano G, Cancedda R and Minuto F (1992) In Vitro Paracrine Regulation of Human Keratinocyte Growth by Fibroblast-Derived Insulin-Like Growth Factors. *J Cell Physiol* 151:262-8.

Bush K and Pins G (2012) Development of Microfabricated Dermal Epidermal Regenerative Matrices to Evaluate the Role of Cellular Microenvironments on Epidermal Morphogenesis. *Tissue Eng Part A* 18:2343-53.

Bush KA, Downing BR, Walsh SE and Pins GD (2007) Conjugation of Extracellular Matrix Proteins to Basal Lamina Analogs Enhances Keratinocyte Attachment. *J Biomed Mater Res A* 80:444-52.

Canady J, Arndt S, Karrer S and Bosserhoff AK (2013) Increased Kgf Expression Promotes Fibroblast Activation in a Double Paracrine Manner Resulting in Cutaneous Fibrosis. *J Invest Dermatol* 133:647-57.

Cornwell KG, Downing BR and Pins GD (2004) Characterizing Fibroblast Migration on Discrete Collagen Threads for Applications in Tissue Regeneration. *J Biomed Mater Res A* 71:55-62.

Downing BR, Cornwell K, Toner M and Pins GD (2005) The Influence of Microtextured Basal Lamina Analog Topography on Keratinocyte Function and Epidermal Organization. *J Biomed Mater Res A* 72:47-56.

El-Ghalbzouri A, Gibbs S, Lamme E, Van Blitterswijk CA and Ponec M (2002) Effect of Fibroblasts on Epidermal Regeneration. *Br J Dermatol* 147:230-43.

El Ghalbzouri A, Hensbergen P, Gibbs S, Kempenaar J, van der Schors R and Ponec M (2004) Fibroblasts Facilitate Re-Epithelialization in Wounded Human Skin Equivalents. *Lab Invest* 84:102-12.

El Ghalbzouri A, Jonkman MF, Dijkman R and Ponec M (2005) Basement Membrane Reconstruction in Human Skin Equivalents Is Regulated by Fibroblasts and/or Exogenously Activated Keratinocytes. *J Invest Dermatol* 124:79-86.

El Ghalbzouri A, Lamme E and Ponec M (2002) Crucial Role of Fibroblasts in Regulating Epidermal Morphogenesis. *Cell Tissue Res* 310:189-99.

Elsdale T and Bard J (1972) Collagen Substrata for Studies on Cell Behavior. *J Cell Biol* 54:626-37.

Erdag G and Sheridan RL (2004) Fibroblasts Improve Performance of Cultured Composite Skin Substitutes on Athymic Mice. *Burns* 30:322-8.

Geer DJ, Swartz DD and Andreadis ST (2005) Biomimetic Delivery of Keratinocyte Growth Factor Upon Cellular Demand for Accelerated Wound Healing in Vitro and in Vivo. *Am J Pathol* 167:1575-86.

Krejci NC, Cuono CB, Langdon RC and McGuire J (1991) In Vitro Reconstitution of Skin: Fibroblasts Facilitate Keratinocyte Growth and Differentiation on Acellular Reticular Dermis. *J Invest Dermatol* 97:843-8.

Maas-Szabowski N, Shimotoyodome A and Fusenig NE (1999a) Keratinocyte Growth Regulation in Fibroblast Cocultures Via a Double Paracrine Mechanism. *J Cell Sci* 112 (Pt 12):1843-53.

Maas-Szabowski N, Shimotoyodome A and Fusenig NE (1999b) Keratinocyte Growth Regulation in Fibroblast Cocultures Via a Double Paracrine Mechanism. *J Cell Sci* 112 (Pt 12):1843-53.

Marionnet C, Pierrard C, Vioux-Chagnoleau C, Sok J, Asselineau D and Bernerd F (2006) Interactions between Fibroblasts and Keratinocytes in Morphogenesis of Dermal Epidermal Junction in a Model of Reconstructed Skin. *J Invest Dermatol* 126:971-9.

Peng C, He Q and Luo C (2011) Lack of Keratinocyte Growth Factor Retards Angiogenesis in Cutaneous Wounds. *J Int Med Res* 39:416-23.

Saiag P, Coulomb B, Lebreton C, Bell E and Dubertret L (1985) Psoriatic Fibroblasts Induce Hyperproliferation of Normal Keratinocytes in a Skin Equivalent Model in Vitro. *Science* 230:669-72.

Smola H, Thiekotter G and Fusenig NE (1993) Mutual Induction of Growth Factor Gene Expression by Epidermal-Dermal Cell Interaction. *J Cell Biol* 122:417-29.

Szabowski A, Maas-Szabowski N, Andrecht S, Kolbus A, Schorpp-Kistner M, Fusenig NE and Angel P (2000) C-Jun and Junb Antagonistically Control Cytokine-Regulated Mesenchymal-Epidermal Interaction in Skin. *Cell* 103:745-55.

Werner S, Breeden M, Hubner G, Greenhalgh DG and Longaker MT (1994a) Induction of Keratinocyte Growth Factor Expression Is Reduced and Delayed During Wound Healing in the Genetically Diabetic Mouse. *J Invest Dermatol* 103:469-73.

Werner S, Krieg T and Smola H (2007) Keratinocyte-Fibroblast Interactions in Wound Healing. *J Invest Dermatol* 127:998-1008.

Werner S, Peters KG, Longaker MT, Fuller-Pace F, Banda MJ and Williams LT (1992) Large Induction of Keratinocyte Growth Factor Expression in the Dermis During Wound Healing. *Proc Natl Acad Sci U S A* 89:6896-900.

Werner S and Smola H (2001) Paracrine Regulation of Keratinocyte Proliferation and Differentiation. *Trends Cell Biol* 11:143-6.

Werner S, Smola H, Liao X, Longaker MT, Krieg T, Hofschneider PH and Williams LT (1994b) The Function of Kgf in Morphogenesis of Epithelium and Reepithelialization of Wounds. *Science* 266:819-22.

Werner S, Weinberg W, Liao X, Peters KG, Blessing M, Yuspa SH, Weiner RL and Williams LT (1993) Targeted Expression of a Dominant-Negative Fgf Receptor Mutant in the Epidermis of Transgenic Mice Reveals a Role of Fgf in Keratinocyte Organization and Differentiation. *The EMBO journal* 12:2635-43.

Wu Y, Chen L, Scott PG and Tredget EE (2007) Mesenchymal Stem Cells Enhance Wound Healing through Differentiation and Angiogenesis. *Stem Cells* 25:2648-59.

Wu Y, Zhao RC and Tredget EE (2010) Concise Review: Bone Marrow-Derived Stem/Progenitor Cells in Cutaneous Repair and Regeneration. *Stem Cells* 28:905-15.

Chapter 4: Microtopography Creates Distinct Keratinocyte Functional Niches and Enhances Epidermal Morphogenesis *In Vitro*

4.1 Introduction

Skin is a complex multilayered tissue that provides the primary barrier between the body and the environment. It serves as a dynamic and highly regulated selectively-permeable barrier which not only acts to prevent infection, but also to regulate tissue homeostasis (Rook and Burns, 2010). Following traumatic disruption of the skin, rapid restoration of the skin barrier is the first line of defense against infection and dehydration to ensure a positive clinical outcome (Macri and Clark, 2009). To better under the cellular mechanisms which direct these tissue responses, several groups have developed *in vitro* models of native skin (Bellas *et al.*, 2012; Gautrot *et al.*, 2012; Powell *et al.*, 2010). While these models elucidate mechanisms that guide epidermal regeneration, they are limited in their capacity to precisely analyze the key topographic and biochemical roles of keratinocyte microniches at the dermal-epidermal junction (DEJ) in directing critical wound healing processes. A common limitation of current tissue engineered skin substitutes, both those used clinically and for *in vitro* studies, is the absence of topography at the dermal-epidermal junction (DEJ).

In native skin, the topography of keratinocyte microniches at the DEJ plays a critical role in maintaining the structure and mechanical properties of the tissue, as well as in directing its regenerative potential (Jones *et al.*, 1995; Lavker and Sun, 1982, 1983). The DEJ is characterized by fingerlike dermal papillae (DP) and epidermal rete ridges that conform to the dermal topography. These features create microniches with dimensions ranging from 50-400 µm width and 50-200 µm depths (Fawcett and Jensh, 1997; Odland, 1950). This interdigitated topography increases the surface area between the dermis and the epidermis, enhancing both the mechanical shear resistance of the skin and the paracrine diffusion between layers. Additionally, microtopographic niches create distinct cellular microenvironments that differentially direct keratinocyte phenotype and cellular function. For example, multiple labs demonstrated that

keratinocyte stem cells preferentially locate to the tips of the DP or the bases of the rete ridges, depending on their anatomical location (Lane *et al.*, 2014; Lavker and Sun, 1982, 1983; Watt, 1998, 2001, 2002; Watt and Huck, 2013). Interestingly, changes in DEJ topography are noted in skin diseases such as psoriasis (lengthening of rete ridges) and in aged skin (flattening of the DEJ), further suggesting an important role for topography in epidermal function (Liao *et al.*, 2013; Montagna and Carlisle, 1979; Murphy *et al.*, 2007). To further investigate the roles of 3D microniches on keratinocyte functions, several groups developed *in vitro* models to characterize the effects of cell geometries and surface chemistries on keratinocyte function (Charest *et al.*, 2009; Gilbert and Blau, 2011; Gobaa *et al.*, 2011; Trappmann *et al.*, 2012). However, a greater understanding of how 3D topographic, biochemical and cellular cues direct keratinocyte proliferation and cellular function will further our understanding of epidermal morphogenesis and skin wound healing and will allow us to harness these cues to develop the next generation skin substitutes.

Keratinocyte stem cells remain a controversial area of research with ongoing debate surrounding epidermal stem cell models as well as specific locations and appropriate markers for epidermal stem cells. Some of this confusion originates from the heterogeneous nature of the epidermal stem cell population. The epidermis contains several distinct stem cell populations, including interfollicular epidermal (IFE) stem cells, hair follicle stem cells and sebaceous gland stem cells, which support epidermal maintenance and tissue regeneration (Pincelli and Marconi, 2013). These physical microniches contain several distinct keratinocyte sub-populations located throughout the epidermis, including both keratinocyte stem cells and terminally committed keratinocytes. In particular, evidence suggests that basal keratinocytes, once considered a homogenous population, represent a heterogeneous cell reservoir. Studies of native skin demonstrated clustering of phenotypically similar keratinocytes. Lavker and Sun suggested the existence of two spatially segregated keratinocyte subpopulation: nonserrated, slow-cycling keratinocytes located at the base of deep rete ridges and serrated keratinocytes located in shallow rete ridges (Lavker and Sun, 1982, 1983). Later, Watt *et al.* examined stem cell patterning in the IFE epidermis by correlating the regional variation in integrin expression levels in human

skin with the colony forming efficiency of keratinocytes (Jones, Harper and Watt, 1995; Watt, 1998, 2001, 2002). Additionally, a recent study of keratinocytes seeded on a microfabricated dermal papilla template showed differential gene expression on micropatterned membranes compared to flat controls (Lammers *et al.*, 2012). Given the continued lack of knowledge regarding the role of microtopography in directing cellular phenotype, function and fate, we suggest that the topography of the dermal-epidermal junction is largely responsible for driving the clustering of these keratinocyte sub-populations and hypothesize that topographical cues can be used to direct keratinocyte phenotype and create stem cell reservoirs. Further, we propose that μDERMs provide a novel platform for systematically investigating the roles of microtopography on cellular function as well as diverse keratinocyte stem cell niches.

In this chapter, we investigated the influence of cellular microniche topography on keratinocyte function. We recently described a method to create micropatterned dermal-epidermal regeneration matrices (μDERMs) that facilitate the investigation of cellular responses to microtopographies (Bush and Pins, 2012). In **Chapter 3: Fibroblasts Enhance the Epidermal Morphology of Cultured μDERM**, we integrated fibroblast paracrine signaling into our model system. In this chapter we have specifically probed the formation of distinct proliferative and synthetic niches within micropatterned keratinocyte microniches. We demonstrated that keratinocytes in narrower channels exhibit a more proliferative phenotype, while keratinocytes in wider channels exhibit enhanced synthesis of the basement membrane (BM) protein laminin-332. Additionally, keratinocytes exhibiting the putative stem cell markers β_1 integrin and p63 preferentially localized to the base of narrow channels and the corners of wider channels. This novel approach to creating 3D model systems with topographical cues that mimic native cellular compartments at the DEJ will enable systematic investigation of the biophysical and biochemical cues that direct cutaneous tissue morphogenesis, epidermal pathologies.

4.2 Materials and Methods

4.2.1 Cell Culture and Media Formulations

Neonatal primary human foreskin keratinocytes (NHKs) and primary human foreskin fibroblasts (NHFs) were isolated from foreskins, obtained as non-identifiable discard tissue from the University of Massachusetts Memorial Medical Center (Worcester, MA), and were approved with exempt status from the New England Institutional Review Board, using previously described methods. Prior to seeding on µDERMs, keratinocytes were cultured on a feeder layer of mitomycin C treated J2s (generously donated by Dr. Stelios Andreadis, State University of New York at Buffalo, Buffalo, NY). NHF medium consisted of Dulbecco's modified Eagle's medium (DMEM) with 10% fetal bovine serum (FBS) and 1% penicillin-streptomycin. HKF medium was comprised of a 3:1 blend of high glucose DMEM and Ham's F12 with 10% fetal bovine serum and 1% penicillin-streptomycin supplemented with adenine (1.8×10^{-14} M), cholera toxin (10^{-10} M), hydrocortisone (0.4 µg/ml), insulin (5 µg/ml), transferring (5 µg/ml), and triiodo-L-thyronine (2×10^{-9} M). After initial NHK plating, medium was replaced with NHK medium containing 10 ng/ml epidermal growth factor (EGF). Seeding medium for µDERM culture consisted of a 3:1 blend of high glucose DMEM and Ham's F12 with 1% fetal bovine serum and 1% penicillin-streptomycin supplemented with cholera toxin (10^{-10} M), hydrocortisone (0.2 µg/ml), insulin (5 µg/ml) and ascorbic acid (50 µg/ml). Priming medium consisted of seeding medium supplemented with 24 µM BSA, 25 µM oleic acid, 15 µM linoleic acid, 7 µM arachidonic acid, 25 µM palmitic acid, 10 µM L-carnitine, and 10 mM L-serine) . Air-liquid interface (A/L) medium was serum-free priming medium supplemented with 1 ng/ml EGF.

4.2.2 *In vitro* µDERM Culture Model

4.2.2.1 µDERM Specifications

The microtopographic features of our µDERMs were designed specifically to enable concurrent histological evaluation of multiple geometries on a single construct, to minimize experimental variations and analysis time. Specifically, 1.25 cm x 2.0 cm patterns were designed with 3 series of parallel channels 200 µm deep, 2500 µm long and with variable widths (50µm, 100µm, 200µm

or 400µm). For histological analysis, µDERMs were sectioned perpendicular to the channels to provide multichannel analysis on each section.

4.2.2.2 µDERM Fabrication

As described in Chapter 3, we incorporated fibroblasts into our previously published µDERM model (Bush and Pins, 2012). Specifically, a pattern was designed with a series of 200µm deep channels with varying widths (50µm, 100µm, 200µm, 400µm) (Bush and Pins, 2012; Downing *et al.*, 2005). Type I acid-soluble collagen (10 mg/ml in 5 mM HCl) was purified from rat tail tendons (Cornwell *et al.*, 2004; Elsdale and Bard, 1972) and 0.3 ml of this collagen solution was self-assembled on the micropatterned molds using 5x DMEM (Invitrogen) with 0.22 M $NaHCO_3$ and 0.1 M NaOH (Sigma) for 18 hours at 37˚C and 10% CO_2. To construct a dermal analog, following polymerization a collagen-GAG sponge was laminated to the back of the micropatterned gel using an additional 0.3 ml of self-assembled collagen and then crosslinked with EDC. µDERMs were then removed from the PDMS patterns and conjugated with fibronectin (FN). µDERMs were sterilized in an antibiotic cocktail (100 IU/ml-100µg/ml penicillin-streptomycin, 2.5µg/ml amphotericin B, 10pg/ml ciprofloxacin, 100µg/ml gentamycin) for a minimum of 24 hours at room temperature and rinsed with DMEM.

4.2.2.3 Cell Seeding and in vitro Culture of µDERMs

For cell seeding, µDERMs were placed on custom-designed cell seeding screens (Figure 3.1 K,L). Medical grade 316 stainless steel screens were embedded in PDMS platforms, leaving the center of the screen open. These PDMS platforms elevated the screens to allow for culture at the air-liquid interface. Initially, $8x10^4$ NHFs/cm^2 in 100µl of NHF medium were seeded on the dermal side of the scaffold and incubated for 2 hours. Following incubation, additional fibroblast medium was added, and µDERMs were cultured for 48 hours (37˚C, 10%CO_2) with daily medium changes (Figure 3.1). µDERMs were inverted onto A/L screens, NHKs were seeded on the micropatterned side at a density of $5x10^5$ cells/cm^2 in 100µl seeding medium for 2 hours then µDERMs were submerged in seeding medium (Figure 3.1I). As a control, de-epidermized dermis (DED) was seeded with keratinocytes and cultured alongside µDERMs, as previously described (Bush and Pins, 2012). After 24 hours, seeding medium was replaced with priming medium for 48 hours.

Finally, priming medium was replaced with A/L interface medium and µDERMs were cultured for 3 or 7 days at the A/L interface (Figure 3.1 M).

4.2.3 Quantitative Morphometric Evaluation of Cultured µDERMs

µDERMs were fixed in neutral buffered formalin, embedded in Paraplast (McCormick Scientific) and sectioned perpendicular to the microchannel topography. Slides were stained with hematoxylin and eosin (Richard Allen Scientific). Channel depth, channel width, epidermal thickness in the channel and epidermal thickness on the neighboring plateaus were measured for each channel using Spot software (Figure 3.2A). For each well, channel depth and epidermal thickness were measured in 3 locations (center and each side) and then averaged to determine channel depth and epidermal thickness. Channel width was measured in 3 places (bottom, top and center) and then averaged to determine channel width. To account for variations in µDERM dimensions, the average epidermal thickness was normalized to the average channel depth of the corresponding well. Plateau thickness was measured immediately adjacent to either side of each channel and then averaged to determine the adjacent plateau thickness (Figure 3.2B). Each µDERM section contained up to 4 replicates of each channel geometry. For each geometry, channels were analyzed on at least 3 separate µDERMs. Sample sizes for normalized epidermal thickness measurements were n=7, 9, 14 and 15, for 3 days of culture (50µm, 100µm, 200µm and 400µm channel widths, respectively); n= 19, 19, 19, and 21, for 7 days of culture with fibroblasts (50µm, 100µm, 200µm and 400µm channel widths, respectively); and n = 4, 5, 3, and 8, for 7 days of culture without fibroblasts (50µm, 100µm, 200µm and 400µm channel widths, respectively). Sample sizes for plateau thickness measurements were n=21, 14, 18, 28, 30, for 3 days of culture (flats, 50µm, 100µm, 200µm and 400µm channel widths, respectively); n= 21, 40, 38, 38, 40, for 7 days of culture with fibroblasts (flats, 50µm, 100µm, 200µm and 400µm channel widths, respectively);and n = 9, 6, 10, 6, 16, for 7 days of culture without fibroblasts (flats, 50µm, 100µm, 200µm and 400µm channel widths, respectively). Epidermal thickness of DED and native foreskin tissue was also measured. Finally, individual channels with mean geometries that deviated from the population mean values by more than two standard deviations were excluded from analysis.

4.2.4 Immunohistochemistry (IHC)

To further evaluate the similarities between our 3D scaffolds and the experimental controls, immunohistochemical analysis was performed on 7 day cultures of μDERMs containing fibroblasts.

4.2.4.1 Laminin-332 Immunohistochemistry

Laminin-332 was detected by staining for the laminin γ_2 chain, using methods based on those described previously (Lu *et al.*, 2001; Zapatka *et al.*, 2007). Briefly, following antigen retrieval (Protease XXIV, 15 minutes) and blocking (5% skim milk in PBS, 10 minutes) sections were incubated with laminin γ_2 antibody diluted (1:200 in blocking solution; D4B5, Millipore) overnight at 4˚C. Subsequently, sections were incubated with AlexaFluor546 secondary goat-anti-mouse antibody (Invitrogen). Nuclei were then stained with Hoechst 33342 (33.3 μg/ml) for 15 minutes. Negative control samples were incubated with blocking buffer, in lieu of primary antibody.

4.2.4.2 Ki67, β_1 integrin and p63 Immunohistochemistry

Antigen retrieval for ki67, β_1 integrin and p63 IHC was performed by boiling paraffin section on slides in a citrate buffer as previously described (Bush and Pins, 2012). Sections were blocked in 10% horse serum for 10 minutes and then incubated with either mouse-antihuman CD29 antibody (β_1 integrin; BioGenex) and rabbit-antihuman p63 antibody (H-137, Santa Cruz) overnight at 4˚C or with prediluted mouse-antihuman Ki67 antibody (Zymed) overnight at room temperature. Subsequently, sections were incubated with both AlexaFluor546 (Invitrogen) secondary goat-anti-mouse antibody and AlexaFluor 488 (Invitrogen) secondary donkey-anti-rabbit antibody (β_1 integrin and p63) or with AlexaFluor 546 alone (ki67). Nuclei were then stained with Hoechst 33342 (33.3 μg/ml) for 15 minutes. Negative control samples were incubated with blocking buffer, in lieu of primary antibody. Foreskin tissue was used as a positive immunohistochemistry control.

4.2.4.3 Involucrin Immunohistochemistry

Involucrin expression was assessed to measure keratinocyte commitment to terminal differentiation. Following deparaffinization and rehydration through xylene and graded alcohols,

antigen retrieval was performed by incubation with 37 C 0.1% trypsin for 5 minutes. Slides were then blocked in 10% normal horse serum for 1 hour at room temperature. Sections were incubated with mouse-anti-human involucrin primary antibody diluted in blocking serum (1:8000, Sigma-Aldrich, St. Louis, MO) for 1 hour at 37 C, rinsed with PBS, and incubated with AlexaFluor546 goat anti-mouse secondary antibody (Invitrogen). Nuclei were then stained with Hoechst 33342 (33.3 μg/ml) for 15 minutes. Negative control samples were incubated with blocking serum without primary antibody. Finally, the thickness of the involucrin positive layer was measured using imageJ.

4.2.5 Statistical Analysis

Statistical differences were evaluated using SigmaPlot Version 11.0 (Systat Software, Inc.). 1-Way Analysis of Variance (ANOVA) and 2-Way ANOVA were performed to determine statistical differences, as indicated. For comparisons between groups, Holm-Sidak post-hoc analysis was performed. For keratinocyte proliferation studies, Dunnett's method was used for post-hoc analysis to compare μDERM conditions to foreskin controls. For all comparisons, a significant difference between groups was indicated by a p value < 0.05.

4.3 Results

4.3.1 Morphological Assessment of Cultured μDERMs

Our fabrication process (Figure 3.1) yielded a μDERM with a collagen gel matrix ranging in average thickness from 87 μm (beneath channels) to 186 μm (plateaus) and collagen dermal sponges 336 μm thick. The average thickness of the flat collagen gel matrix was 129 μm.

4.3.2 Microtopography Enhances Epidermal Morphology

Keratinocyte stratification in channels (50μm, 100μm, 200μm and 400μm in width; 200 μm in depth) and flat regions of μDERMs containing fibroblasts was evaluated following 3 and 7 days of culture at the air-liquid interface (A/L) (Figure 4.1, Columns 1 and 2). In μDERMs containing fibroblasts, scaffolds contain distinctly stratified epidermal morphology, which closely

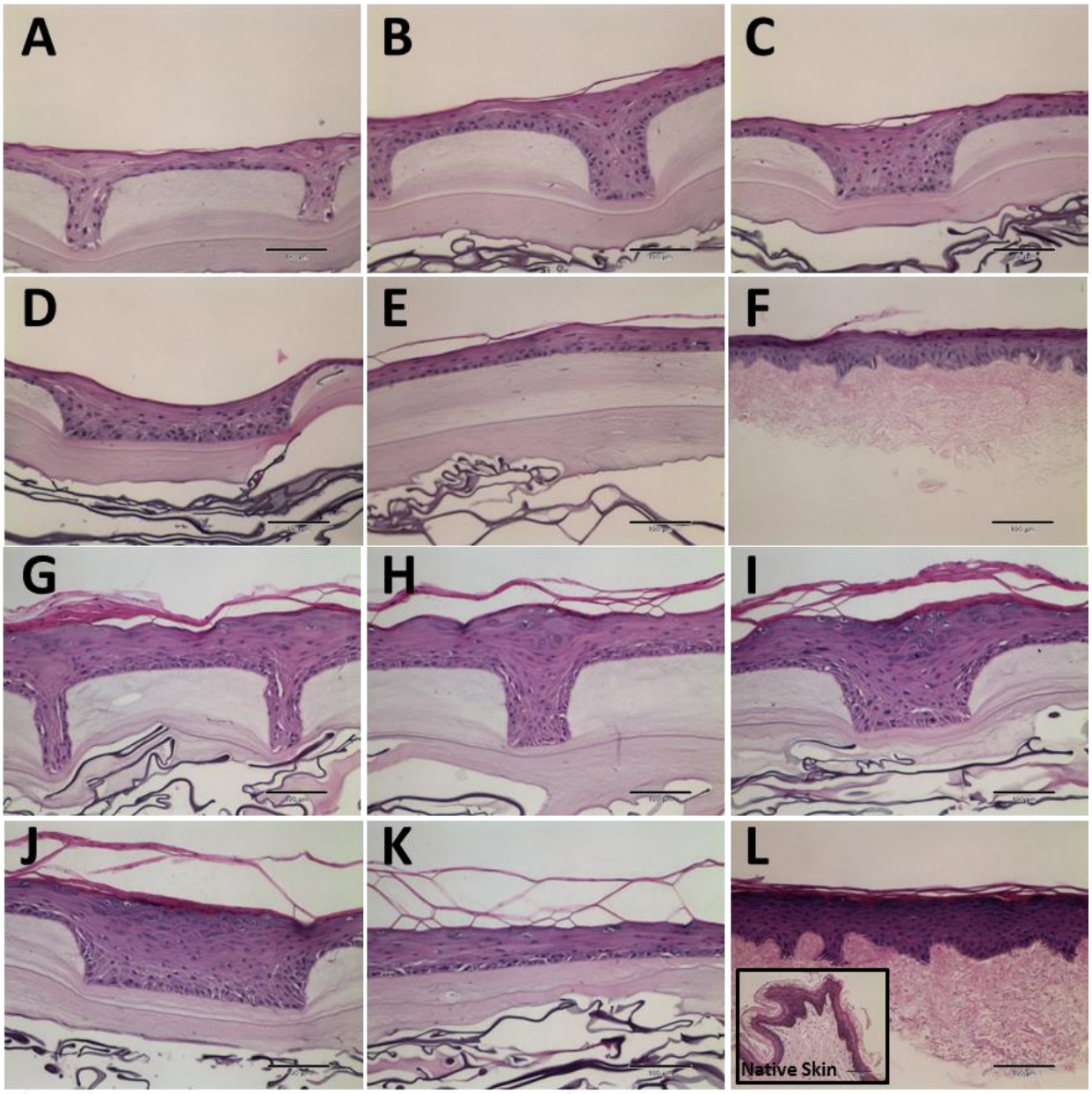

Figure 4.1 Morphology of cultured µDERMs at 3 and 7 days. Hematoxylin and eosin stain of µDERMs cultured for 3 days (A-E) and 7 days (G-K) containing 50µm (A,G), 100µm (B,H), 200µm(C,I), or 400µ(D,J) channels or flat control regions(E,K). Keratinocytes cultured on µDERM form a stratified epidermis that resembles keratinocytes seeded on DED for 3 days (F) and 7 days (L),. Notably, keratinocytes cultured on flats stratify, but lack a defined stratum granulosum present in microtopographies. Additionally, epidermal thickness is increased by channel topographies. In contrast, Scale bar = 100µm.

recapitulates the morphologies observed on neonatal foreskin tissue controls and keratinocyte-seeded, DED scaffold controls (Figure 4.1, row 6).

In µDERMs with channels, four distinct, stratified keratinocyte layers can be observed in the epidermal layer by 7 days of A/L culture. We also observed an increase in stratification in regions of the graft containing topographic features (50µm, 100µm, 200µm, and 400µm channels) compared to in flat regions (Figure 4.1M, O). These regions of the grafts exhibit pronounced stratum granulosum layers comparable to native skin tissue (Figure 4.1R), regardless of channel dimension. In contrast, intermediate stratum granulosum and spinosum layers are not readily distinguished in comparable flat regions of control grafts. At 3 days, epidermal stratification is limited to the stratum corneum and a partially organized basal layer.

4.3.3 Epidermal Thickness is Increased In and Near Narrow Microniches

4.3.3.1 Quantitative Morphometric Analysis of Normalized Epidermal Thickness

To further characterize the effects of microtopography, we quantitatively assessed the thickness of the cultured epidermis in different microniche dimensions (Figure 4.2 A, B). Overall, normalized epidermal thickness is increased in narrow (50µm and 100µm) channels compared to wide (200µm and 400µm channels). At 3 days, the normalized epidermal thickness in 50µm and 100µm channels is statistically increased compared to wider 200µm and 400µm channels ($p<0.05$, Figure 3C). This result persists at 7 days.

Consistent with the enhanced epidermal morphology noted in histological evaluations, epidermal thickness increased significantly between 3 and 7 days ($p<0.05$, Figure 3A, C). This trend of increased epidermal thickness was most pronounced in the 200µm and 400µm channels where thickness was increased by 35% and 65% respectively between 3 and 7 days. Epidermal thickness on plateaus was also thicker at 7 days ($p<0.05$, Figure 3D). Interestingly, in 400µm channels, epidermal thickness at 3 days does not exceed channel depth (normalized thickness < 1) (Figure 4.2B), resulting in an invagination on the surface of the stratum corneum (Figure 4.1J). By 7 days, epidermal thickness exceeded channel depth for all dimensions, including 400µm channels and surface depressions are not readily apparent.

4.3.1.2 Quantitative Morphometric Analysis of Epidermal Thickness on Plateaus in Proximity to Channels

We observed that the increased epidermal thickness on µDERMs containing narrow channels was not limited to the channel itself but appeared to extend to the immediately adjacent shoulder regions. To evaluate this, we compared the thickness of the epidermis on flat plateaus immediately adjacent to microchannels (Figure 4.2B) to the thickness on control flat regions. Again, epidermal thickness increased significantly between 3 and 7 days of A/L culture, independent of topography ($p<0.05$). Interestingly, the presence of microtopography affected epidermal thickness on adjacent plateaus compared to control flat regions. When compared to flat regions, epidermal thickness was increased in regions adjacent to narrow channels and decreased in regions adjacent to wide channels (Figure 4.1 and Figure 4.2B). After 3 days in culture, epidermal thickness near 100µm channels and was significantly greater than the epidermal thickness on flat controls and on plateaus in proximity to all other channel dimensions.

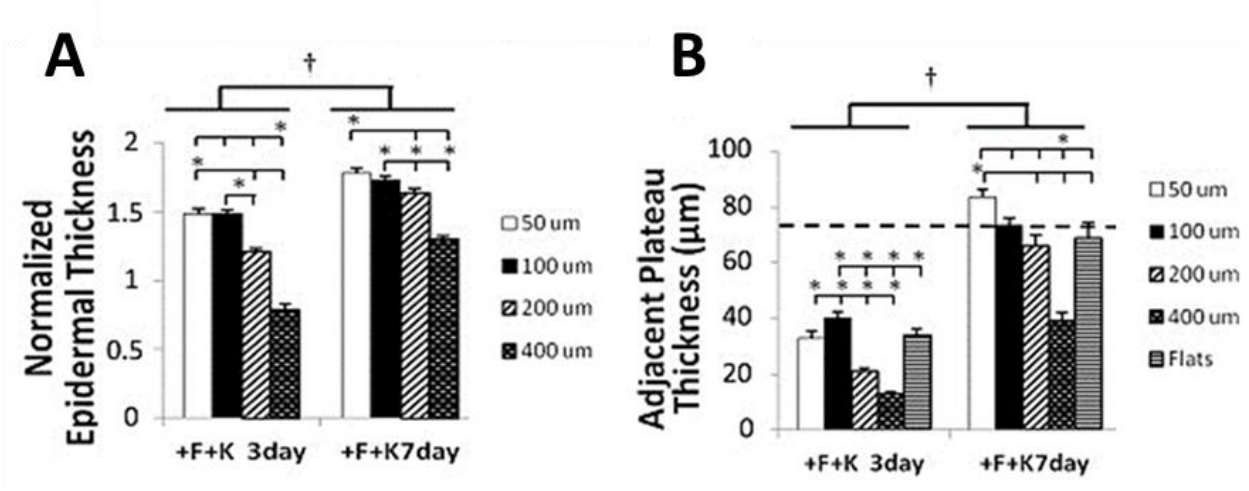

Figure 4.2 Quantitative morphometric analysis of epidermal thickness on cultured µDERMs. Normalized epidermal thickness increased from days 3 to 7, independent of topography (A). Additionally, normalized epidermal thickness in narrow channels is statistically increased compared to wider channels cultured under the same conditions. Plateau thickness was measured immediately adjacent to each channel topography and in the center of control flats. Plateau thickness increased adjacent to narrow channels and decreased adjacent to wide channels relative to flats (B). Data presented as mean±SEM. †indicates statistical difference between groups, $p<0.05$. * indicates statistical difference between indicated channel dimensions, $p<0.05$.

In contrast, epidermal thicknesses for proximal plateaus of wider 200µm and 400µm channels were decreased compared to flats; epidermal thickness adjacent to 400µm channels also decreased compared to 200µm channels. The results at 7 days were similar. Specifically,

epidermal thickness on plateaus adjacent to 50µm channels was increased significantly compared to flat regions and plateaus adjacent to 200µm and 400µm channels, while epidermal thickness on proximal plateaus near 400µm channels decreased significantly compared to all other dimensions. At 7 days, plateau thicknesses on flats and near 50µm, 100µm and 200µm channels were comparable to epidermal thickness on DED and native foreskin tissue.

4.3.4 Proliferation is Increased In Narrow Microniches

To investigate the mechanisms contributing to the increased epidermal thickness in and near narrow microniches, we analyzed proliferation of basal keratinocytes. µDERMs cultured for 7 days A/L were stained for ki67, a nuclear protein that is present during G_1, G_2, S phase and mitosis but absent in quiescent cells (G_0) making it a definitive marker for cell proliferation (Bullwinkel *et al.*, 2006; Scholzen and Gerdes, 2000). Representative images are shown for the various microniche geometries in Figure 4.3A-F. The number of ki67+ cells/mm of DEJ length was calculated for each well dimension (Figure 4.3G). The number of ki67+ cells/mm was not statistically different on DED compared to µDERMs for all topographic dimensions, but 100 µm channels had a significantly increased density of ki67+ keratinocytes in the basal layer compared to 400 µm channels. It is also interesting to note that the ki67+ cell density in these wells was statistically comparable to the ki67+ cell density in native foreskin tissue.

One feature inherent to microtopography is an increase in total surface area. In this way, the surface are of µDERMs more closely approximates the surface area of the native DEJ than flat, planar control scaffolds. To determine whether this increased surface area increases the ki67+ cell density, we measured the number of ki67+ cells/planar graft length (Figure 4.3H). Overall ki67+ keratinocyte density was increased in regions with 50µm channels compared to 200 and 400 µm channels, flat controls and DED controls. Additionally ki67+ keratinocyte density in regions with 50µm channels approximated the density in foreskin control. Taken together, these results suggest that narrow microniches enhance keratinocyte proliferation.

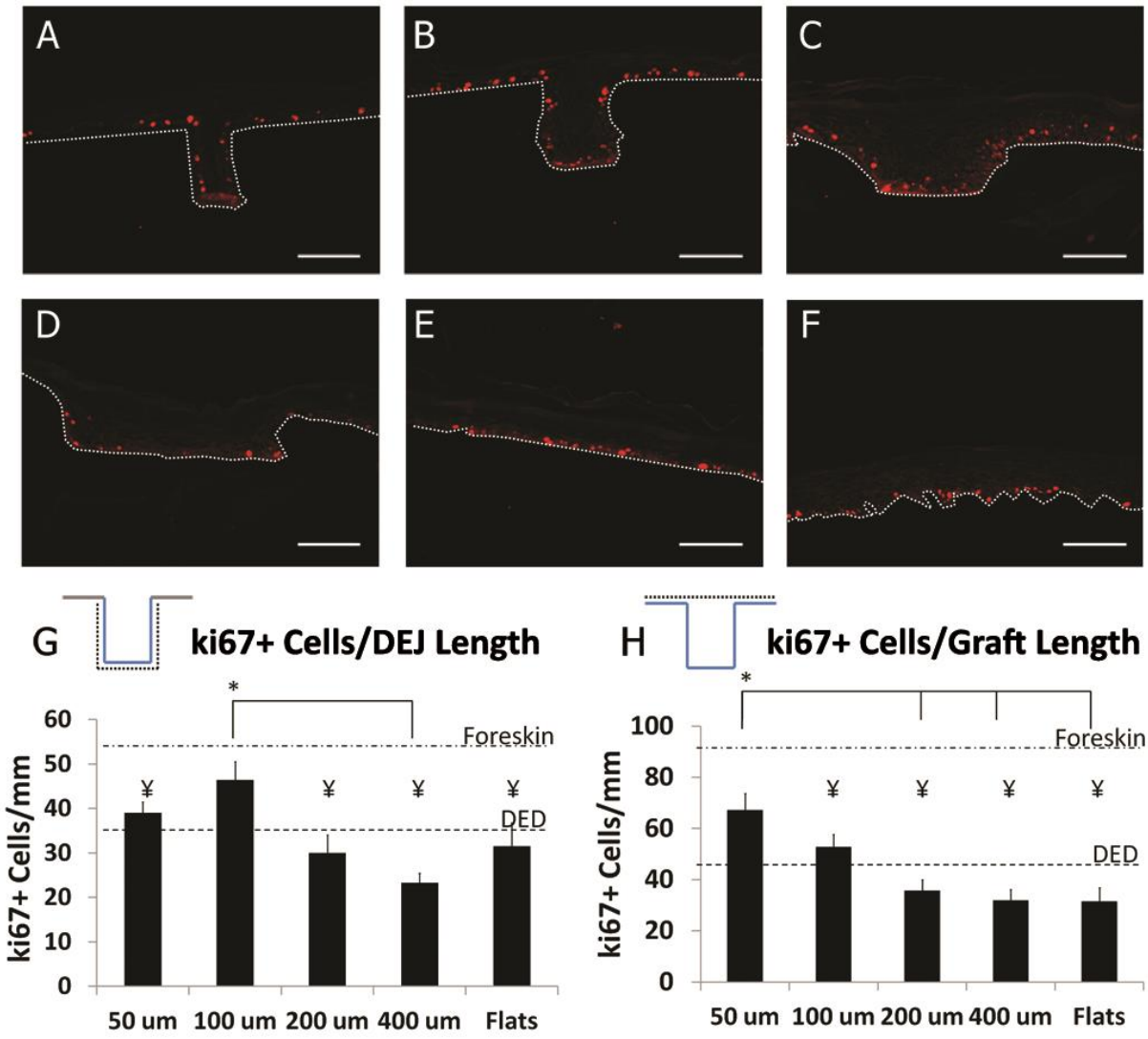

Figure 4.3 Proliferation of keratinocytes seeded on µDERMs after 7 days A/L interface culture. Representative images of ki67 expression on µDERMs with 50µm (A), 100µm (B), 200µm (C), and 400µm (D) channels, on flat µDERM (E) and on DED (F). Dotted white line indicates DEJ. The linear density of ki67+ keratinocytes was calculated by normalizing against DEJ length (G) and planar graft length (H). Ki67+ cell density along the length of the DEJ within 100 µm channels is increased compared to 200 µm channels, 400 µm channels and flats. Ki67+ cell density along the length of the graft is significantly increased in regions containing 50 µm channels compared to 200 µm channels, 400 µm channels, and flats. Additionally, the graft density of ki67+ cells in narrow channeled regions is not statistically different from native foreskin. Scale bar = 100µm. Data presented as Mean ±SEM. * denotes statistical differences between specified microniche dimensions, ¥ indicates statistical difference from foreskin control, $p<0.05$

4.3.5 Involucrin Expression is Increased in Narrow Microniches

To determine the effect of microniche topography on differentiation, histological sections from µDERMs cultured for 7 days at the A/L interface were immunostained for involucrin, a marker of terminal differentiation.

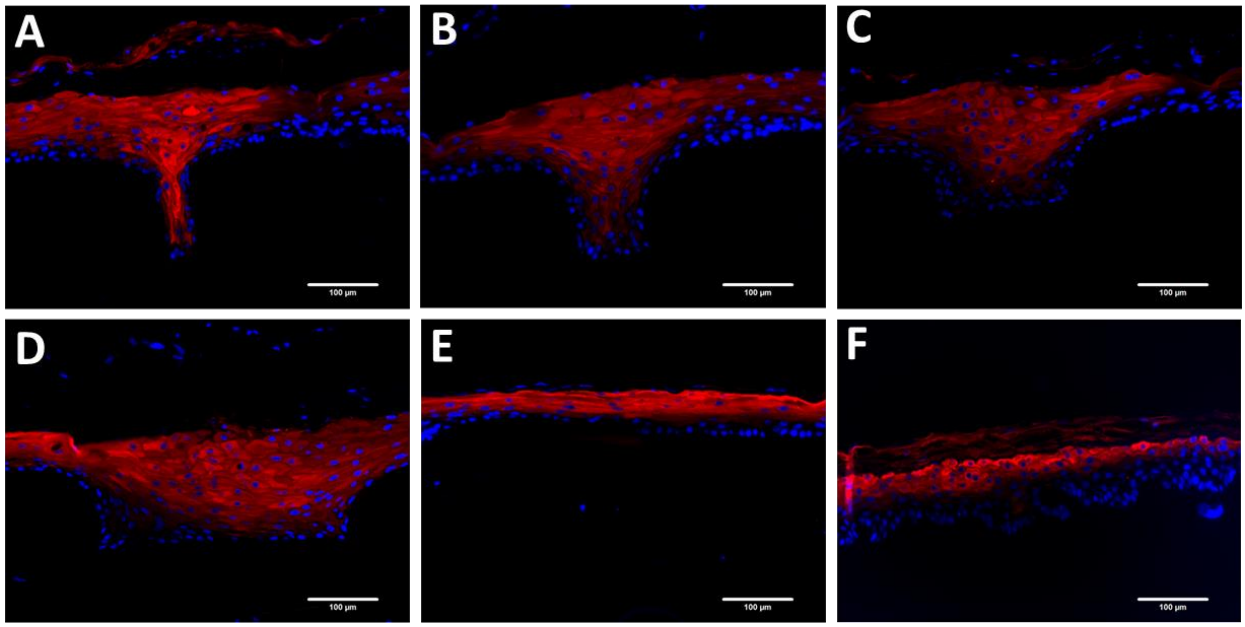

Figure 4.4 Involucrin Expression on µDERM after 7 days A/L Culture Representative images of involucrin expression (red) and Hoechst staining (blue) on µDERMs with 50µm (A), 100µm (B), 200µm (C), and 400µm (D) channels, on flat µDERM (E) and on DED (F). Involucrin is expressed in the suprabasal layers of all channel topographies and DED controls.

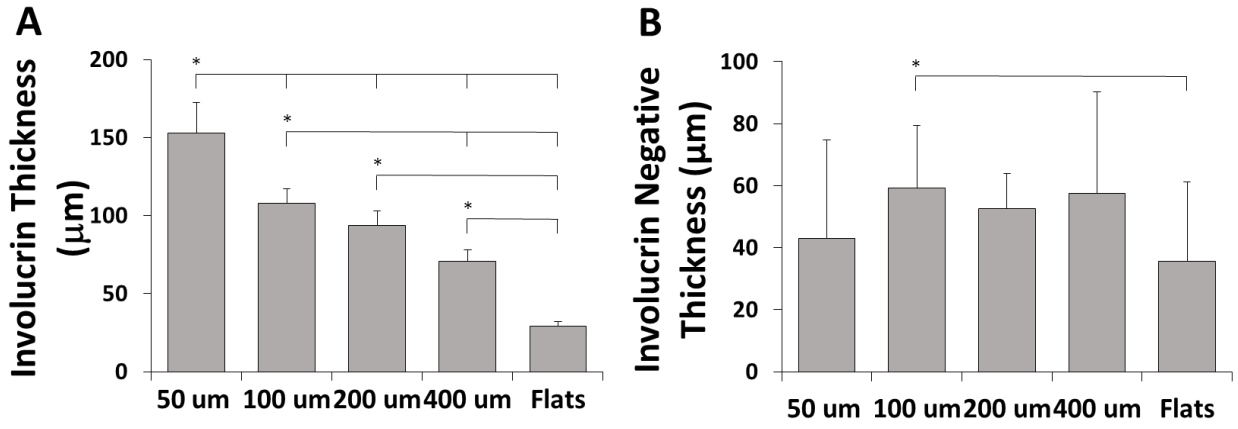

Figure 4.5 Involucrin expression is increased in narrow channels of µDERM. (A) Shows the thickness of the involucrin positive layer in channels of different dimensions on cultured µDERM. Involucrin expression is significantly increased in narrow channels. (B) Shows the thickness of the basal involucrin negative layer. There is a trend of increased involucrin negative thickness in channel topographies. * indicates statistically significant increase compared to indicated groups ($p<.05$). n=12, 25, 20, 20 and 13 for 50 µm, 100 µm, 200 µm, 400 µm channels and flats respectively.

The involucrin positive layer appeared thicker in microchannels (A, B, C and D) than on flat regions of µDERM (E). Involucrin expression was quantified by measuring the thickness of the involucrin positive epidermal layer (Figure 4.5A). Not only was the thickness of the involucrin positive layer increased in channels of all dimensions compared to flats, but involucrin thickness was

significantly increased in narrow channels compared to wider channels, which strongly correlates with the trend of increased epidermal thickness in narrow microchannels.

We also examined the effect of topography on the thickness of the involucrin negative layer, which consisted primarily of the basal layer, but in some microniches extended up into the suprabasal keratinocytes. We showed a trend of increased involucrin negative thickness in 100 μm, 200 μm, and 400 μm channels compared to flats, although this increase was only statistically significant in 100 μm channels. We observed a high degree of variability in this involucrin negative thickness within channel dimensions, as evidenced by the high standard deviations. Post hoc analysis yielded a power of only 0.464, indicating a need for further studies with larger sample numbers to determine if topography plays a significant role in the positional induction of involucrin expression.

4.3.6 Laminin 332 Synthesis is Increased in Wide Microniches

To investigate the effects of keratinocyte microniches on BM synthesis, scaffolds were analyzed after 7days of culture at the A/L. Histological sections were immunostained for laminin-332 (γ2 chain) and nuclei were counterstained with Hoechst (Figure 4.6 A-F). A continuous layer of laminin deposition was observed at the dermal-epidermal junction of all μDERM topographies, flat controls and DED. To visualize areas of increased laminin-332 deposition, false colorization was applied after background subtraction (blue = top 1/3 intensity, green = mid 1/3 intensity, and red = lowest 1/3 intensity normalized to the maximum intensity in the image set) (Figure 4.6 G-L). To quantify laminin-332 deposition and distribution, the average relative fluorescence intensity/length of laminin γ2 chain expression localized to the DEJ was determined for the plateaus, base and sides of each dimension. There was no significant difference in laminin deposition between regions of individual channels (plateaus, bases, and sides). However, overall laminin deposition was decreased in 50μm and 100μm channels compared to 200μm channels, 400μm channels and flats. In 400μm channels, laminin deposition was increased over flat controls

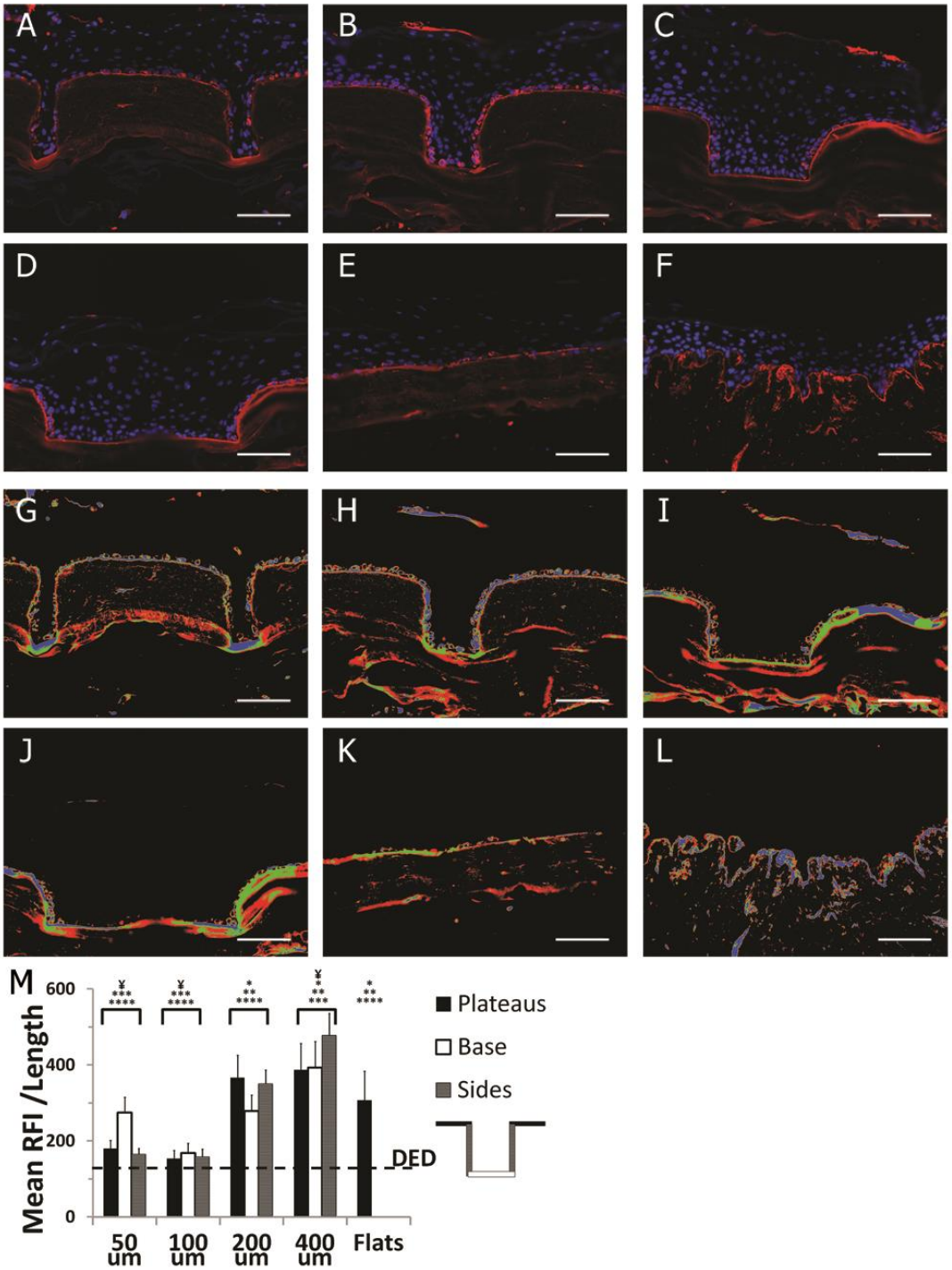

Figure 4.6 Laminin-332 deposition on µDERMs after 7 days A/L culture. Representative images of laminin-332 expression (Alexafluor546) on cultured µDERMs with 50µm (A), 100µm (B), 200µm (C), and 400µm (D) channels, on flat µDERM (E) and on DED (F). LUT false colorization of laminin 332 expression (G-L); blue = highest 1/3 laminin γ2 expression, green = mid 1/3 laminin γ2 expression, red = lowest 1/3 laminin γ2 expression. Laminin deposition was quantified by normalizing the relative fluorescent intensity (RFI) of γ2 expression at the DEJ against DEJ length (M). Laminin 332 deposition is increased in wider channels and decreased in narrow channels compared to flat control features. There was no statistical difference in regional expression of laminin-332 within microniches (plateaus, channel base, channel sides) of a specific dimension. Data presented as mean ±SEM. c. Asterisks indicate statistical difference from : *50 µm channels, **100µm channels, *** 200µm channels, ****400µm channels. ¥ Indicates statistical difference from flats control, $p<0.05$.

and in both 400µm and 200µm channels, laminin deposition increased relative to DED controls. This suggests that wider keratinocyte niches promote a synthetic phenotype.

4.3.7 Keratinocyte Stem Cells Localize to Narrow Microniches and Corners of Wide Microniches

To further examine the presence of distinct keratinocyte niches in µDERMs, we performed immunohistochemistry for β_1 integrin and p63 – putative keratinocyte stem cell markers (Figure 4.7). In suprabasal keratinocytes, β_1 integrin expression was low (bottom 1/3 brightness, β_1^{dim}) or completely absent. The majority of basal keratinocytes expressed moderate (middle 1/3 brightness, β_1^{mid}) or high (top 1/3 brightness, β_1^{bri}) levels of β_1 integrin. Additionally, p63 expression was predominately localized to the basal keratinocytes, with clusters of $p63^+$ cells overlapping clusters of β_1^{bri} cells.

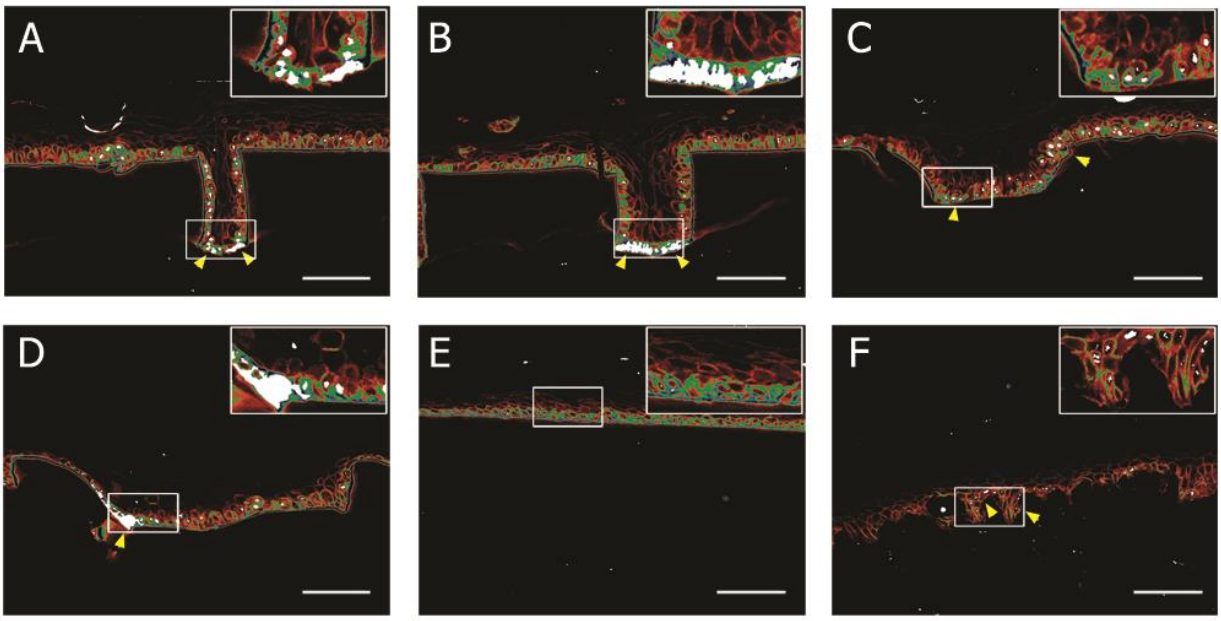

Figure 4.7 β1brip63+ keratinocyte localization on µDERMs cultured at the A/L interface for 7 days. LUT false colorization of β1 integrin and p63 expression with 50µm (A), 100µm (B), 200µm (C), and 400µm (D) channels, on flat µDERM (E) and on DED (F); blue = highest 1/3 β1 expression, green = mid 1/3 β1 expression, red = lowest 1/3 β1 expression, white = p63+ nuclei. Insets show indicated regions of interest at high magnification. $\beta_1^{bri}p63^+$ keratinocytes preferentially localize to the bases of 50µm (A) and 100µm (B) channels and the corners of 400µm channels (D). In contrast, β_1^{bri} cells are randomly distributed on flat regions and p63 expression is limited. On DED, β1brip63+ cells are located in niches (F). Scale bar = 100µm.

These clusters of $\beta_1^{bri}p63^+$ keratinocytes were located predominately in the bottoms of narrow 50µm and 100µm channels (Figure 4.7A and B) and in the corners of wide 200 µm and 400µm

channels (Figure 4.7C and D). In contrast, $\beta_1^{bri}p63^+$ keratinocytes were randomly distributed within the basal layer of keratinocytes cultured on flat interfaces (Figure 4.7E). This suggests the ability of microtopography to sequester phenotypically similar keratinocytes.

4.4 Discussion

Future innovations to skin substitutes necessitate the development of a 3D *in vitro* skin model that enables facile systematic evaluations of the effect of microtopographic features on keratinocyte function in cellular niches that mimic the physical topography of the DEJ. This study builds upon our µDERM model (Bush and Pins, 2012) to demonstrate that topographic features can drive keratinocyte compartmentalization into proliferative, synthetic and $\beta_1^{bri}p63^+$ keratinocyte niches. In this study, we found that epidermal thickness was increased in and near narrow channel geometries and that µDERMs containing channel topography exhibited a more defined stratum granulosum and a robust basal layer of keratinocytes, suggesting that topographic features contribute to keratinocyte-mediated epidermal morphogenesis. Further, the density of $ki67^+$ keratinocytes was increased in cellular regions with narrow channel geometries, while the amount of laminin-332 deposited on µDERM surfaces was increased in regions with wide channels. Additionally, we found that $\beta_1^{bri}p63^+$ keratinocytes clustered in the bases of narrow channels and the corners of wider channels. Together, these results support the hypothesis that keratinocytes cultured on µDERM may aggregate into distinct cell subpopulations in response to topographic cues. These findings also suggest that, independent of biochemical cues, microtopography may be used to drive cellular function.

In nature, the epidermis conforms to the complex series of rete ridges and papillary plateaus of the DEJ, creating 3D biophysical and biochemical microniches that regulate keratinocyte phenotype and cellular functions. In this study, we seek to precisely recapitulate the keratinocyte microenvironments of the DEJ. Importantly, we have found that incorporation of this topography improves the overall epidermal morphology. Notably, the basal cells on µDERMs containing microchannels exhibit the characteristic cuboidal shape seen in native skin and appear to be well attached to the collagen gel. We also not the presence of a more defined stratum granulosum in

channel topographies. The stratum granulosum is critical for the development of barrier function, providing a strong clinical motivation for incorporation of DEJ topography in future skin substitutes.

In our μDERM model, we see a statistically significant increase in the number of proliferative keratinocytes in narrow channels compared to wide channels and flat controls. Our new μDERM model incorporates fibroblasts into the dermal layer and creates a more biomimetic *in vitro* model system that enables the evaluation of the effect of microtopography on keratinocyte proliferation. Importantly, in first generation μDERMs lacking fibroblasts there were no significant differences in ki67^{+} cell density between channels of different dimensions (Bush and Pins, 2012). However, an increase in laminin-332 deposition was demonstrated in wider channels. Since both proliferative and synthetic keratinocytes are essential for proper epidermal morphogenesis, DEJ topography may regulate these two functions as a response to soluble factors. In future studies we will further probe this by quantifying the effect of exogenous KGF on keratinocytes cultured in different microtopographies.

Our results with μDERMs containing fibroblasts suggest that microtopography may contribute to modulating keratinocyte proliferation. These findings significantly augment our previously proposed space filling mechanism to explain increased epidermal thickness in narrow channels of keratinocyte microniches (Bush and Pins, 2012). In our earlier studies on bioengineered skin substitutes containing microfabricated basal lamina analogs lacking fibroblasts, we observed a decrease in proliferating keratinocyte following initial seeding: first in narrow channels (3 days) and then in wide channels (7 days), and we found no statistically significant differences in ki67+ keratinocyte density in channels of different dimensions (Bush and Pins, 2012). This led us to propose a space filling mechanism to explain the increased epidermal thickness in narrow channels. However, here we show that in μDERMs containing fibroblasts (after 7 days A/L), the density of proliferating cells along the DEJ is higher in narrow (100μm) channels. Further, the density of proliferating cells on the scaffold is also higher in narrow (50μm) channels. This suggests that channel topography can direct cellular proliferation and indicates that a space filling

mechanism is not solely responsible for increased epidermal thickness. Previous work has demonstrated the importance of keratinocyte-fibroblast paracrine signaling to the maintenance of the proliferative keratinocyte phenotype. We hypothesized that the absence of fibroblast signaling in our previous work may have resulted in a quiescent phenotype, limiting our ability to fully investigate microtopographic cues. To address this limitation and to generate a more physiologically relevant model, we incorporated dermal fibroblasts into our µDERM model. Our results which demonstrate a thicker, more robust epidermal layer in the presence of fibroblasts are consistent with previously published works and suggest that the incorporation of fibroblasts into our model system allows us to more explicitly probe the ability of microtopography to create distinct keratinocyte niches. Incorporating fibroblasts into the dermal sponge may be particularly important for future *in vivo* studies. A previous study using a murine transplantation model demonstrated that incorporation of fibroblasts into a composite skin substitute not only improved epidermal formation but also enhanced vascularization and reduced graft contraction *in vivo* (Erdag and Sheridan, 2004). Despite these enhancements to our model system, our understanding of the mechanisms that govern the topographic modulation of epidermal thickness remain incomplete. Although we have demonstrated increased keratinocyte proliferation in narrow microchannels, our previous results with fibroblast-free µDERMs suggest that the increased epidermal thickness observed in narrow channels may be a result of more than increased proliferation. In the future, it would be interesting to characterize the initial seeding of keratinocytes on µDERMs and to determine whether or not the change in the epidermal thickness can be predicted by the keratinocyte proliferation rate when normalized to the initial cell attachment density.

In addition to proliferation, we looked at keratinocyte commitment to terminal differentiation by immunostaining for involucrin. Involucrin was expressed in the suprabasal layers and excluded from the basal layers of all µDERM. Although in native tissue involucrin expression is confined to the upper strata, on many of the µDERMs, the involucrin positive layer contained all of the suprabasal cells. This is consistent with previous reports that show that *in vitro* keratinocyte cultures exhibit hyper-involucrin expression with only the basal layer retaining involucrin

negative cells (Banks-Schlegel and Green, 1981; Watt *et al.*, 1987). Additionally, *in vivo* during the early stages of wound healing or areas of hyperproliferation thicker involucrin layers are observed (Bernard *et al.*, 1986; Chen *et al.*, 2013; Li *et al.*, 2000). Interestingly, in some of the microchannels, we noted multiple layers of involucrin negative keratinocytes. We quantified the thickness of the involucrin negative basal-suprabasal layer and found that there was a slight increase in the thickness of the involucrin negative layer in channels compared to flat. Although this difference was only significant in the 100 µm channels, it may suggest that channel geometries can create a more physiologically relevant model for studying keratinocyte differentiation. However, post hoc power analysis indicated that the power was less than 0.8 so future studies are necessary to determine the potential significance of channel topography on special localization of involucrin.

We also examine the influence of microtopography on the deposition of the BM protein laminin-332 (Aumailley *et al.*, 2005). Importantly, keratinocytes seeded on µDERMs deposited a continuous layer of laminin-332 along the surfaces of all of the microniches at the DEJ. In quiescent skin, laminin-332 is part of the anchoring filaments at the DEJ and is essential for keratinocyte adhesion to the underlying dermis via the $\alpha_6\beta_4$ integrin (Baker *et al.*, 1996; Burgeson and Christiano, 1997; Miyazaki, 2006). Mutations in the genes coding for the laminin-332 subunits (LAMA3, LAMB3, and LAMC2) lead to junctional epidermolysis bullosa (JEB) which is characterized by severe blistering at the lamina lucida (Fine *et al.*, 2000; Meng *et al.*, 2003). Additionally, following skin wounding laminin-332 is secreted by epidermal keratinocytes to facilitate wound re-epithelialization (Amano *et al.*, 2004; Nguyen *et al.*, 2000; Santoro and Gaudino, 2005). We showed increased laminin synthesis was inversely related to proliferating keratinocyte density. In wide (200µm and 400µm) channels, laminin deposition was increased compared to narrow channels. In 400µm channels, laminin deposition was also increased compared to flat controls. This relationship suggests a synthetic keratinocyte niche may exist in wide channels. Since both keratinocyte proliferation and BM deposition are critical for wound healing, these results suggest the importance of including microtopographic features of multiple dimensions in complete tissue engineered skin grafts.

Finally, we examine the influence of microtopography on the localization of the stem-like $\beta_1^{bri}p63^+$ keratinocyte population. We demonstrated clustering of these cells in the base of narrow channels and the corners of wide channels, supporting the role of cellular adhesion in keratinocyte stem cell maintenance. In native skin, keratinocyte stem cells are found to preferentially locate to the tips of the DP or the base of the rete ridges (Lavker and Sun, 1982, 1983; Watt, 1998, 2001, 2002). However, on flat skin substitutes, these cells are randomly distributed. The ability of μDERM to recreate this patterning *in vitro* provides an important platform for future studies. Further, the heterogeneity of β_1 integrin and p63 expression in basal keratinocytes and the clustering of $\beta_1^{bri}p63^+$ keratinocytes further supports the theory that distinct keratinocyte microniche topographies on μDERMs modulate keratinocyte function. These results suggest that μDERMs may promote stem cell clustering; however, given the controversy over epidermal stem cell markers and distinct stem cell populations, further evaluation is necessary. To further probe this clustering phenomenon and to better elucidate the feasibility of creating an *in vitro* stem cell niche, future studies will focus on isolating and characterizing keratinocytes from microniches for clonal analysis via microdissection. Importantly, the existence of a keratinocyte response to morphological cues may help explain the heterogeneous basal keratinocyte population that is observed as keratinocytes respond to their local microenvironments.

The mechanism by which microtopography promotes cell sequestering both *in vitro* and *in situ* is not completely understood. One hypothesis is that cell phenotype and function is driven by variable nutrient availability due to the diffusion and mass transport profile through the substrate. In the μDERM model, the channel bases are in closer proximity to the dermal sponge than the plateaus, which we hypothesize will result in a higher concentration of fibroblast secreted cytokines in channels compared to plateau regions. This may be partially responsible for the differences in cell function between channel regions, plateau regions and flats. However, the differences in laminin 332 deposition, keratinocyte proliferation, epidermal thickness and $\beta_1^{bri}p63^+$ keratinocyte localization between channels of different dimensions suggest mass transport of paracrine signals through the collagen gel may not be the only mechanism involved

in the keratinocyte response to microtopography. Differential oxygen diffusion through the keratinocyte layers may also create localized regions of hypoxia. Importantly, regional hypoxia is present in native skin, particularly in hair follicles and dermal glands (Rosenberger *et al.*, 2007). *In vitro* studies have shown that keratinocytes grown under hypoxic conditions exhibit reduced laminin 332 synthesis (O'Toole *et al.*, 1997). Here we have demonstrated that keratinocytes grown in narrow channels generate a thicker epidermal layer and also exhibit reduced laminin 332 synthesis compared to wide channels and flat controls. The increased epidermal thickness may create regional hypoxia which results in a reduction of laminin synthesis. However, hypoxia alone cannot account for the differences in laminin 332 synthesis because laminin deposition in 400µm channels is increased compared to on flats, despite having a much thicker epidermal layer within the channel. Finally, microtopographic mechanical cues may drive cellular function through static compressive and tensile forces induced by the topography. Previously, Fratzl *et al.* demonstrated that geometric cues such as channel surface area and local substrate curvature influenced the rate of bone tissue growth (Rumpler *et al.*, 2008). It is likely that multiple microtopographic-mediated mechanisms are responsible for the observed phenomenon. Future studies will investigate the specific contributions of mass transport and nutrient diffusion, hypoxic gradients and static mechanical stresses on keratinocyte phenotype and function in an attempt to further elucidate the importance of the microtopographic environment of the DEJ.

By integrating microfabrication technologies into the biomaterials design process, this work provides a robust research platform which we began to use to conduct systematic analyses of the fundamental relationships between the precise dimensions of the 3D cellular microenvironments and keratinocyte functions that significantly enhance the regeneration of robust epidermal layers on the surfaces of our skin substitutes. One benefit of the µDERM platform is that the micropatterned tissue analog is implantable, making it versatile for future *in vivo* wound healing studies as well as *in vitro* assays. Using this platform, we will continue to identify design parameters for the clinical development of robust skin substitutes that would benefit the growing need for treatment of burns, chronic wounds and diabetic ulcers.

Our findings from this study suggest a key role for microtopography in the segregation and promotion of keratinocyte niches. Strategic selection of microtopographic features can be used to design more advanced engineered skin constructs targeted to specific functions for both *in vitro* models as well as for clinical use. To reach the full potential of microtopographic regulation of keratinocyte phenotype, further research is necessary to elucidate the mechanisms behind niche formation. In the future we plan to examine the temporal synthesis of different BM proteins and the development of barrier function on μDERM with different topographical geometries. Our findings suggest that these novel μDERMs will serve as a platform for the development of highly tailored tissue engineered skin substitutes for use in the treatment of full-thickness wounds and as an *in vitro* organ system to study skin morphogenesis, wound healing, epidermal pathologies and drug screening assays.

4.5 Acknowledgments

This research was funded by the NIH (EB-005645). Special thanks to Dr. Mehmet Toner and Octavio Hurtado at the BioMicroElectroMechanical Systems (BioMEMS) Resource Center, Massachusetts General Hospital, Boston, MA (NIH Grant: P41 EB02503 [MT]), for their assistance with the microfabrication processes. I would like to thank my advisor, Professor George Pins, for his scientific contribution to the work. I would also like to thank Jen Molignano and Tom Moutinho for technical assistance, the Department of Obstetrics and Gynecology at UMMS (Worcester, MA) for providing us with neonatal foreskins for keratinocyte isolations and Russell Kronengold, Ph.D., at the Kensey Nash Corporation (Exton, PA), for his generous donations of SEMED-S collagen.

4.6 References

Amano S, Akutsu N, Ogura Y and Nishiyama T (2004) Increase of Laminin 5 Synthesis in Human Keratinocytes by Acute Wound Fluid, Inflammatory Cytokines and Growth Factors, and Lysophospholipids. *Br J Dermatol* 151:961-70.

Aumailley M, Bruckner-Tuderman L, Carter WG, Deutzmann R, Edgar D, Ekblom P, Engel J, Engvall E, Hohenester E, Jones JC, Kleinman HK, Marinkovich MP, Martin GR, Mayer U, Meneguzzi G, Miner JH, Miyazaki K, Patarroyo M, Paulsson M, Quaranta V, Sanes JR, Sasaki T, Sekiguchi K,

Sorokin LM, Talts JF, Tryggvason K, Uitto J, Virtanen I, von der Mark K, Wewer UM, Yamada Y and Yurchenco PD (2005) A Simplified Laminin Nomenclature. *Matrix Biol* 24:326-32.

Baker SE, Hopkinson SB, Fitchmun M, Andreason GL, Frasier F, Plopper G, Quaranta V and Jones JC (1996) Laminin-5 and Hemidesmosomes: Role of the Alpha 3 Chain Subunit in Hemidesmosome Stability and Assembly. *J Cell Sci* 109 (Pt 10):2509-20.

Banks-Schlegel S and Green H (1981) Involucrin Synthesis and Tissue Assembly by Keratinocytes in Natural and Cultured Human Epithelia. *J Cell Biol* 90:732-7.

Bellas E, Seiberg M, Garlick J and Kaplan DL (2012) In Vitro 3d Full-Thickness Skin-Equivalent Tissue Model Using Silk and Collagen Biomaterials. *Macromol Biosci* 12:1627-36.

Bernard BA, Reano A, Darmon YM and Thivolet J (1986) Precocious Appearance of Involucrin and Epidermal Transglutaminase During Differentiation of Psoriatic Skin. *Br J Dermatol* 114:279-83.

Bullwinkel J, Baron-Luhr B, Ludemann A, Wohlenberg C, Gerdes J and Scholzen T (2006) Ki-67 Protein Is Associated with Ribosomal Rna Transcription in Quiescent and Proliferating Cells. *J Cell Physiol* 206:624-35.

Burgeson RE and Christiano AM (1997) The Dermal-Epidermal Junction. *Curr Opin Cell Biol* 9:651-8.

Bush K and Pins G (2012) Development of Microfabricated Dermal Epidermal Regenerative Matrices to Evaluate the Role of Cellular Microenvironments on Epidermal Morphogenesis. *Tissue Eng Part A* 18:2343-53.

Charest JL, Jennings JM, King WP, Kowalczyk AP and Garcia AJ (2009) Cadherin-Mediated Cell-Cell Contact Regulates Keratinocyte Differentiation. *J Invest Dermatol* 129:564-72.

Chen JQ, Man XY, Li W, Zhou J, Landeck L, Cai SQ and Zheng M (2013) Regulation of Involucrin in Psoriatic Epidermal Keratinocytes: The Roles of Erk1/2 and Gsk-3beta. *Cell Biochem Biophys* 66:523-8.

Cornwell KG, Downing BR and Pins GD (2004) Characterizing Fibroblast Migration on Discrete Collagen Threads for Applications in Tissue Regeneration. *J Biomed Mater Res A* 71:55-62.

Downing BR, Cornwell K, Toner M and Pins GD (2005) The Influence of Microtextured Basal Lamina Analog Topography on Keratinocyte Function and Epidermal Organization. *J Biomed Mater Res A* 72:47-56.

Elsdale T and Bard J (1972) Collagen Substrata for Studies on Cell Behavior. *J Cell Biol* 54:626-37.

Erdag G and Sheridan RL (2004) Fibroblasts Improve Performance of Cultured Composite Skin Substitutes on Athymic Mice. *Burns* 30:322-8.

Fawcett DW and Jensh RP (1997) *Concise Histology*. Chapman and Hall: New York, NY.

Fine JD, Eady RA, Bauer EA, Briggaman RA, Bruckner-Tuderman L, Christiano A, Heagerty A, Hintner H, Jonkman MF, McGrath J, McGuire J, Moshell A, Shimizu H, Tadini G and Uitto J (2000) Revised Classification System for Inherited Epidermolysis Bullosa: Report of the Second International Consensus Meeting on Diagnosis and Classification of Epidermolysis Bullosa. *J Am Acad Dermatol* 42:1051-66.

Gautrot JE, Wang C, Liu X, Goldie SJ, Trappmann B, Huck WT and Watt FM (2012) Mimicking Normal Tissue Architecture and Perturbation in Cancer with Engineered Micro-Epidermis. *Biomaterials* 33:5221-9.

Gilbert PM and Blau HM (2011) Engineering a Stem Cell House into a Home. *Stem Cell Res Ther* 2:3.

Gobaa S, Hoehnel S, Roccio M, Negro A, Kobel S and Lutolf MP (2011) Artificial Niche Microarrays for Probing Single Stem Cell Fate in High Throughput. *Nat Methods* 8:949-55.

Jones PH, Harper S and Watt FM (1995) Stem Cell Patterning and Fate in Human Epidermis. *Cell* 80:83-93.

Lammers G, Roth G, Heck M, Zengerle R, Tjabringa GS, Versteeg EM, Hafmans T, Wismans R, Reinhardt DP, Verwiel ET, Zeeuwen PL, Schalkwijk J, Brock R, Daamen WF and van Kuppevelt TH (2012) Construction of a Microstructured Collagen Membrane Mimicking the Papillary Dermis Architecture and Guiding Keratinocyte Morphology and Gene Expression. *Macromol Biosci* 12:675-91.

Lane SW, Williams DA and Watt FM (2014) Modulating the Stem Cell Niche for Tissue Regeneration. *Nat Biotechnol* 32:795-803.

Lavker RM and Sun TT (1982) Heterogeneity in Epidermal Basal Keratinocytes: Morphological and Functional Correlations. *Science* 215:1239-41.

Lavker RM and Sun TT (1983) Epidermal Stem Cells. *J Invest Dermatol* 81:121s-7s.

Li ER, Owens DM, Djian P and Watt FM (2000) Expression of Involucrin in Normal, Hyperproliferative and Neoplastic Mouse Keratinocytes. *Exp Dermatol* 9:431-8.

Liao YH, Chen SY, Chou SY, Wang PH, Tsai MR and Sun CK (2013) Determination of Chronological Aging Parameters in Epidermal Keratinocytes by in Vivo Harmonic Generation Microscopy. *Biomed Opt Express* 4:77-88.

Lu W, Miyazaki K, Mizushima H and Nemoto N (2001) Immunohistochemical Distribution of Laminin-5 Gamma2 Chain and Its Developmental Change in Human Embryonic and Foetal Tissues. *Histochem J* 33:629-37.

Macri L and Clark RA (2009) Tissue Engineering for Cutaneous Wounds: Selecting the Proper Time and Space for Growth Factors, Cells and the Extracellular Matrix. *Skin Pharmacol Physi* 22:83-93.

Meng X, Klement JF, Leperi DA, Birk DE, Sasaki T, Timpl R, Uitto J and Pulkkinen L (2003) Targeted Inactivation of Murine Laminin Gamma2-Chain Gene Recapitulates Human Junctional Epidermolysis Bullosa. *J Invest Dermatol* 121:720-31.

Miyazaki K (2006) Laminin-5 (Laminin-332): Unique Biological Activity and Role in Tumor Growth and Invasion. *Cancer Sci* 97:91-8.

Montagna W and Carlisle K (1979) Structural Changes in Aging Human Skin. *J Invest Dermatol* 73:47-53.

Murphy M, Kerr P and Grant-Kels JM (2007) The Histopathologic Spectrum of Psoriasis. *Clin Dermatol* 25:524-8.

Nguyen BP, Ryan MC, Gil SG and Carter WG (2000) Deposition of Laminin 5 in Epidermal Wounds Regulates Integrin Signaling and Adhesion. *Curr Opin Cell Biol* 12:554-62.

O'Toole EA, Marinkovich MP, Peavey CL, Amieva MR, Furthmayr H, Mustoe TA and Woodley DT (1997) Hypoxia Increases Human Keratinocyte Motility on Connective Tissue. *J Clin Invest* 100:2881-91.

Odland GF (1950) The Morphology of the Attachment between the Dermis and the Epidermis. *Anat Rec* 108:399-413.

Pincelli C and Marconi A (2013) Keratinocyte Stem Cells: Biology and Clinical Applications. In: *Regenerative Medicine and Cell Therapy* (Baharvand H, Aghdami N, eds): Humana Press, 57-64.

Powell HM, McFarland KL, Butler DL, Supp DM and Boyce ST (2010) Uniaxial Strain Regulates Morphogenesis, Gene Expression, and Tissue Strength in Engineered Skin. *Tissue Eng Part A* 16:1083-92.

Rook A and Burns T (2010) Rook's Textbook of Dermatology. (Wiley-Blackwell: Chichester, West Sussex, UK ; Hoboken, NJ.

Rosenberger C, Solovan C, Rosenberger AD, Jinping L, Treudler R, Frei U, Eckardt KU and Brown LF (2007) Upregulation of Hypoxia-Inducible Factors in Normal and Psoriatic Skin. *J Invest Dermatol* 127:2445-52.

Rumpler M, Woesz A, Dunlop JW, van Dongen JT and Fratzl P (2008) The Effect of Geometry on Three-Dimensional Tissue Growth. *J R Soc Interface* 5:1173-80.

Santoro MM and Gaudino G (2005) Cellular and Molecular Facets of Keratinocyte Reepithelization During Wound Healing. *Exp Cell Res* 304:274-86.

Scholzen T and Gerdes J (2000) The Ki-67 Protein: From the Known and the Unknown. *J Cell Physiol* 182:311-22.

Trappmann B, Gautrot JE, Connelly JT, Strange DG, Li Y, Oyen ML, Cohen Stuart MA, Boehm H, Li B, Vogel V, Spatz JP, Watt FM and Huck WT (2012) Extracellular-Matrix Tethering Regulates Stem-Cell Fate. *Nat Mater* 11:642-9.

Watt FM (1998) Epidermal Stem Cells: Markers, Patterning and the Control of Stem Cell Fate. *Philos Trans R Soc Lond B Biol Sci* 353:831-7.

Watt FM (2001) Stem Cell Fate and Patterning in Mammalian Epidermis. *Curr Opin Genet Dev* 11:410-7.

Watt FM (2002) The Stem Cell Compartment in Human Interfollicular Epidermis. *J Dermatol Sci* 28:173-80.

Watt FM, Boukamp P, Hornung J and Fusenig NE (1987) Effect of Growth Environment on Spatial Expression of Involucrin by Human Epidermal Keratinocytes. *Arch Dermatol Res* 279:335-40.

Watt FM and Huck WT (2013) Role of the Extracellular Matrix in Regulating Stem Cell Fate. *Nat Rev Mol Cell Biol* 14:467-73.

Zapatka M, Zboralski D, Radacz Y, Bockmann M, Arnold C, Schoneck A, Hoppe S, Tannapfel A, Schmiegel W, Simon-Assmann P and Schwarte-Waldhoff I (2007) Basement Membrane Component Laminin-5 Is a Target of the Tumor Suppressor Smad4. *Oncogene* 26:1417-27.

Chapter 5: Keratinocyte Attachment and Stem Cell Localization on Multi-Dimensional Dermal Papillae Analogs

5.1 Introduction

In vitro cell culture has long provided investigators with a powerful research tool, however until recently the majority of cell culture was performed in 2-D on non-physiologically relevant substrates. Recently, there has been a paradigm shift towards 3-D cell culture that better represents the *in vivo* situation to increase the physiological relevance of *in vitro* experiments (Haycock, 2011; Justice *et al.*, 2009; Pampaloni *et al.*, 2007). These 3-D cell culture models allow for the study of epidermal morphogenesis and epidermal processes including proliferation, differentiation and basement membrane protein deposition in the context of cell-cell, cell-soluble and cell-matrix interactions (Bellas *et al.*, 2012; Gotz *et al.*, 2012a; Gotz *et al.*, 2012b; Groeber *et al.*, 2011; Huang *et al.*, 2010). While these models represent significant scientific advancements, what is missing is a model system which allows investigators to probe cellular responses to microtopographical features.

Three-dimensional tissue engineered skin constructs are popular *in vitro* models for systematically studying cell-cell and cell-matrix interactions that direct epidermal morphogenesis and influence tissue pathologies. One method for generating these constructs is to culture keratinocytes on a fibroblast populated collagen gel, raised to the air-liquid interface to allow for epidermal stratification. Morphologically, these tissue engineered skin substitutes resemble native skin with a stratified keratinocyte layer on a dermal substrate. However, the dermal-epidermal interface in native skin is marked by a complex interdigitated topography. The keratinocyte layer conforms to the rete ridges and dermal papillae resulting in distinct keratinocyte microniches. The majority of current tissue engineered skin substitutes incorporate a flat interface which lacks this topography. One exception to this is the use of de-epithelialized dermis (DED) for the dermal substrate. Although DED provides topographical cues, it also provides numerous biochemical cues and therefore does not allow for interrogation of

topographical effects in a fully defined model system. As such, there remains a need for a facile model system that facilitates systemic analyses of the cell-cell and cell-matrix interactions that direct keratinocyte stem cell clustering, skin morphogenesis, tissue regeneration and the pathogenesis of disease progression.

The purpose of this study is to create an *in vitro* model system (platform) to evaluate the interactions between keratinocytes and dermal-epidermal junction topography in three dimensions by recreating the physical keratinocyte microniche. An understanding of how these cellular microniches regulate keratinocyte proliferation, migration and differentiation will facilitate the development of a more robust skin model system and aid in the development of the next generation skin substitutes. Recently, we demonstrated that microchannel topography creates distinct keratinocyte functional niches on the surface of 3D micropatterned dermal-epidermal regeneration matrices (μDERMs) using cross-sectional histology and quantitative immunohistochemistry (Clement *et al.*, 2013). While these studies provide important insight into the importance of microtopographic cues, the channel topographies do not fully recreate the dermal papillae structure of the DEJ. We hypothesize that this topographic interface promotes keratinocyte stem cell clustering and directs keratinocyte functions that facilitate epidermal regeneration. To test this hypothesis, our laboratory has developed a facile technique for creating precisely defined micropatterned collagen dermal-epidermal junction templates to study how keratinocytes respond to microtopographical features and cellular microniches. This paper describes the fabrication of these 3D analogs and methods for immunostaining and confocal microscopy to investigate keratinocyte stem cell clustering on DEJ templates that mimic native skin.

5.2 Materials and Methods

5.2.1 Micropatterned DEJ Geometric Design

Two different geometric configurations were explored for whole mount analysis on micropatterned DEJ templates: an array of hexagonal wells and an array of multi-scale hexagonal posts. Hexagonal arrays consisted of 200 μm diameter hexagonal wells separated by 200 μm

plateaus (Figure 5.1). The hexagonal well arrays were used initially to establish whole mount microscopy and immunostaining methods.

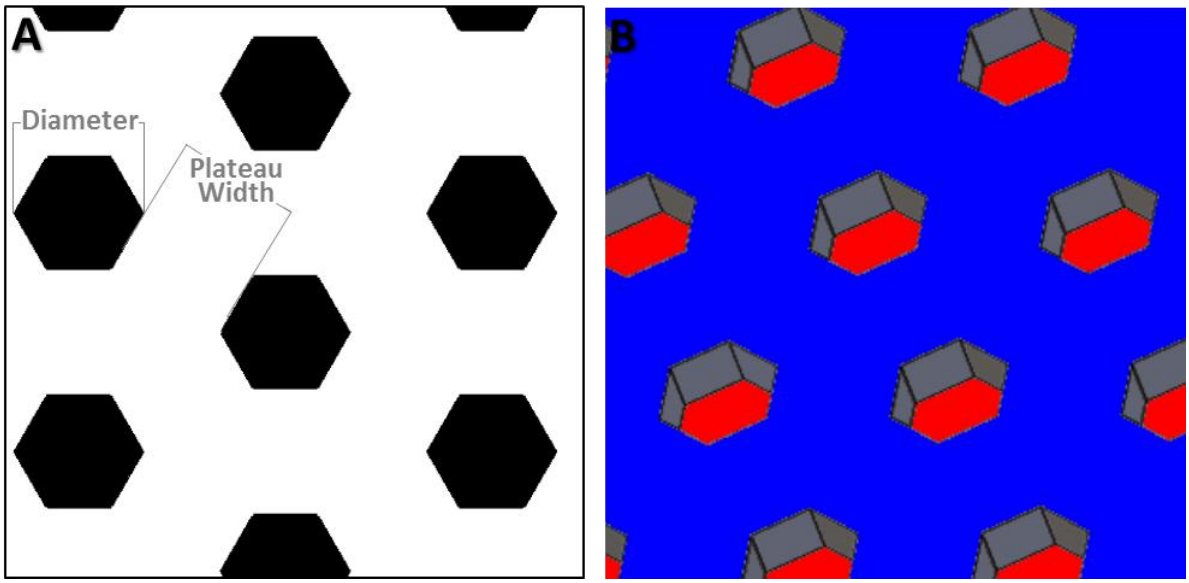

Figure 5.1 Design of Hex-Well DEJ Analogs
(A) Schematic of the photolithography mask used for patterning hexagonal wells (black) separated by plateaus (white) illustrating dimensions. Hex well diameter, plateau width and depth were each specified to be 200µm. (B) 3D rendering of hexagonal well DEJ analog. Hexagonal wells (red) are separated by raised plateaus (blue).

To create topographic features that more closely mimic native tissue architecture, we developed arrays of multi-scale hexagonal posts that mimicked the dermal papillae of the DEJ, using dimensions identified by our histological analyses presented in Chapter 4 (Figure 5.2). Specifically, large 400 µm and small 54 µm posts (LP and SP respectively) were separated by both wide (200 µm) and narrow (50 µm) channels (WC and NC respectively) in order to incorporate both synthetic and proliferative keratinocyte niches.

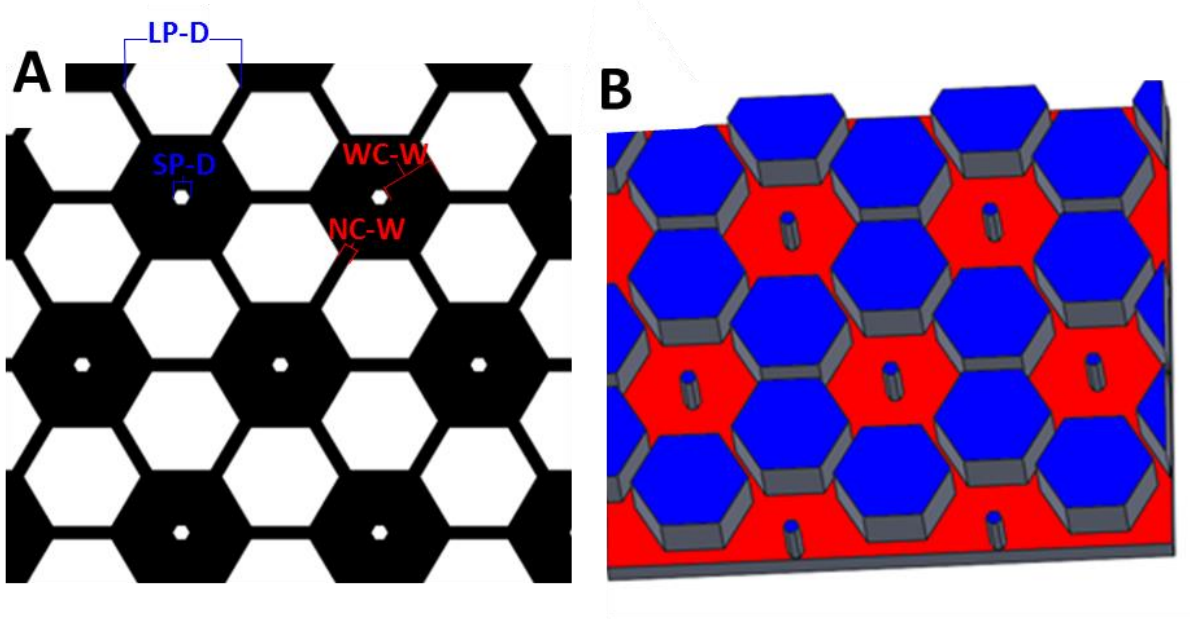

Figure 5.2 Design of Dermal Papillae Analogs (A) Schematic of the photolithography mask used for patterning hexagonal papillae (white) separated by channels (black) illustrating channel dimensions. LP-D = Large papilla diameter. SP-D = Small papilla diameter. WC-W = Wide channel width. NC-W = Narrow channel width. (B) 3D rendering of dermal papillae analogs. Papillae tops are shown in blue and channel bottoms in red.

5.2.2 Fabrication of Micropatterned DEJ Templates

Micropatterned DEJ templates were created by polymerizing type I collagen on a patterned negative mold as illustrated in Figure 5.3.

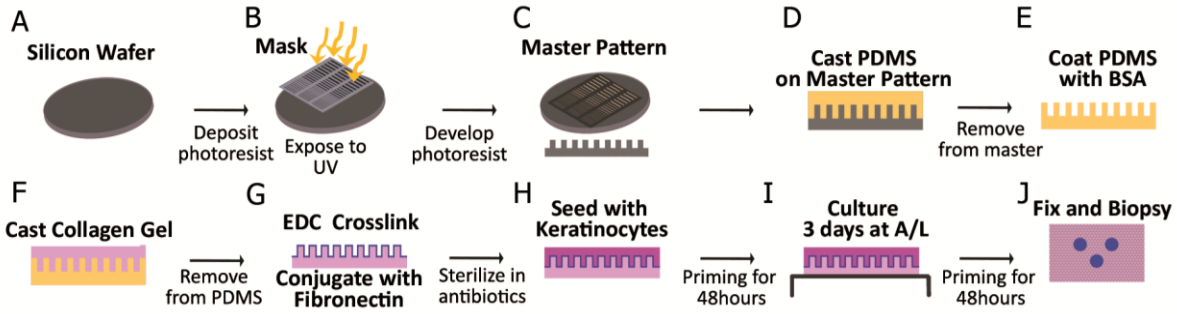

Figure 5.3 DEJ Analog Fabrication. Photolithography was used to create a silicon wafer with microtopographic features resembling the DEJ (A-C). Polydimethylsiloxane silicone elastomer (PDMS, 10:1 base to curing agent; Sylgard184; Dow Corning) was cured on the wafer's surface creating a negative mold (D). PDMS is coated with 1% BSA (E) and then type I collagen was self-assembled on the micropatterned molds (F). DEJ analogs were crosslinked with 5mM EDC, conjugated with fibronectin (FN, 32 μg/cm^2) and sterilized in antibiotics (G). Then the micropatterned DEJ surface was seeded with keratinocytes (H) and following 48 hours, submerged culture, DEJ analogs were raised to the air-liquid interface. (I) Finally, DEJ analogs were fixed and punch biopsies were acquired for IHC analysis.

Specifically, a master silicon wafer with hexagonal papillae separated by narrow channels and wide hexagonal wells was generated using photolithography. Hexagonal papillae were designed with a diameter of 400um, spacing of 50 μm and a depth of 200 um (Figure 5.2A). Polydimethylsiloxane silicone elastomer (PDMS, 1:10 base to curing agent) was poured over the silicon master, degassed under vacuum and then polymerized at 60 °C to create a negative mold. PDMS molds were coated in 1% bovine serum albumin for 30 minutes, rinsed in phosphate buffered saline (PBS) and air dried.

Type 1 collagen was extracted and purified from rat tail tendons (tissue harvested from animals euthanized for other IACUC approved protocols at Worcester Polytechnic Institute) according to previously published methods. Collagen was lyophilized and resuspended in 5mM HCL at 10 mg/ml. 0.8 ml of collagen was neutralized with 5x Dulbecco's Modified Eagle Medium (DMEM) with 0.22 M $NaHCO_3$ and 0.1 N NaOH, cast onto PDMS molds and then polymerized at 37°C overnight. Following polymerization, the DEJ matrices were carefully removed from the molds and cross-linked with 5mM 1-ethyl-3-(3-dimethylaminopropyl) carbodiimide hydrochloride (EDC) for 4 hours at room temperature. DEJ matrices were then passively adsorbed with 32 μg/cm^2 fibronectin overnight. Finally, DEJ matrices were sterilized in an antibiotic cocktail (100 IU/ml-100 μg/ml penicillin-streptomycin, 2.5 μg/ml amphotericin B, 10 μg/ml ciprofloxacin, 100 μg/ml gentamycin) for 24 hours in preparation for keratinocyte culture.

5.2.3 Cell Culture and Media Formulations

Using previously described methods, primary neonatal human foreskin keratinocytes (NHKs) were isolated from foreskins obtained as non-identifiable discard tissue from the University of Massachusetts Memorial Medical Center (Worcester, MA) and approved with exempt status from the New England Institutional Review Board. Prior to experimental use, keratinocytes were cultured on a feeder layer of mitomycin C treated J2s (generously donated by Dr. Stelios Andreadis, State University of New York at Buffalo, Buffalo, NY). NHKs were cultured in a 3:1 blend of high glucose DMEM and Ham's F12 with 10% fetal bovine serum and 1% penicillin–streptomycin supplemented with adenine (1.8×10^{-14} M), cholera toxin (10^{-10} M), hydrocortisone

(0.4 μg ml^{-1}), insulin (5 μg ml^{-1}), transferrin (5 μg ml^{-1}) and triiodo-L-thyronine (2×10^{-9} M). After initial NHK plating, medium was replaced with NHK medium containing 10 ng ml^{-1} epidermal growth factor (EGF). Keratinocytes were seeded onto DEJ matrices in seeding medium, a 3:1 blend of high glucose DMEM and Ham's F12 with 1% fetal bovine serum and 1% penicillin–streptomycin supplemented with cholera toxin (10^{-10} M), hydrocortisone (0.2 μg ml^{-1}), insulin (5 μg ml^{-1}) and ascorbic acid (50 μg ml^{-1}). Following seeding the medium was replaced with priming medium (seeding medium supplemented with 24 μM BSA, 25 μM oleic acid, 15 μM linoleic acid, 7 μM arachidonic acid, 25 μM palmitic acid, 10 μM L-carnitine and 10 mM L-serine). For air–liquid interface (A/L) culture, DEJ matrices were cultured in serum-free priming medium supplemented with 1 ng ml^{-1} EGF. Both keratinocytes and seeded matrices were maintained at 37°C and 10% CO_2.

5.2.4 Micropatterned DEJ Matrix Seeding

Following detachment with 0.05% trypsin, NHKs were spun down, resuspended in seeding medium and seeded on micropatterned DEJ matrices at a density of $2.5x10^5$ cells/cm^2 for 2 hours. Following incubation, unattached cells were rinsed off and cell-seeded matrices were cultured overnight submerged in seeding medium. Seeding medium was then replaced with priming medium for 48 hours at which point the DEJ matrices were raised to the A/L interface for up to 3 days with daily medium exchanges.

5.2.5 Verification of Topgraphical Features of Micropatterns

Quantitative light microscopy was used to validate the dimensions of micropatterned DEJ. Matrices were imaged using a Nikon Eclipse TS100 inverted microscope and images were acquired with an RT Color Spot camera (Diagnostic Instruments). Hexagonal well and post diameter was determined by averaging the length of the three diagonals. Well spacing was determined by taking the average of the distance between each well edge and its nearest neighbor (Figure 5.2b). Measurements were taken of at least 30 wells on 3 scaffolds. Well depth was estimated using z-stacks obtained with confocal microscopy.

5.2.6 Analysis of Initial Keratinocyte Seeding on Micropatterned DEJ Matrices

Following the 24 hours seeding period, micropatterned DEJ matrices were fixed in 10% buffered formalin for 1 hour. DEJ matrices were rinsed with PBS and then incubated with Hoechst (20 µg/ml) were placed epidermal side down in a 35 mm diameter glass bottom specimen chamber with a 0.19 mm thick coverslip bottom (MatTek Corporation, Ashland, MA) and imaged using a Leica SP5 point scanning confocal microscope at 10x (dry) or 20x (oil immersion). Z-stack images were acquired throughout the entire thickness of the cell layer. Maximum projections were created from the individual z-stack images for the top plane (plateaus of hexagonal papillae) and the bottom plane (channels and hexagonal wells) as well as the full z-stack.

5.2.7 Immunofluorescent Staining and Image Analysis

Micropatterned DEJ matrices were immunostained for β_1 integrin and p63 to determine the initial seeding distribution of the β_1^{bri} keratinocytes and p63+ keratinocytes on micropatterns using methods protocols were adapted from methods previously published by Jensen *et al* (Jensen *et al.*, 1999). Briefly, the constructs were fixed in 10% buffered formalin for 2 hours at room temperature and then rinsed with PBS. A 5mm biopsy punch was used to take up to 3 samples from the centers of each graft for immunostaining. Samples were blocked and permeablized in permeabilization buffer comprised of 0.25% gelatin from cold water fish skin (Sigma), 0.5% skim milk, 0.5% Triton X-100 (Sigma) in 20mM HEPES with 0.9% sodium chloride (pH 7.2) for 30 minutes on a shaker plate. Following permeabilization, micropatterned DEJ matrices were incubated overnight on a shaker plate at room temperature in either mouse anti-human β_1 integrin primary (P5D2; Developmental Studies Hybridoma Bank) or rabbit anti-human p63 (H-137, Santa Cruz) diluted 1:200 in permeabilization buffer. Following three exchanges of PBS with 0.2% Tween20, samples were rinsed in PBS+Tween for 4 hours on a shaker plate with exchanges every 20 minutes. Then samples were incubated in species matched secondary antibody (goat anti-mouse or goat anti-rabbit AlexaFluor 568 secondary; Life Technologies) diluted 1:100 in permeabilization buffer overnight at room temperature. To removes unbound secondary, following three exchanges of PBS+Tween, samples were incubated in permeabilization buffer for 2 hours on a shaker plate with exchanges every 20 minutes, overnight

on the shaker plate, and then rinsed for an additional 2 hours with exchanges every 20 minutes. Samples were then stained with Hoechst (20µg/ml) and incubated overnight in permeabilization buffer before imaging.

5.3 Results

5.3.1 Micropatterned Collagen Matrices Replicate Patterns on Negative Replicates

Micropatterned collagen matrices were generated by polymerizing a type 1 collagen gel on a PDMS replicates. Micropatterns were designed with either hexagonal wells or hexagonal papillae. For hexagonal well matrices, the specified well diameter was 200µm while the measured diameter was 211.4 µm. The specified depth was 200µm while the measured depth 103.8µm (Figure 5.4).

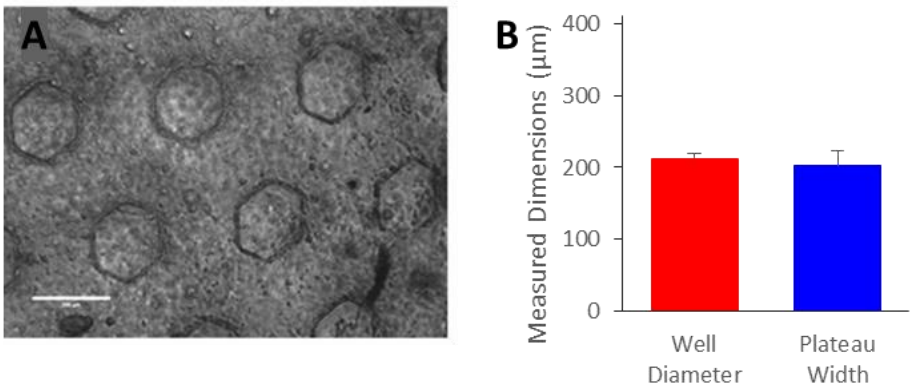

Figure 5.4 Characterization of hexagonal well DEJ analogs. (A) Bright field image of hexagonal well DEJ analog. Scale bar = 250 µm. (B) Measured dimensions of hexagonal wells patterned on collagen gels. The measured dimensions approximated the specified dimensions (200 µm diameter hexagonal wells separated by 200 µm plateaus).

For hexagonal papillae matrices, the specified papillae diameters were 400µm and 54 µm and the specified channel dimensions were 50µm and 200µm. Due to challenges patterning the tall, narrow 54 µm papillae, these structures did not pattern on all µDERM. This resulted in larger hexagonal wells instead of the specified 200µm annular channels. For fully patterned papillae matrices, actual papillae widths were measured at 50.9 µm and 388.1 µm separated by channels measured at 42.1 µm and 186.6 µm. In absence of the smaller papillae, the measured diameter of the resulting hexagonal well was 476.7 µm. Ultimately, patterned papillae matrices still contained both narrow proliferative niches and wide synthetic niches. Similar to the hexagonal

well matrices, the specified depth was 200µm but the measured depth was only 129 µm, approximately half the designated depth (Figure 5.5).

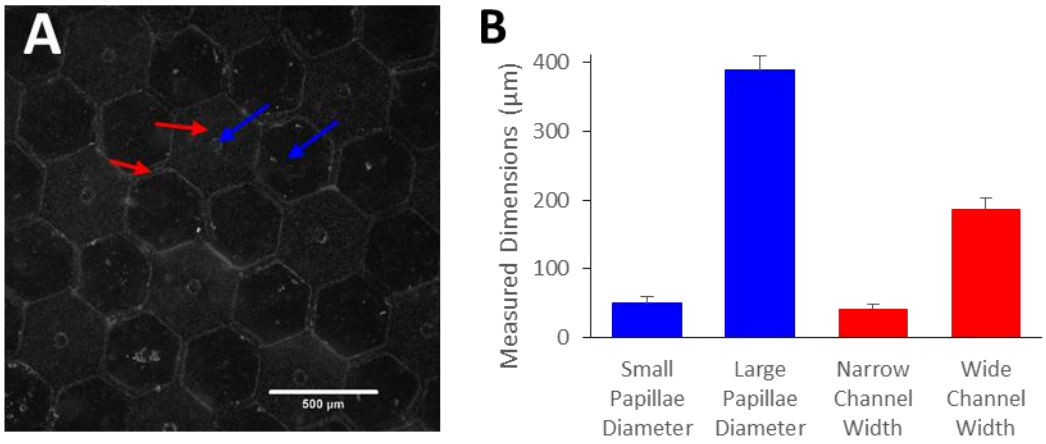

Figure 5.5 Characterization of dermal papillae DEJ analogs. (A) Bright field image of dermal papillae analog. Scale bar = 500 µm. (B) Measured dimensions of hexagonal papillae (blue) and channels (red) patterned on collagen gels. The measured dimensions approximated the specified dimensions.

5.3.2 Keratinocytes Conform to the Topography of Micropatterned DEJ Analogs

In order to assess our ability to study cellular response to micropatterned collagen matrices, keratinocytes were seeded at a density of 2.5 x 10^5 cell/cm^2 on micropatterned matrices for 24 hours. Seeded cells conform to the topography of the micropatterned collagen matrices and approximate a monolayer. Figure 5.6 and Figure 5.7 show confocal images of keratinocytes on micropatterned matrices. Notably, instead of filling the wells, cells formed a confluent monolayer on the top surface of the matrices and on the well and channel bottoms of the matrices. Initially, the false color max projection of Figure 5.6C seems to show that multiple layers of keratinocytes may be present within the narrow microchannels. However, examination of the sides of the wide hexagonal wells and the full z-stacks suggests that these multiple layers simply represent a uniform monolayer of keratinocytes on the vertical surface of the channels.

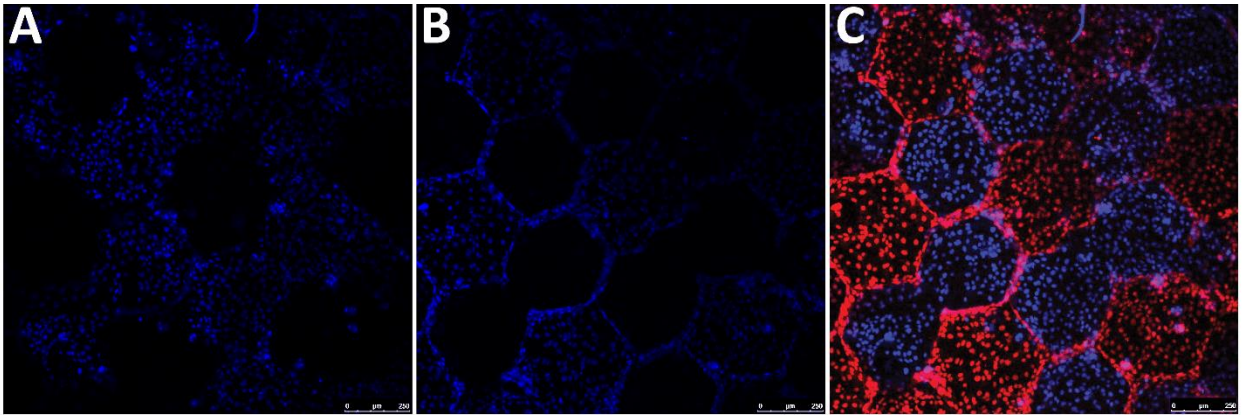

Figure 5.6 Confocal microscopy images of keratinocytes seeded on micropatterned papillae DEJ analogs for 24 hours. (A) Max projection of Z-stack of the top plane (papillae plateaus). (B) Max projection of Z-stack of the bottom plane (channel bottoms). (C) False color max projection of the complete Z-stack with the bottom plane (channel bottoms) displayed in red and the remaining planes displayed in blue.

These observations are confirmed through examination of keratinocytes seeded on hexagonal well DEJ analogs (Figure 5.7). Examination of the 3D rotation shows keratinocytes along the bottoms and sides of the wells (B) while the holes in the top plane (D) indicate the keratinocytes do not fill the wells, but rather formed a monolayer conforming to the surface topography.

5.3.3 Keratinocytes Expressing High Levels of β_1 Integrin Localize to Hexagonal Wells after 24 Hours A/L Culture

Following 24 hours of culture at the A/L interface, micropatterned hexagonal well DEJ analogs were fixed and immunostained for β_1 integrin and imaged using confocal microscopy (Figure 5.8). β_1 integrin is expressed on the cell membrane of keratinocytes in the basal layer. In particular, β_1 integrin expression is increased in keratinocytes at the bottoms of hexagonal wells and on plateaus near wells. This is more readily apparent when images are false colored to indicate areas of high β_1 integrin expression (blue; Figure 5.9 B and D)

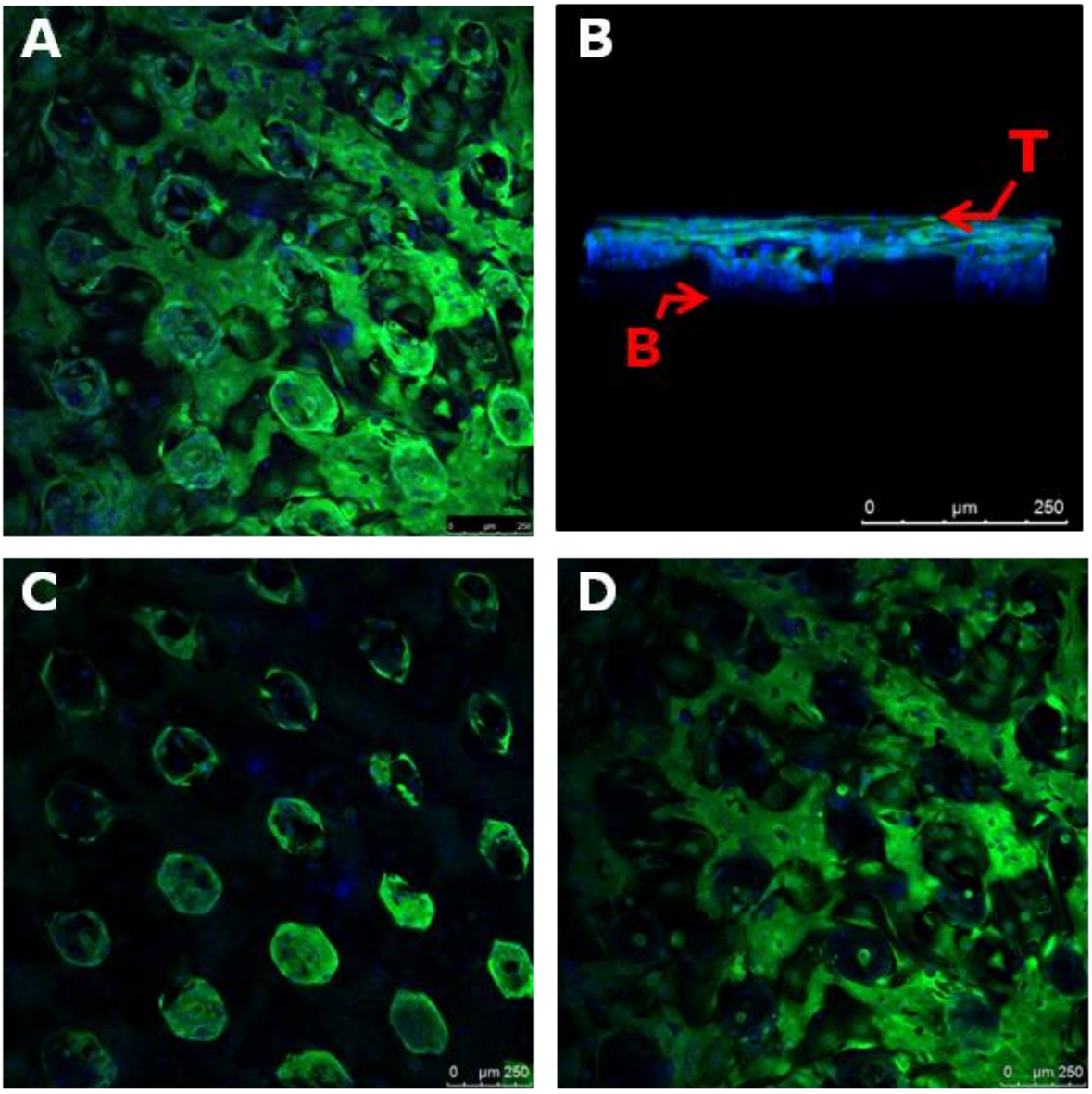

Figure 5.7 Keratinocytes seeded on micropatterned DEJ containing hexagonal wells for 24 hours approximate a monolayer. Keratinocytes were loaded with calcein AM (green) and stained with Hoechst (blue). (A) Confocal max projection of keratinocytes seeded on hexagonal wells. (B) 3D rotation of confocal Z-stack. T and B indicate the top and bottom of the construct respectively. (C) Max projection of bottom plane (well bottoms). (D) Max projection of top plane (plateaus).

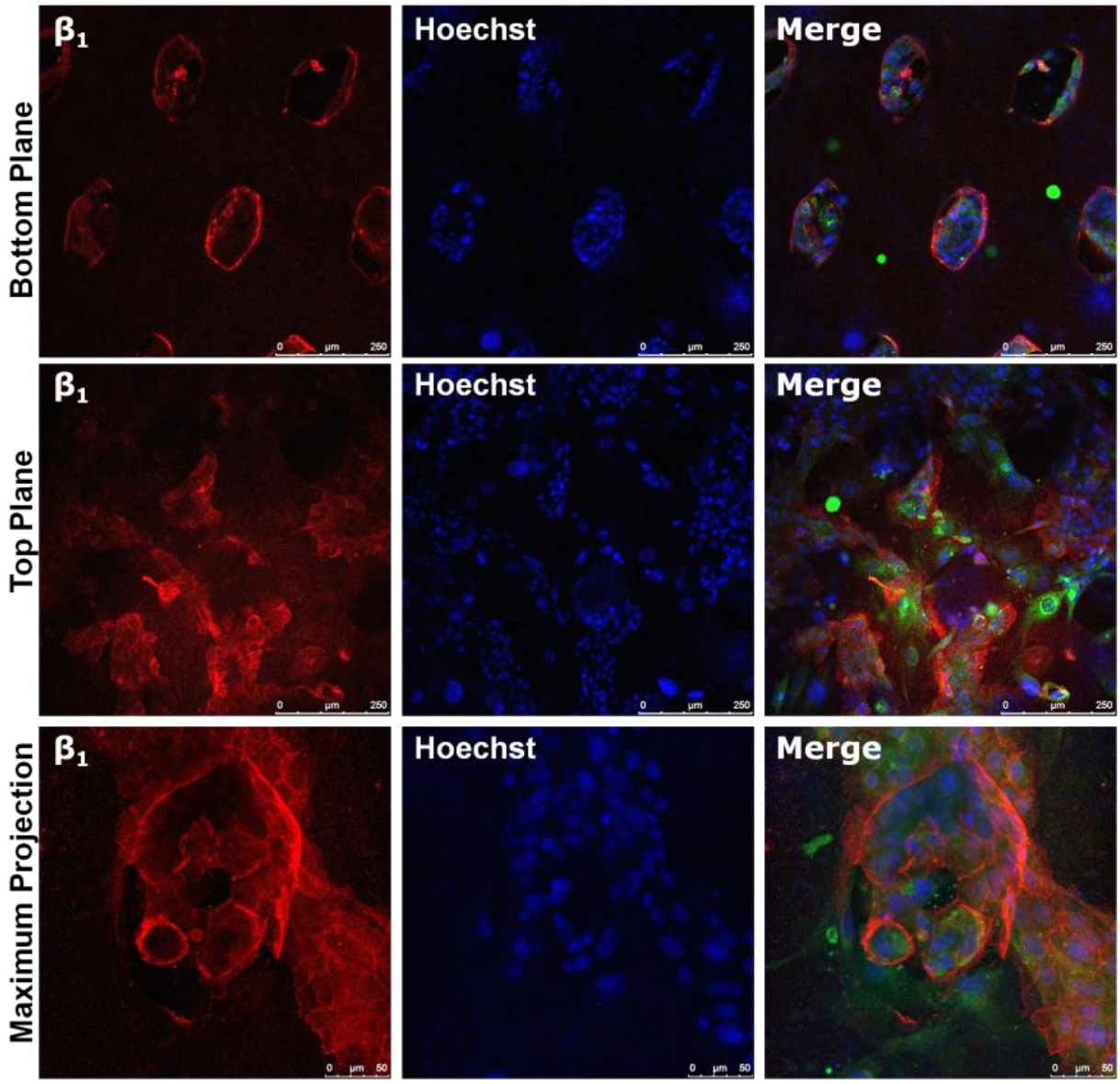

Figure 5.8 β_1 integrin expression in keratinocytes cultured at the A/L interface on DEJ containing hexagonal wells for 24 hours. β_1 integrin (red), Hoechst (blue) and calcein (green) labeled keratinocytes. Maximum projection (bottom row) shown at higher magnification. β_1 integrin expression is observed on the cell membrane of basal keratinocytes, especially those located within or near hexagonal wells.

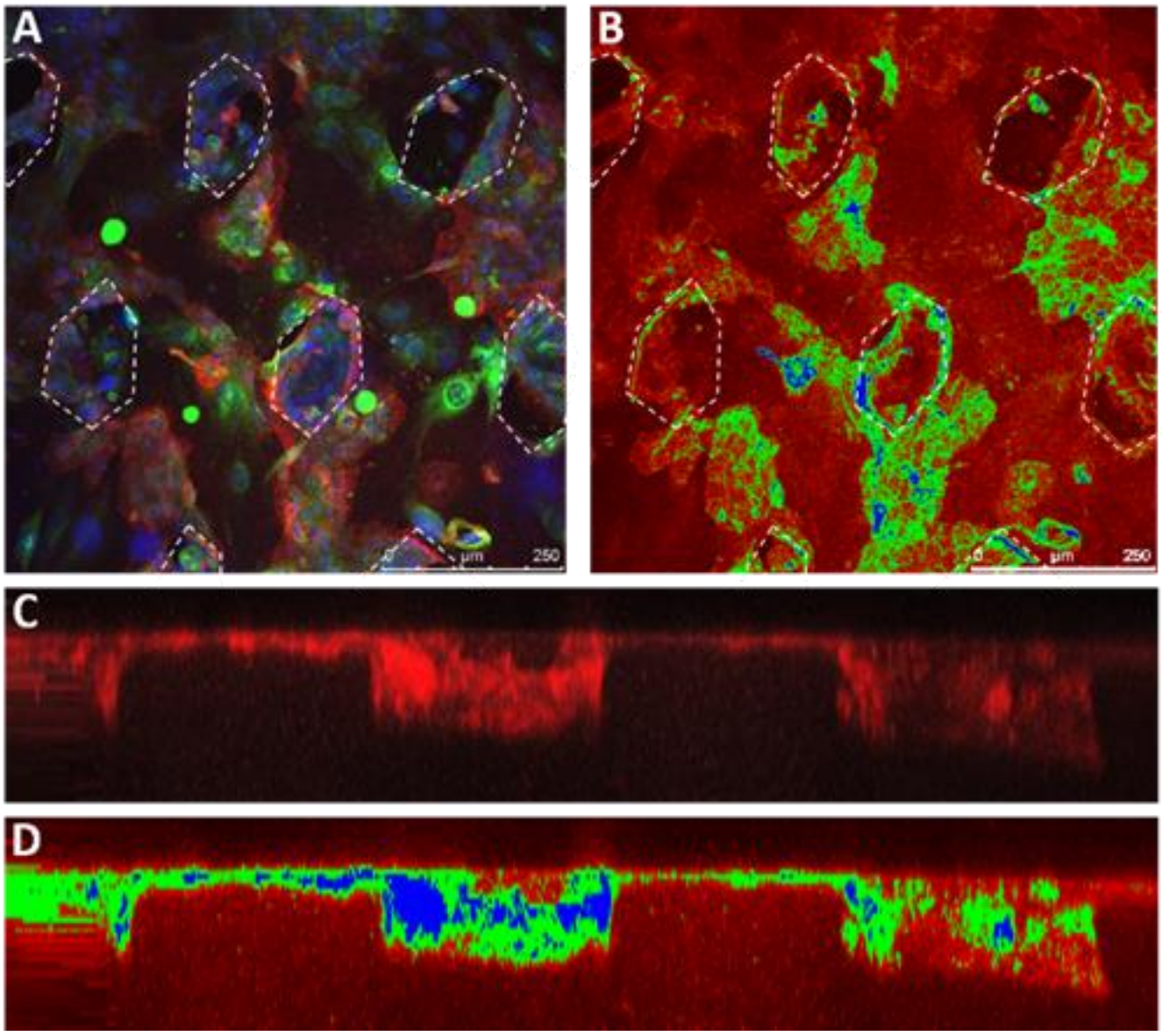

Figure 5.9 False colorization of β1 integrin expression in keratinocytes seeded on DEJ analogs containing hexagonal wells. (A) Maximum projection of true color image. (B) False color image of β_1 integrin expression indicating areas of high (blue), mid (green) and low (red) β_1 staining intensity. (C) Cross-section of true color β_1 integrin expression. (D) Cross-section of false-color β_1 integrin expression.

5.3.4 Keratinocytes Expressing High Levels of β_1 Integrin Localize at the Bases of Hexagonal Papillae at 3 Days

After 3 days of culture at the air-liquid interface, seeded matrices were fixed and stained for β_1 integrin. Figure 5.10 shows confocal images of β_1 integrin stained keratinocytes on micropatterned matrices. β_1 integrin expression was confined to the basal layer

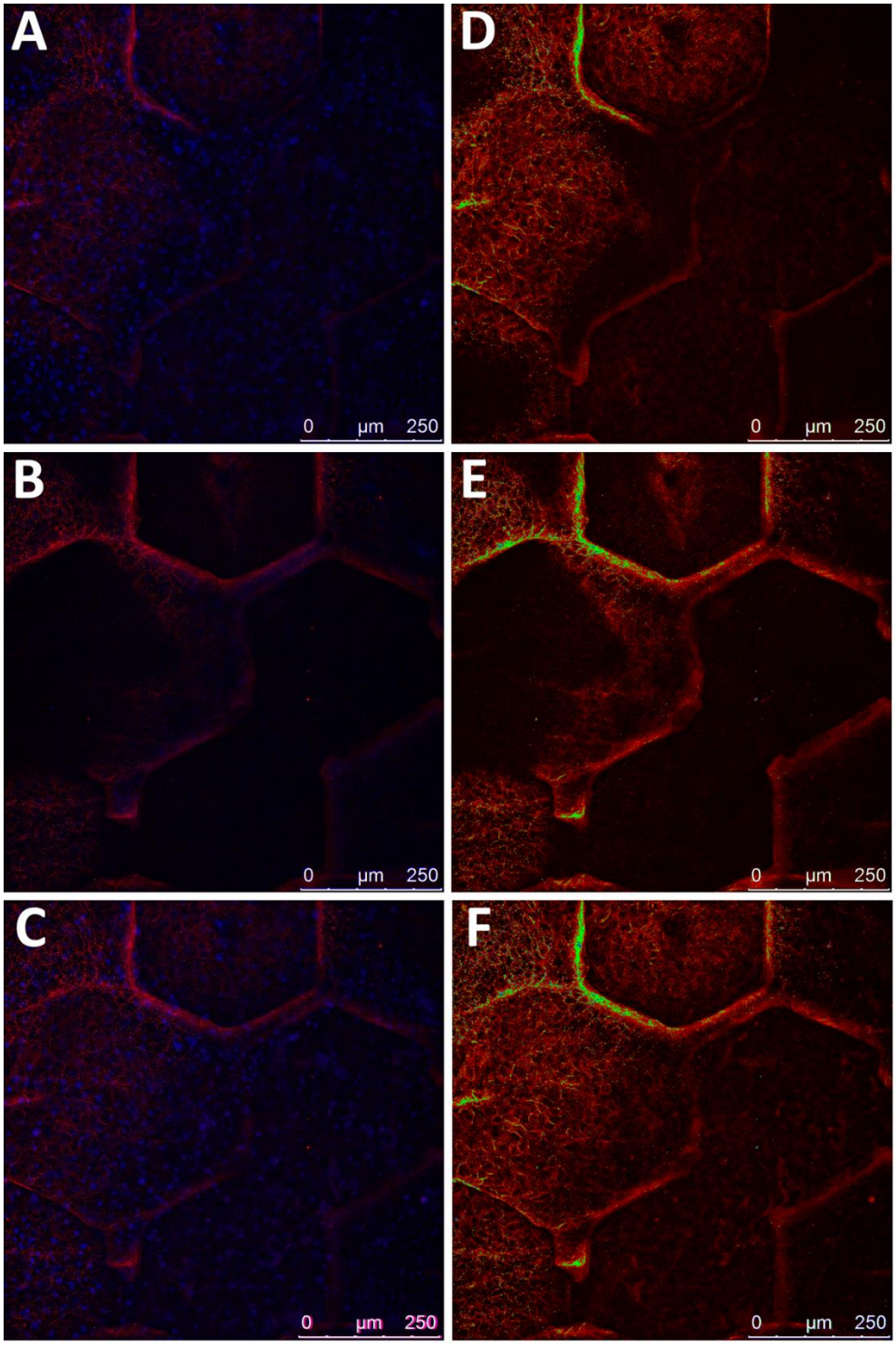

Figure 5.10 β_1 integrin expression in keratinocytes cultured on DEJ analogs containing hexagonal papillae for 3 days at the A/L interface. (A – C) True color image of keratinocytes stained for $\beta_1$integrin expression (red) and labelled with Hoechst (blue). (D-F) False colored imaged of β_1 integrin expression showing high (blue), mid (green) and low (red) levels of β_1 integrin. A and D show the top planes of the confocal Z- stack, including the tops of the papillae through the upper keratinocyte strata. B and E show the bottom planes of the confocal Z-stack including only the bottoms of the hexagonal wells and narrow channels. C and F are max projections of the full confocal Z-stack. β_1 integrin is expressed in keratinocytes located throughout the basal layer, but keratinocytes at the bases of hexagonal papillae and in the bottoms of narrow channels have higher levels of β_1 integrin expression.

of keratinocytes, where the majority of the cells had detectable expression. The areas with the highest β_1 integrin expression are located in the bottoms of microwells and on the top surface of matrices in close proximity to microwells, as illustrated by the presence of blue and green regions on the false colored images (Figure 5.10 D-F).

5.3.5 $p63^+$ Keratinocytes are Found in the Basal Layer

To further investigate keratinocyte clustering on DEJ analogs, we examined p63 expression on analogs containing hexagonal papillae. Although p63 expression was confined to the basal layer, the majority of basal keratinocytes stained positive for p63, with no discernable patterning. Notably, despite the relative uniformity in the distribution of p63+ nuclei within the basal layer, the keratinocytes in narrow channels appeared to express higher levels of p63 compared to the keratinocytes located on plateaus or wider channels.

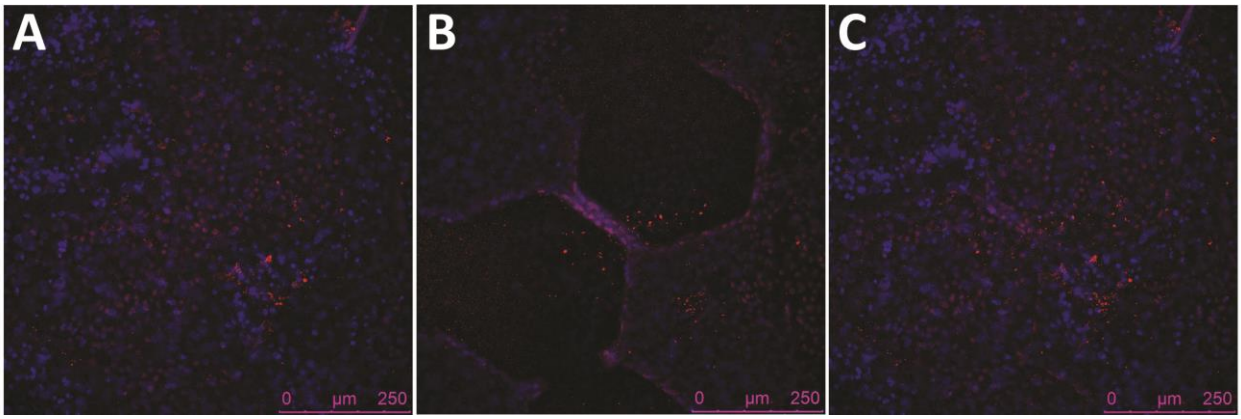

Figure 5.11 p63 Expression on Dermal Papillae Analogs. Max projections of top plane. (A), bottom plane (B) and full stack (C) of confocal z-stack. p63+ keratinocytes are located in the basal layer both in channels and on hexagonal papillae.

5.4 Discussion

The development of both the next generation clinical skin substitutes and advanced *in vitro* skin models for drug screening and the study of wound healing and disease pathogenesis requires a greater understanding of how topographic cues drive cellular function. Ultimately, incorporating these cues in a logical and precise manner will allow for skin substitutes that more closely mimic native skin and provide more physiologically relevant data. Previously, we utilized topographic features to drive keratinocyte clustering in proliferative (narrow), synthetic (wide) and $\beta_1^{bri}p63^+$

(corners) keratinocyte niches. However, these results were obtained through analysis of 2D histological sections. In order to more fully understand the organization of keratinocytes in three-dimensions, it is beneficial to characterize the distribution of keratinocyte sub-populations across the entire basal surface. To this end we have developed a novel method for whole mount analysis of keratinocyte responses to microtopographical features. Using this model system, we have shown that clustering of β_1^{bri} keratinocytes in channels is apparent following only 3 days of A/L culture and some clustering may be observed as early as 1 day. Further, these results support our previous histological findings that β_1^{bri} keratinocytes cultured on μDERM aggregate in narrow channels and channel corners.

Whole mount analysis with confocal microscopy can provide a more complete picture of cellular distribution on micropatterned templates than cross-sectional analysis because it is not limited to only a small section of the construct. Fluorescent labeling of cells in conjunction with fluorescently labeled immunostaining provides a way to easily visualize the topographical localization of keratinocyte subpopulations. Additionally, in the future these confocal methods can be adapted to provide for non-destructive graft imaging.

We have used this method to demonstrate preferential clustering of β_1 integrin bright keratinocytes near hexagonal microwells at 1 day and in both narrow microchannels and corners of wide wells at the base of hexagonal papillae after 3 days culture at the air-liquid interface. Additionally, we have demonstrated p63 expression throughout the basal compartment. These results support our conclusion in Chapter 4 that DEJ topography creates keratinocyte stem cell microniches.

It is interesting that we observed β_1 integrin bright keratinocyte clustering on the top surface of micropatterned templates near the well openings as well as in the corners of wells. In our histological analyses of keratinocytes seeded on microchannel topographies (Chapter 4), we demonstrated clustering in the bottoms of channels after 7 days air-liquid culture, but did not note clustering in the proximity of channels. One possible explanation for this is that cross-sectional analysis of skin grafts is limited to a 2-D interpretation of our 3-D constructs, limiting

our ability to fully observe the clustering phenomenon. Another possibility is that there is a temporal dependence to the clustering phenomenon and that at longer time points clustering is limited to the bottoms of wells. This would suggest that the mechanism for clustering is either cellular migration to preferential locations or phenotypic switch based on location as opposed to cellular segregation upon initial seeding due to topography. Further studies in both our cross-sectional and whole mount analysis systems are necessary to completely elucidate this phenomenon. One advantage of confocal imaging is that it allows for non-destructive imaging of the DEJ analogs. In the future, this may allow us to perform temporal analysis of keratinocyte clustering on a single construct through cellular tracking. One strategy would be to seed genetically modified keratinocytes engineered to express GFP tagged β_1 integrin onto the DEJ analogs. These constructs could then be imaged over time to determine whether or not β_1^{bri} keratinocytes are localized to microniches upon initial seeding. Analysis of initial β_1^{bri} keratinocyte seeding patterns is of particular interest because β_1 integrin expression is involved in the regulation of keratinocyte adhesion (Levy *et al.*, 2000) and therefore may contribute to the phenomenon of putative keratinocyte stem cell clustering observed in our μDERM and DEJ analog cultures.

Interestingly, while p63 expression was confined to the basal layer, the majority of basal cells were $p63^{+}$ with not observable clustering of $p63^{+-}$ cells in wells or channels. This is in contrast to our 7 day A/L cross-sectional data presented in Chapter 4. This expression profile may be indicative of an immature basal layer that has not yet attained steady state. Rather at 3 days, the basal keratinocytes cultured on DEJ analogs remain in an activated proliferative state. Additionally, previous studies have shown that the $p63^{+}$ keratinocyte population can be enriched through selective adherence using type IV collagen (Radu *et al.*, 2002). Previous work also suggests that $\alpha_6^{bri}10G7^{dim}$ keratinocytes, putative keratinocyte stem cells, rapidly adhere to collagen I substrates (Kaur and Li, 2000). Although it was determined that the rapidly adhering cells were not exclusively stem cells, the short attachment time used in our experiments may lead to an enrichment of the p63+ phenotype in the basal layer at early time points. Future studies will examine additional time points to elucidate the temporal relationship of keratinocyte

stem cell clustering. In particular, we will look at the p63 expression pattern on 7 day DEJ analogs to determine if they replicate the clustering observed in the histological analysis of the µDERM model.

Importantly, this chapter establishes a method for the whole mount analysis of keratinocytes seeded on micropatterned substrates. This provides a valuable platform for assessing the role of 3D topographic microniches in regulating cellular function. Here we examine the role of topography in keratinocyte stem cell clustering but in the future this method can be used to further characterize the formation of the proliferative and synthetic keratinocyte microniches *in vitro*.

Additionally, although here we used immunohistochemistry on fixed DEJ analogs, in the future this method can be modified to provide for non-terminal live cell imaging. This will allow us to look at the temporal dependence of keratinocyte clustering. In particular, we can use this system to evaluate keratinocyte re-epithelialization in response to a cryoburn *in vitro* by tracking calcein loaded keratinocytes. This will provide greater insight into how microtopography can direct keratinocyte migration and proliferation. Further, this platform can be used to assess the response of other cell types to microtopographic features. In particular, the epithelium of the gastrointestinal tract features basement membranes with distinct topographic features (Barrett and Rabould, 2008).

5.5 Acknowledgments

This research was funded by the NIH (EB-005645). Special thanks to Dr. Mehmet Toner and Octavio Hurtado at the BioMicroElectroMechanical Systems (BioMEMS) Resource Center, Massachusetts General Hospital, Boston, MA (NIH Grant: P41 EB02503 [MT]) and Professor Anjana Jain at WPI, for their assistance with the microfabrication processes. I would like to thank my advisor, Professor George Pins, for his scientific contribution to the work. I would also like to thank Vicki Huntress for confocal assistance, Jen Molignano, Tom Moutinho, Kathryn Volk and MacKenzie Brandes for laboratory assistance, and the Department of Obstetrics and Gynecology at UMMS (Worcester, MA) for providing us with neonatal foreskins for keratinocyte isolations.

5.6 References

Barrett K and Rabould H (2008) Functional Anatomy and General Principles of Regulation in the Gastrointestinal Tract. In: *Berne and Levy Physiology* (Koeppen B, Stanton B, eds), Philadelphia, PA: Elsevier, 487-95.

Bellas E, Seiberg M, Garlick J and Kaplan DL (2012) In Vitro 3d Full-Thickness Skin-Equivalent Tissue Model Using Silk and Collagen Biomaterials. *Macromol Biosci* 12:1627-36.

Clement AL, Moutinho T and Pins GD (2013) Micropatterned Dermal-Epidermal Regeneration Matrices Create Functional Niches That Enhance Epidermal Morphogenesis. *Acta Biomater* 9:9474-84.

Gotz C, Pfeiffer R, Tigges J, Blatz V, Jackh C, Freytag EM, Fabian E, Landsiedel R, Merk HF, Krutmann J, Edwards RJ, Pease C, Goebel C, Hewitt N and Fritsche E (2012a) Xenobiotic Metabolism Capacities of Human Skin in Comparison with a 3d Epidermis Model and Keratinocyte-Based Cell Culture as in Vitro Alternatives for Chemical Testing: Activating Enzymes (Phase I). *Exp Dermatol* 21:358-63.

Gotz C, Pfeiffer R, Tigges J, Ruwiedel K, Hubenthal U, Merk HF, Krutmann J, Edwards RJ, Abel J, Pease C, Goebel C, Hewitt N and Fritsche E (2012b) Xenobiotic Metabolism Capacities of Human Skin in Comparison with a 3d-Epidermis Model and Keratinocyte-Based Cell Culture as in Vitro Alternatives for Chemical Testing: Phase Ii Enzymes. *Exp Dermatol* 21:364-9.

Groeber F, Holeiter M, Hampel M, Hinderer S and Schenke-Layland K (2011) Skin Tissue Engineering--in Vivo and in Vitro Applications. *Adv Drug Deliver Rev* 63:352-66.

Haycock JW (2011) 3d Cell Culture: A Review of Current Approaches and Techniques. *Methods Mol Biol* 695:1-15.

Huang S, Xu Y, Wu C, Sha D and Fu X (2010) In Vitro Constitution and in Vivo Implantation of Engineered Skin Constructs with Sweat Glands. *Biomaterials* 31:5520-5.

Jensen UB, Lowell S and Watt FM (1999) The Spatial Relationship between Stem Cells and Their Progeny in the Basal Layer of Human Epidermis: A New View Based on Whole-Mount Labelling and Lineage Analysis. *Development* 126:2409-18.

Justice BA, Badr NA and Felder RA (2009) 3d Cell Culture Opens New Dimensions in Cell-Based Assays. *Drug Discov Today* 14:102-7.

Kaur P and Li A (2000) Adhesive Properties of Human Basal Epidermal Cells: An Analysis of Keratinocyte Stem Cells, Transit Amplifying Cells, and Postmitotic Differentiating Cells. *J Invest Dermatol* 114:413-20.

Levy L, Broad S, Diekmann D, Evans RD and Watt FM (2000) Beta1 Integrins Regulate Keratinocyte Adhesion and Differentiation by Distinct Mechanisms. *Mol Biol Cell* 11:453-66.

Pampaloni F, Reynaud EG and Stelzer EH (2007) The Third Dimension Bridges the Gap between Cell Culture and Live Tissue. *Nat Rev Mol Cell Biol* 8:839-45.

Radu E, Simionescu O, Regalia T, Dumitrescu D and Popescu LM (2002) Stem Cells (P63(+)) in Keratinocyte Cultures from Human Adult Skin. *J Cell Mol Med* 6:593-8.

Chapter 6: µDERM Enhance Wound Healing *In Vivo*

6.1 Introduction

Wound healing is a multi-billion dollar market with over 4 million traumatic and chronic skin wounds treated annually in the United States alone (American Burn Association, 2007, 2013; Sen *et al.*, 2009). While several composite skin and dermal substitutes have achieved some clinical success in restoring damaged skin, limited mechanical stability, sub-optimal wound healing, infection, scarring and prolonged healing times remain persistent problems. As such, there is a continued need for a bi-layered skin substitute that promotes rapid tissue regeneration (cellular ingrowth and angiogenesis), maintains the mechanical stability of the tissue, and provides barrier function (microbial resistance) for the wound site (MacNeil, 2007; Shevchenko *et al.*, 2010). A common limitation of current skin substitutes is the absence of topography at the dermal-epidermal junction. In Chapters 3-5, we have shown that microtopography increases epidermal thickness and creates microniches that support proliferative and synthetic keratinocyte phenotypes *in vitro.* Although there are 3D *in vivo* models to study skin wound healing (Geer *et al.*, 2004; Vaccariello *et al.*, 1999), currently there are no *in vivo* models available to study how microtopography at the dermal-epidermal junction directs wound healing. To address these needs, we have developed a micropatterned dermal-epidermal regeneration matrix (µDERM) composed of a fibroblast populated collagen-GAG sponge laminated to a micropatterned collagen gel seeded with keratinocytes and cultured at the air-liquid interface to promote epidermal stratification.

In the proposed study, we plan to use a well-established animal model for full thickness wound injuries (Medalie and Morgan, 1999) to evaluate the cellular and tissue responses to these novel skin substitutes. This study aims to validate our *in vitro* findings *in vivo* and establish a model for investigating aspects of wound healing not easily assessed *in vitro,* such as angiogenesis. Additionally, we aim to validate the µDERM model system as an implantable system with an

eventual goal of developing a better clinical skin substitute. To do this, we will compare the implantation of flat and micropatterned μDERMs to cultured de-epithelialized dermis (DED) in a full thickness excisional skin wound on the dorsum of athymic mice. Additionally, we will determine the effect of 1-ethyl-3-(3-dimethylaminopropyl) carbodiimide (EDC) crosslinking concentration on *in vivo* μDERM performance and μDERM topography.

6.2 Materials and Methods

In order to evaluate the formation of functional keratinocyte microniches *in vivo*, μDERMs containing microchannel topography and cultured at the air-liquid interface for 7-10 days were implanted into full thickness wounds on the dorsum of athymic mice.

6.2.1 Fabrication of μDERMs

μDERMs containing a series of parallel channels (200 μm depth) with varying widths (50μm, 100μm, 200μm, 400μm) were fabricated for implantation as described in Chapters 3 and 4 and previously published (Bush and Pins, 2012; Clement *et al.*, 2013; Downing *et al.*, 2005). Briefly, 10 mg/ml collagen I from rat tail tendons was self-assembled on the micropatterned PDMS negative molds using 5x DMEM with 0.22 M $NaHCO_3$ and 0.1 M NaOH for 18 hours (37˚C and 10% CO_2). Following polymerization, a collagen-GAG sponge was laminated to the back of the micropatterned gel using an additional layer of self-assembled collagen I. μDERMs were crosslinked with either 5mM or 60mM 1-ethyl-3-(3-dimethylaminopropyl) carbodiimide (EDC) for 4 hours at room temperature. Crosslinked μDERMs were removed from the PDMS molds and conjugated with 32 μg/cm^2 fibronectin (FN). Prior to cell seeding, μDERMs were sterilized in an antibiotic cocktail (100 IU/ml-100μg/ml penicillin-streptomycin, 2.5μg/ml amphotericin B, 10pg/ml ciprofloxacin, 100μg/ml gentamycin) for a minimum of 24 hours at room temperature.

After rinsing with sterile DMEM, the dermal sponges of the μDERMs were seeded with 8x10^4 neonatal human fibroblasts/cm^2 in 100μl of NHF medium (high glucose DMEM supplemented with 10% FBS and 1% penicillin-streptomycin) and cultured for 48 hours (37˚C, 10%CO_2). μDERMs were then inverted onto air-liquid (A/L) interface culture screens and the micropatterned surfaces were seeded with 5x10^5 keratinocytes/cm^2 in serum free medium for 2 hours. Following

72 hours of submerged culture, µDERM were raised to the air-liquid interface and cultured for 7-10 days with daily medium changes prior to implantation. As a control, de-epidermized dermis (DED) was seeded with keratinocytes and cultured alongside µDERMs, as previously described (Bush and Pins, 2012).

6.2.2 Creation of a Full Thickness Wound and µDERM Implantation

All animal care and experimental procedures were approved by the Worcester Polytechnic Institute Institutional Animal Care and Use Committee and conform to the NIH guidelines for the care and use of laboratory animals. A well-established full-thickness excisional wound model was used for implantation studies (Hamoen *et al.*, 2002; Medalie and Morgan, 1999).

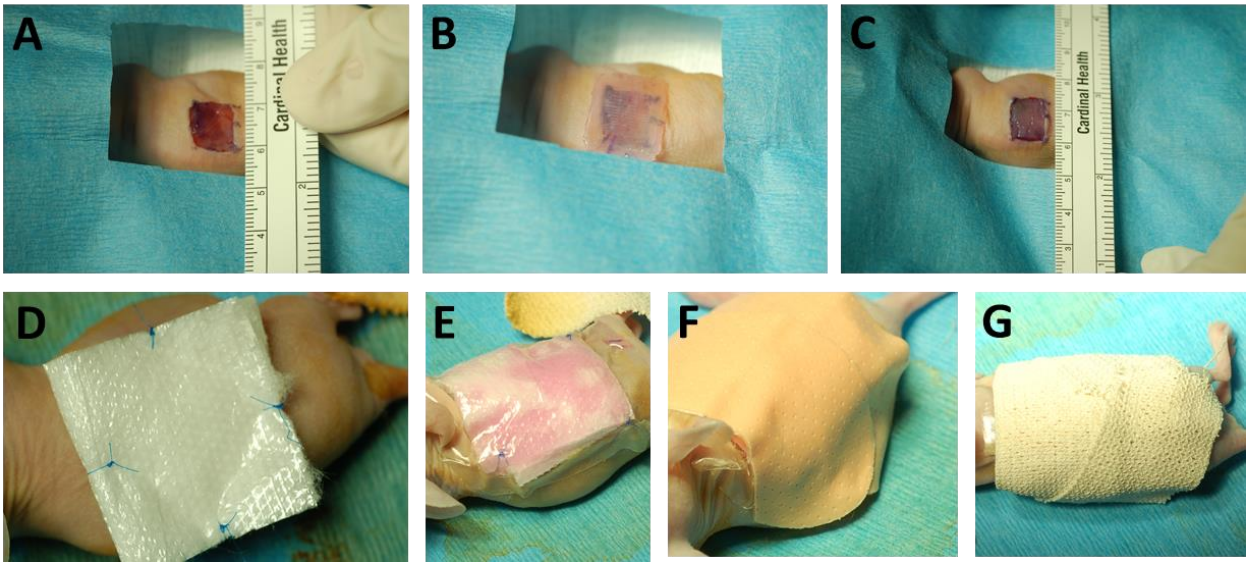

Figure 6.1 Implantation of cultured µDERM. (A) A 1 cm2 square of skin is excised from the dorsal side of the mouse. (B) A graft is placed in the wound bed and (C) trimmed to fit precisely. (D) The graft is covered with two layers of Telfa, the second of which is secured with four sutures. € A layer of Tegaderm is applied to the dressings and injected with keratinocyte medium to maintain moisture. (F) The Tegaderm is covered with a Band-Aid and (G) the mouse is wrapped with flexible sports bandage to prevent graft and dressing cannibalization.

Four to eight week old athymic nude mice (Foxn1^{nu}, Harlan) were anesthetized for the duration of the surgical procedure using continuous isoflurane. After cleaning the surgical site with ethanol and betadine, a 1 cm^2 square region is marked on the mouse's dorsum to the right of the spine and inferior to the shoulder blade. Surgical scissors were used to create the full thickness wound and excise the skin, including the underlying panniculus carnosus (Figure 6.1A). Grafts (microchanneled µDERM, flat µDERM or positive control DED) were placed in the wound bed and

trimmed to size (Figure 6.1 B and C). Grafts were covered by a piece of Telfa (Kendall Brands, Mansfield, MA) coated with triple antibiotic (Neosporin, Johnson and Johnson, New Brunswick, NJ). A second Telfa dressing was layered over the first and secured with a minimum of one suture (6-0 Prolene, Securos, Fiskdale, MA) on each side (Figure 6.1D). The skin surrounding the Telfa was coated with adhesive tincture of Benzoin and then a piece of occlusive Tegaderm (3M, St. Paul, MN) was used to seal the graft site. In order to keep the grafts moist and provide nutrient support prior to engraftment, keratinocyte medium was injected through the Tegaderm immediately following surgery and daily thereafter (Figure 6.1E). Finally, to further secure the graft and dressings, a Band-Aid (Johnson and Johnson, New Brunswick, NJ) was sutured over the Tegaderm layer and the mouse was wrapped in a flexible adhesive bandage (Figure 6.1F and G). Buprenorphine was supplied in the drinking water (0.02 mg/ml) for 48 hours post surgery.

In order to assess µDERM performance *in vitro*, multiple types of grafts were evaluated: DED (positive control), flat µDERM, and µDERM containing microchannels. Additionally, based on previous studies by Powell and Boyce (Powell and Boyce, 2007), we were concerned about the high concentration of EDC (60 mM) used for crosslinking during the fabrication of our µDERM. Therefore, the EDC concentration was reduced to 5 mM for flat µDERM. Due to concerns about the effect of a lower EDC concentration on micropattern fidelity, microchanneled µDERM were crosslinked with either 5 mM or 60 mM EDC. This setup is detailed in Figure 6.1.

Table 6.1 Experimental group design for implantation studies.

	EDC Concentration	Number of Mice
DED	N/A	4
Flat µDERM	5 mM	2
Microchanneled µDERM	5 mM	3
	60 mM	3

6.2.3 Characterization of the Effect of EDC Crosslinking Concentration on µDERM Morphology

In order to assess the effect of EDC crosslinking concentration on µDERM morphology, µDERMs were fixed in neutral buffered formalin, embedded in Paraplast (McCormick Scientific) and

sectioned perpendicular to the microchannel topography. Slides were stained with hematoxylin and eosin (Richard Allen Scientific). Channel depth, channel width and epidermal thickness in the channels were measured for each channel using Spot software as previously described in Chapter 3 and 4. Epidermal thickness on flat controls was also measured.

6.3 Results

6.3.1 Mouse Survival Following Graft Implantation

In order to assess implant success and validate the wound model and implantation protocol, mice were monitored regularly for signs of distress. Although all mice survived the initial surgical procedure, the overall 7 day survival rate was 67% (Figure 6.2). All mice surviving for 7 days survived until the prescribed end of experiment and showed no signs of distress or discomfort following recovery from anesthesia. Three of four mice implanted with control DED grafts survived for at least 7 days following implantation. The sole control death is believed to be a result of bandaging failure. At 24 hours, the bandage had come loose resulting in an exposed wound bed. Despite re-bandaging, the graft site appeared to become infected resulting in death at 3 days. Five of five mice implanted with µDERM cross-linked using 5 mM EDC survived to 7 days. In contrast, zero of three mice implanted with 60mM cross-linked µDERM survived to 5 days (Figure 6.2). All mice treated with 60 mM EDC cross-linked grafts died or were euthanized due to body weight loss between two and four days. These mice began to show signs of distress and dehydration at 2 to 3 days and failed to improve with treatment with gel recovery fluids.

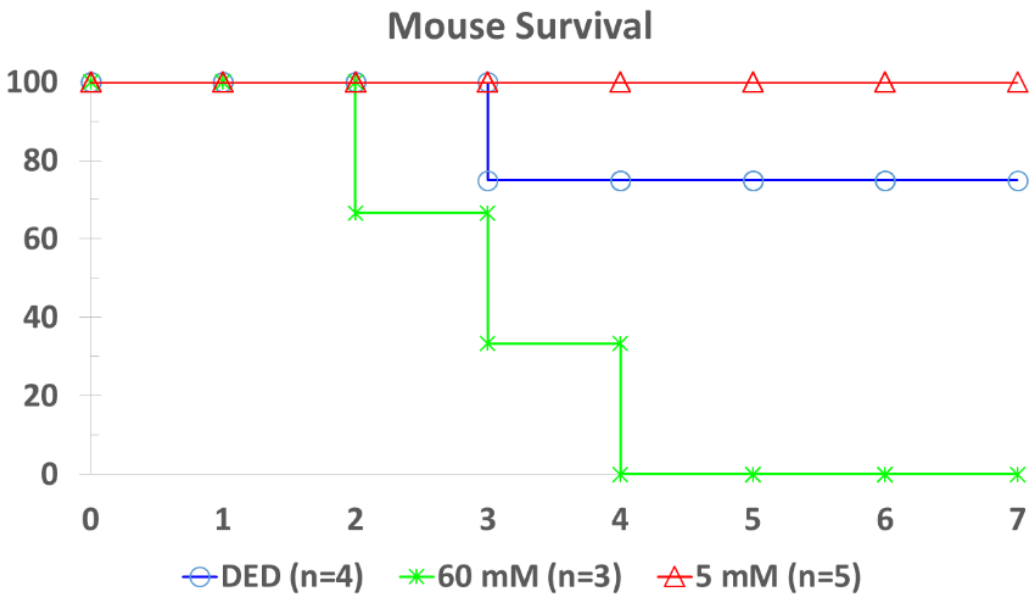

Figure 6.2 Mouse survival for the first 7 days following µDERM implantation. Mice implanted with 60 mM EDC crosslinked µDERM died between two and four days. The majority of mice treated with DED and 5 mM EDC grafts survived until the end of the experiment.

6.3.2 Wound Closure on Athymic Mice

6.3.2.1 Cultured DED Implants Integrate with Surrounding Skin at 7 days

Figure 6.3 shows a DED graft on an athymic mouse 7 days after implantation. The DED is well integrated with the surrounding skin on the left and bottom sides of the graft. Although the upper right hand corner of the DED graft is sheared from the wound bed, there are no signs of infection and there are signs of re-epithelialization of the margin. This, in conjunction with the buckling observed in the center of the graft suggests that the graft may have been disrupted soon after implantation. Importantly, the epidermal layer on the DED appears dry and intact, suggesting the presence of a well formed, stratified, stratum corneum.

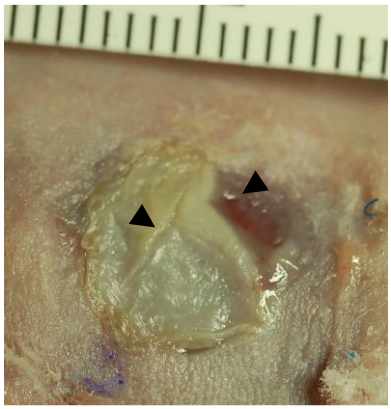

Figure 6.3 Cultured DED graft 7 days after implantation. The majority of the graft is well integrated at the wound margins, although there is some graft blistering and shearing (arrows).

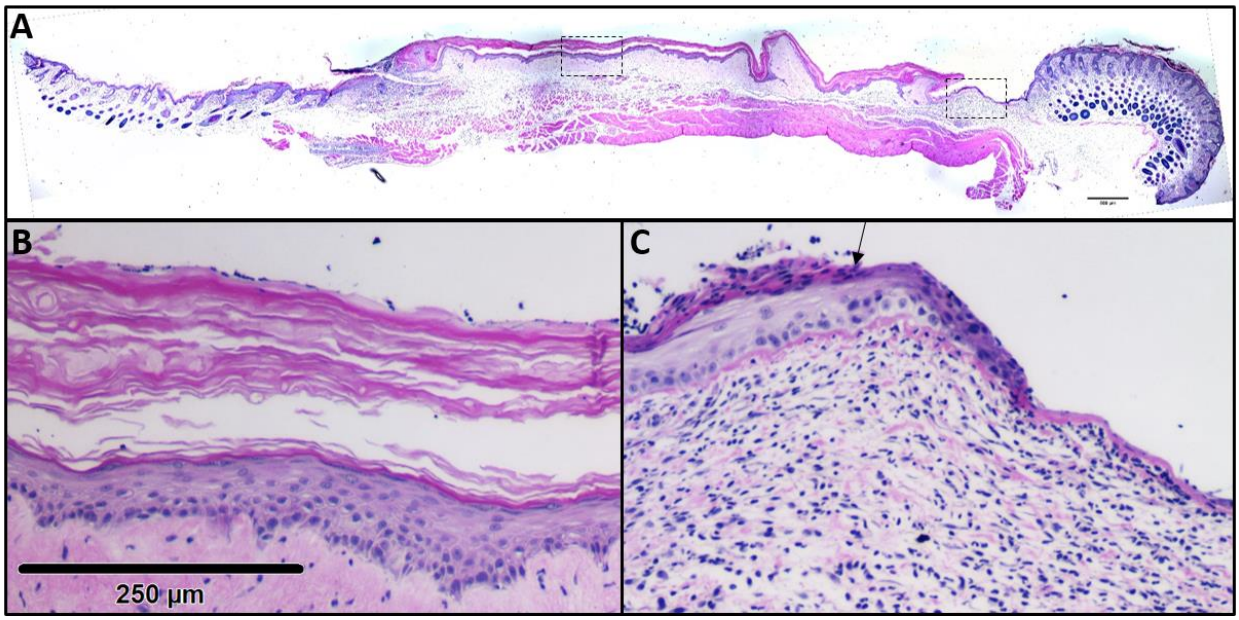

Figure 6.4 H&E of cross-section of the excised DED graft at 7 days. (A) Photo merge of entire graft length and wound margin. (B) High magnification image of the center of the DED graft. (C) High magnification image of the wound margin and migrating epithelial tongue (arrow).

Histological evaluation of the excised graft (Figure 6.4) shows a migrating epithelial tongue between the wound margin and the implant. The graft has a robust epidermal layer with a distinct stratum corneum. Additionally, cellular infiltration into the graft is apparent.

6.3.2.2 µDERM Implants Crosslinked with 5mM EDC are Well-Integrated with Surrounding Murine Skin at7 Days

Figure 6.5 shows an graft 7 days following implantation of a 5 mM EDC-crosslinked µDERM. The µDERM appears to be better integrated than the DED. In particular, the graft appears dry and there is no indication of dehiscence or wound contraction. Additionally, there are no signs of infection and the epidermal layer on the µDERM appears dry and intact. Evaluation of the reverse side of implanted µDERM shows evidence of vascularization of the wound bed (Figure 6.5B).

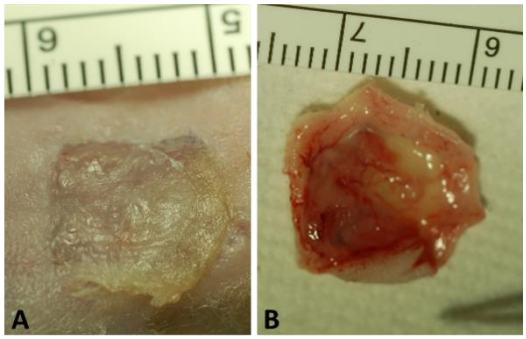

Figure 6.5 µDERM crosslinked with 5 mM EDC, 7 days after implantation. (A) µDERM is well integrated with the surrounding murine tissue. (B) Reverse side of implanted µDERM showing vascularization.

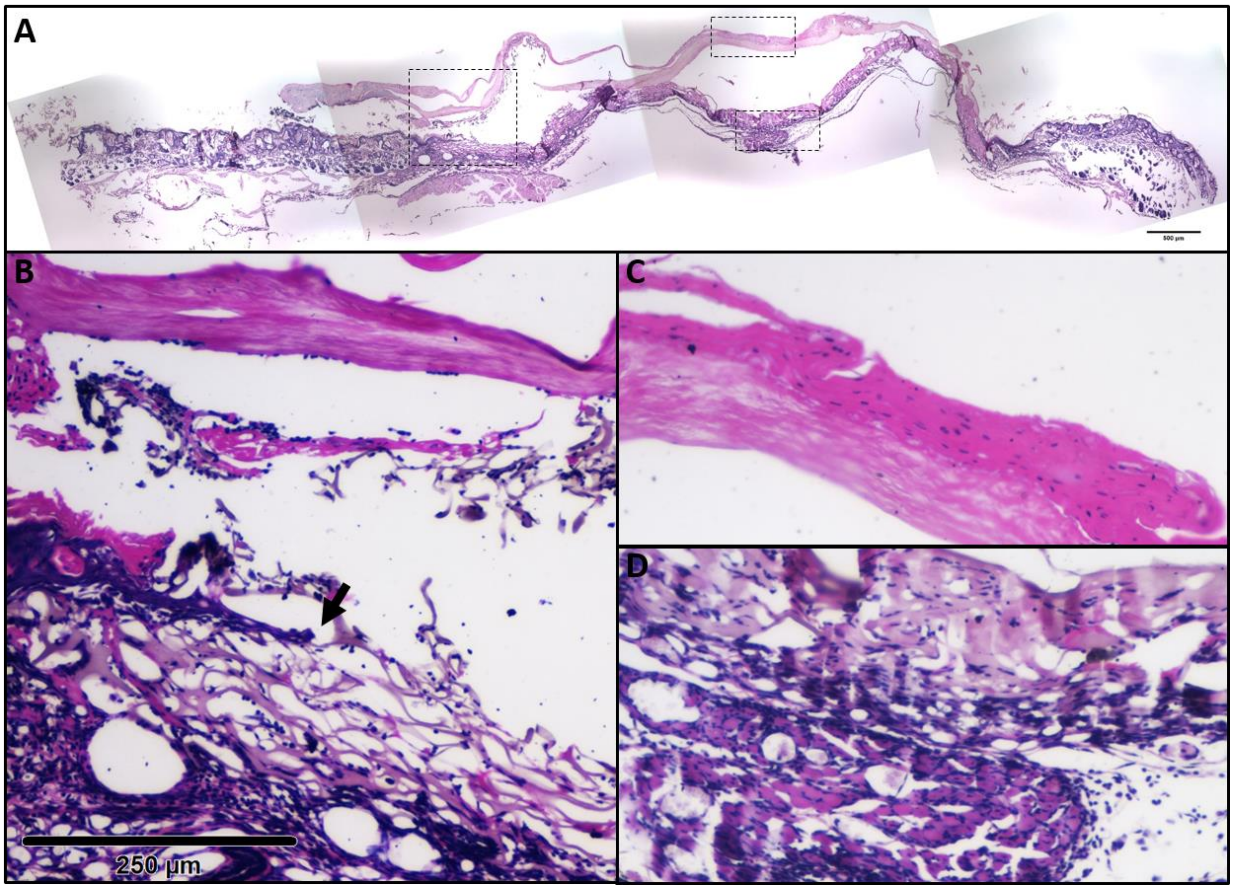

Figure 6.6 H&E of cross-section of an implanted lightly cross-linked (5 mM EDC) µDERM graft 7 days following surgery.
(A) Composite image of entire graft length and wound margin. (B) High magnification image of the wound margin and migrating epithelial tongue (arrow). (C) High magnification image of the epidermal layer of µDERM. (D) High magnification image of infiltrated sponge. Scale bar = 500 µm (A) or 250 µm (B-D).

A histological cross-section of an excised 5mM EDC crosslinked graft is shown in Figure 6.6. A migrating epithelial tongue is clearly visible at the wound margin (Figure 6.6B), however the keratinocytes appear to be migrating between the sponge and collagen gel layer of the µDERM. An epidermal layer is still visible on the surface of the µDERM collagen gel (Figure 6.6C), although it lacks the clear basal organization and stratification seen in µDERM pre-implantation. Interestingly, there was no evidence of micropatterning on the excised graft. Finally, the excised µDERM graft shows evidence of cellular infiltration of the dermal sponge analog (Figure 6.6D).

6.3.2.3 µDERM Implants Crosslinked with 60mM EDC are Poorly Integrated at Early Time Points

Although no mice implanted with 60 mM EDC-crosslinked µDERMs survived until 7 days, grafts were harvested for analysis. Here, results are presented for a µDERM graft implanted for 2 days before the mouse was euthanized for extreme body mass loss. Figure 6.7 shows the explanted graft. In contrast to the DED (Figure 6.3) and 5 mM crosslinked µDERM (Figure 6.5), gross morphological observations suggest that 60 mM EDC crosslinked µDERM are poorly integrated with the surrounding tissue. .

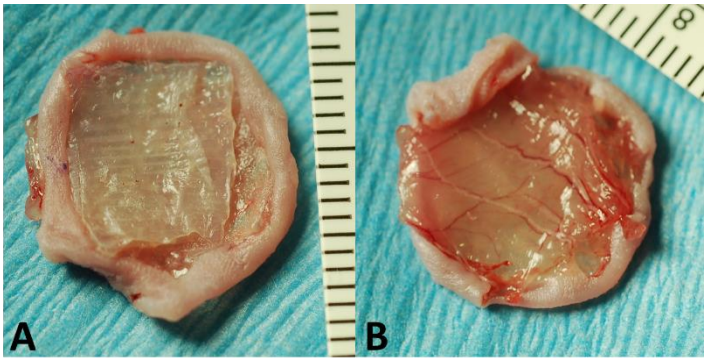

Figure 6.7 µDERM crosslinked with 60 mM EDC, 2 days after implantation. (A) µDERM is not integrated with the surrounding murine tissue. Note that the microchannel pattern is still clearly visible. (B) Reverse side of implanted µDERM. Not the limited re-vascularization.

Histological evaluation (Figure 6.8) of implanted 60 mM EDC crosslinked µDERM shows poor cellular infiltration and limited graft integration with the surrounding tissue. Interestingly, the µDERM retains its micropatterning and exhibits a thick epidermal layer, although this layer shows early signs of breakdown including disorganization of the strata and pyknotic nuclei (Figure 6.8B). Although there is some evidence of cellular infiltration within the sponge, there is no indication of infiltration into the gel layer (Figure 6.8C). Additionally, the epithelial tongue appears to be migrating between the dermal sponge and the micropatterned collagen gel layer of the µDERM (Figure 6.8D).

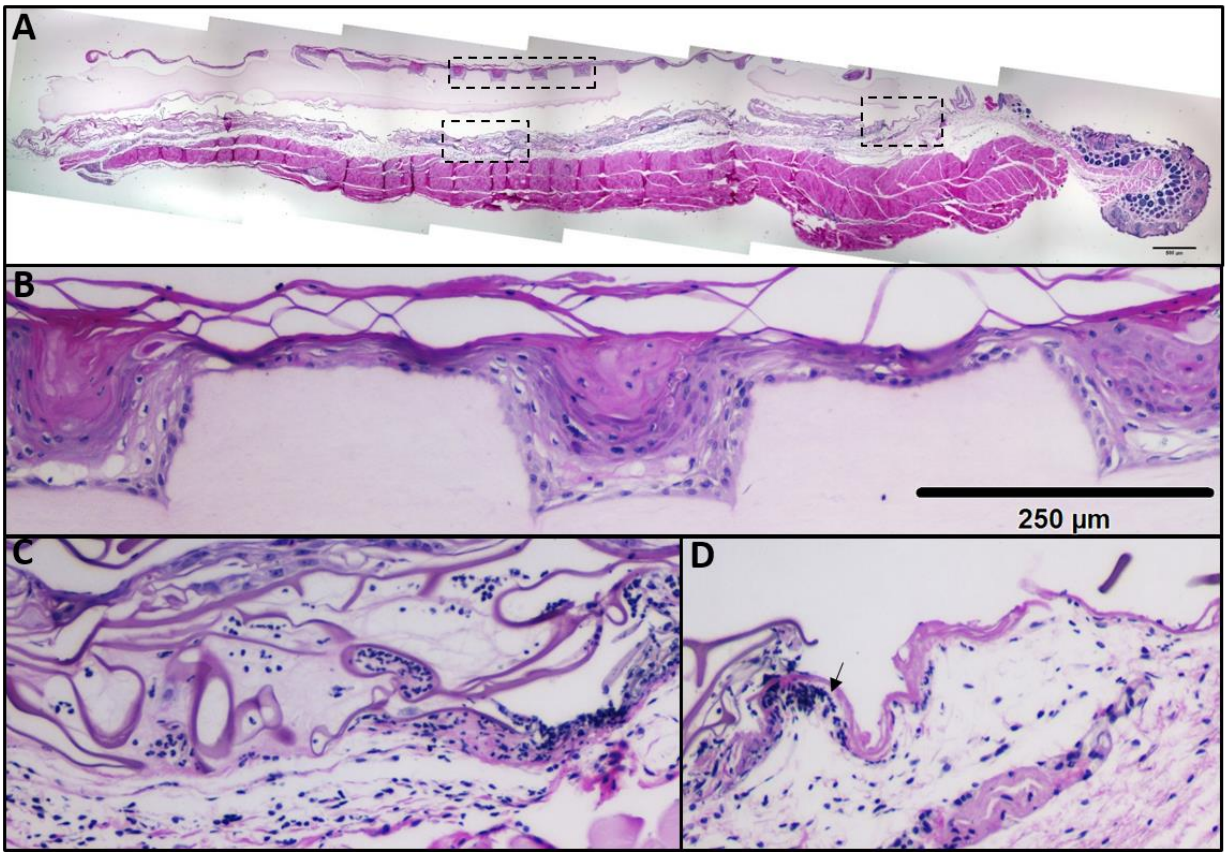

Figure 6.8 H&E of cross-section of an implanted highly cross-linked (60 mM EDC) µDERM graft 2 days following surgery.
(A) Composite image of entire graft length and wound margin. (B) High magnification image of the center of the epidermal layer of the µDERM graft. Note the persistence of the micro-channel topography and the epidermal layer on the µDERM. (C) High magnification image of infiltrated µDERM sponge. (D) High magnification image of the wound margin and migrating epithelial tongue (arrow). Scale bar = 500 µm (A) or 250 µm (B-D)

6.3.3 The Adverse Effect of Crosslinking Concentration on Epidermal Thickness is Mitigated by Microtopography i*n vitro*

Previous studies by Powell *et al* have associated high EDC crosslinking concentrations (50 mM) with poor epidermal morphology (Powell and Boyce, 2006, 2007), however in our previous work with highly crosslinked µDERMs (60 mM EDC), we noted the formation of a robust, well-organized epidermal layer, especially in microchannels, *in vitro* (Bush and Pins, 2012; Clement, Moutinho and Pins, 2013). In order to determine how EDC crosslinking concentration affects epidermal morphology on µDERMs, we assessed the epidermal morphology of µDERM crosslinked with low (5mM) or high (60mM) concentrations of EDC. Representative H&E images of channels and flat regions of µDERMs crosslinked with 5 mM and 60 mM EDC are shown in Figure 6.9. As in Chapter 4, we observed enhanced epidermal morphology in channel

topographies compared to flat regions on µDERMs crosslinked with both low (Figure 6.9 A-C) and high (Figure 6.9 D-F) concentrations of EDC. Using quantitative morphometric analysis of H&E stained sections of µDERM cultured for 7 days at the A/L interface, we evaluated the effect of crosslinking concentration of epidermal morphology and epidermal thickness. Interestingly, we found that epidermal thickness was increased on the flat surfaces of µDERM crosslinked with 5mM EDC compared to those crosslinked with 60 mM EDC (Figure 6.10). However, within microchannels, epidermal thickness was increased in µDERM crosslinked with 60 mM EDC compared to lightly crosslinked µDERM (Figure 6.10A).

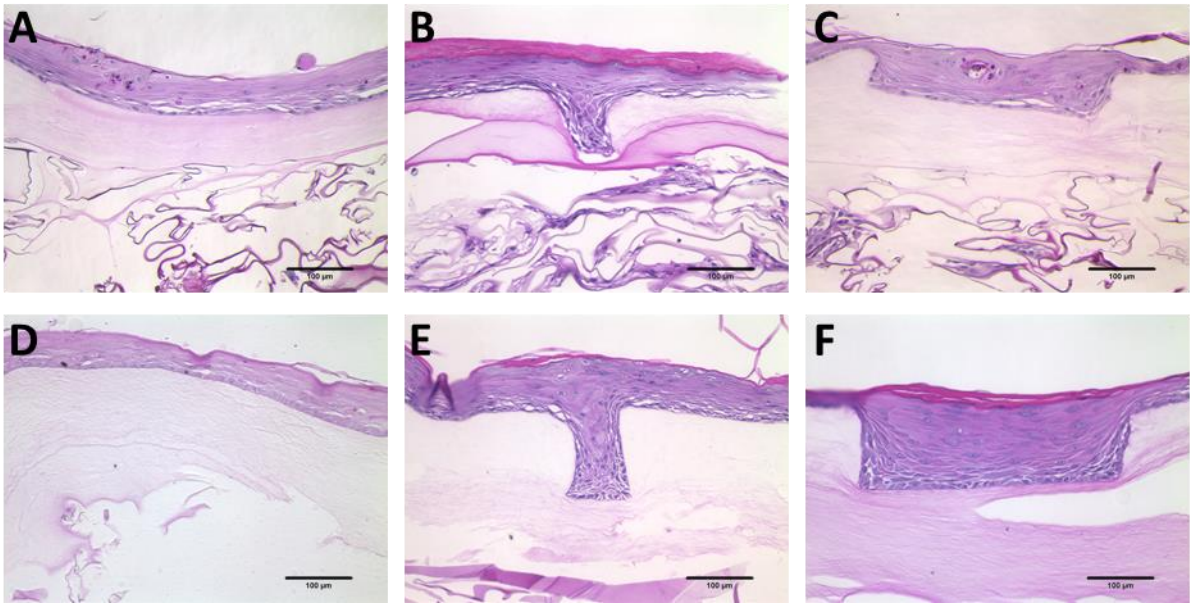

Figure 6.9 H&E of µDERM cultured at the air-liquid interface for 8 days (pre-implantation). µDERMs were crosslinked with 5 mM EDC (A-C) or 60 mM EDC (D-F) prior to fibronectin conjugation and sterilization. Representative images are shown of flat regions (A, D), narrow 50 µm channels (B, E) and wide 400 µ channels (C-F). Note the difference in channel depth between the different crosslinking concentrations.

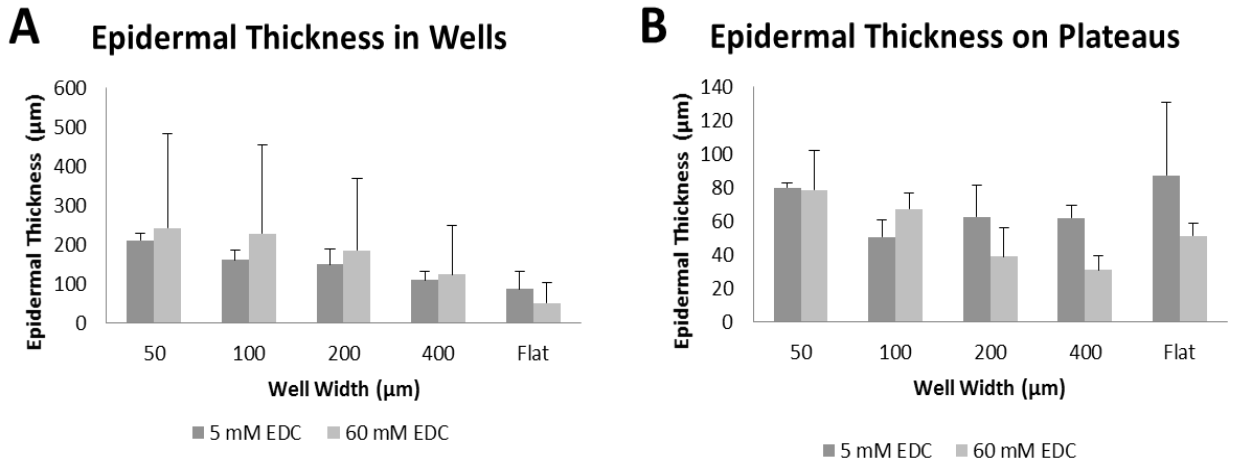

Figure 6.10 Epidermal thickness in wells and on plateaus of µDERM crosslinked with 5 mM or 60 mM EDC
For 5 mM EDC crosslinked grafts n=3, 7, 14, 7, and 25 for 50 µm, 100 µm, 200 µm, 400 µm channels and flats respectively. For 60 mM EDC crosslinked grafts n= 7, 27, 27, 21 and 4 for 50 µm, 100 µm, 200 µm, 400 µm channels and flats respectively.

6.4 Discussion

This chapter presents the results of preliminary implantation studies with our new µDERM skin grafts. We have validated our excisional skin wounding model and surgical implantation technique using cultured DED grafts. To our knowledge, this is the first implantation model that allows for *in vivo* study of the role of topography in regulating keratinocyte function and epidermal wound healing. Interestingly, we noted a marked difference in the *in vivo* performance of µDERM depending on the degree of EDC crosslinking used in graft fabrication. Mice grafted with highly cross-linked (60 mM EDC) µDERM did not survive past 4 days and exhibited poor graft integration at these early time points. In contrast, mice grafted with lightly cross-linked (5 mM EDC) µDERM quickly recovered from the implantation surgery. These grafts were well integrated with the surrounding wound margins by 7 days and the graft surface resembled DED. Although the sample size is small, these results suggest a correlation between EDC crosslinking concentration and the tissue response to graft implantation.

Previous studies have shown that although crosslinking with high concentrations of EDC prevents contraction of collagen-GAG scaffolds *in vitro*, wounds closed with the highly crosslinked (50 mM EDC) scaffold contracted more and had lower rates of cellular engraftment compared to lightly crosslinked scaffolds (1 and 5 mM EDC) (Powell and Boyce, 2007). Interestingly, these studies

also showed that keratinocytes cultured *in vitro* on collagen-GAG scaffolds crosslinked with 50 mM EDC exhibited poor viability and epidermal organization (Powell and Boyce, 2006). Therefore, we also compared the overall morphology and epidermal thickness of keratinocytes seeded on µDERMs crosslinked with 5 mM EDC to those seeded on µDERMs crosslinked with 60 mM EDC.

On flat µDERM we noted decreased epidermal thickness and basal keratinocyte organization on highly crosslinked scaffolds, consistent with the results published by Powell and Boyce. However, on patterned µDERMs the presence of microtopography appears to mitigate this negative effect. In fact, within the channels of highly crosslinked µDERM, epidermal thickness is increased compared to lightly crosslinked µDERM. Importantly, the fidelity of channel topography is much higher on these highly crosslinked µDERM, yielding channels with deeper features. Together these results suggest that although crosslinking with high concentrations of EDC can inhibit cellular responses to µDERMs, the ability of these highly crosslinked scaffold to maintain the topography of the cellular microniches is important for enhanced tissue response.

Although the mechanical properties of µDERM have not yet been characterized, in handling both 5 mM EDC crosslinked µDERM and 60 mM EDC crosslinked µDERM, we noted that the highly cross-linked scaffolds were less compliant. It is well established that cells respond to substrate stiffness (Discher *et al.*, 2005). Trappmann *et al* demonstrated that keratinocytes stem cells seeded on stiff collagen coated polyacrylimide hydrogels spread more and maintained their stem cell phenotype compared to cells cultured on more compliant hydrogels (Trappmann *et al.*, 2012). They further concluded that this change in cell behavior was due to differences in mechanical feedback from the anchored collagen fibres. Additionally, Wang *et al* showed that keratinocyte proliferation and migration were increased on stiffer substrates (Wang *et al.*, 2012). These results suggest that substrate stiffness is an important consideration for the design of implantable scaffolds and that future studies to determine the mechanical properties of highly crosslinked and lightly crosslinked µDERMs may be warranted.

In this pilot study, we validated our *in vivo* wound healing model using control DED implants. We also identified several challenges that will need to be addressed to further the μDERM model. First, we note re-epithelialization between the sponge and collagen gel layer in both lightly and highly EDC crosslinked μDERMs. This may be caused by the thickness of the μDERM relative to the athymic mouse skin. During surgeries, we noted that the surface of the μDERM protruded above the surrounding skin. In the future, making μDERMs thinner may help address this concern. Another concern, is the lack of infiltration of the micropatterned collagen gel, which may be a result of the high density of the gel. Using our current fabrication method, the high collagen concentration is necessary to reproduce the micropatterns with high fidelity. However, in the future it may be possible to create a micropatterned collagen-GAG sponge and eliminate the gel layer entirely. This would allow the graft to prevent wound contraction by providing structural support within the wound bed and also create a template for epidermal regeneration including important topographic cues. Finally, while a high degree of crosslinking is necessary to maintain microtopography, highly EDC crosslinked scaffolds have been shown to negatively affect cellular growth and μDERM implantation. Thus it is critical for future studies to identify the minimum amount of crosslinking necessary to maintain the precisely engineered microtopography of the μDERMs or examine different methods of crosslinking.

6.5 Acknowledgments

This research was funded by the NIH (EB-005645). Special thanks to Dr. Mehmet Toner and Octavio Hurtado at the BioMicroElectroMechanical Systems (BioMEMS) Resource Center, Massachusetts General Hospital, Boston, MA (NIH Grant: P41 EB02503 [MT]), for their assistance with the microfabrication processes. I would like to thank my advisor, Professor George Pins, for his scientific contribution to the work. Special thanks to Professor Glenn Gaudette and the members of Gaudette Lab for providing surgical expertise, consultations and support for the *in vivo* studies. I would also like to thank Jen Molignano and Tom Moutinho for surgical assistance, Kevin Ackerman, MacKenzie Brandes and Alyssa Bornstein for laboratory assistance and the Department of Obstetrics and Gynecology at UMMS (Worcester, MA) for providing us with neonatal foreskins for keratinocyte isolations.

6.6 References

American Burn Association (2007) Burn Incidence and Treatment in the U.S.: 2007 Fact Sheet.

American Burn Association (2013) Burn Incidence and Treatment in the United States: 2013 Fact Sheet.

Bush K and Pins G (2012) Development of Microfabricated Dermal Epidermal Regenerative Matrices to Evaluate the Role of Cellular Microenvironments on Epidermal Morphogenesis. *Tissue Eng Part A* 18:2343-53.

Clement AL, Moutinho TJ, Jr. and Pins GD (2013) Micropatterned Dermal-Epidermal Regeneration Matrices Create Functional Niches That Enhance Epidermal Morphogenesis. *Acta Biomater* 9:9474-84.

Discher DE, Janmey P and Wang YL (2005) Tissue Cells Feel and Respond to the Stiffness of Their Substrate. *Science* 310:1139-43.

Downing BR, Cornwell K, Toner M and Pins GD (2005) The Influence of Microtextured Basal Lamina Analog Topography on Keratinocyte Function and Epidermal Organization. *J Biomed Mater Res A* 72:47-56.

Geer DJ, Swartz DD and Andreadis ST (2004) In Vivo Model of Wound Healing Based on Transplanted Tissue-Engineered Skin. *Tissue Eng* 10:1006-17.

Hamoen K, Erdag G, Cusick J, Rakhorst H and Morgan J (2002) Genetically Modified Skin Substitutes. In: *Gene Therapy Protocols* (Morgan J, ed) Vol. 69: Springer New York, 203-17.

MacNeil S (2007) Progress and Opportunities for Tissue-Engineered Skin. *Nature* 445:874-80.

Medalie D and Morgan J (1999) Preparation and Transplantation of a Composite Graft of Epidermal Keratinocytes on Acellular Dermis. In: *Tissue Engineering Methods and Protocols* (Morgan J, Yarmush M, eds) Vol. 18: Humana Press, 407-21.

Powell HM and Boyce ST (2006) Edc Cross-Linking Improves Skin Substitute Strength and Stability. *Biomaterials* 27:5821-7.

Powell HM and Boyce ST (2007) Wound Closure with Edc Cross-Linked Cultured Skin Substitutes Grafted to Athymic Mice. *Biomaterials* 28:1084-92.

Sen CK, Gordillo GM, Roy S, Kirsner R, Lambert L, Hunt TK, Gottrup F, Gurtner GC and Longaker MT (2009) Human Skin Wounds: A Major and Snowballing Threat to Public Health and the Economy. *Wound Repair Regen* 17:763-71.

Shevchenko RV, James SL and James SE (2010) A Review of Tissue-Engineered Skin Bioconstructs Available for Skin Reconstruction. *J R Soc Interface* 7:229-58.

Trappmann B, Gautrot JE, Connelly JT, Strange DG, Li Y, Oyen ML, Cohen Stuart MA, Boehm H, Li B, Vogel V, Spatz JP, Watt FM and Huck WT (2012) Extracellular-Matrix Tethering Regulates Stem-Cell Fate. *Nature materials* 11:642-9.

Vaccariello MA, Javaherian A, Parenteau N and Garlick JA (1999) Use of Skin Equivalent Technology in a Wound Healing Model. *Methods in molecular medicine* 18:391-405.

Wang Y, Wang G, Luo X, Qiu J and Tang C (2012) Substrate Stiffness Regulates the Proliferation, Migration, and Differentiation of Epidermal Cells. *Burns : journal of the International Society for Burn Injuries* 38:414-20.

Chapter 7: Conclusions and Future Work

7.1 Introduction

This thesis evaluates the role of topography on epidermal morphogenesis and keratinocyte function *in vitro* and explores the creation of a full thickness skin substitute for potential future clinical applications. In contrast to other tissue-engineered skin model systems which are characterized by a flat dermal-epidermal interface, our model utilizes a micropatterned collagen gel that can recreate the topography of the native dermal-epidermal junction (DEJ). Our research suggests that the topographic cues of the DEJ may play an important role in wound healing by differentially driving cellular functions including proliferation and laminin 332 synthesis and through the creation of a physical keratinocyte stem cell niche.

7.2 Summary of Results and Conclusions

7.2.1 Part 1: Identification of microchannel niche dimensions that regulate cell function on bilayered skin analogs containing fibroblast paracrine signaling cues

In order to advance current skin substitutes for clinical and *in vitro* model use, we began by incorporating fibroblast signaling into our previously described Micropatterned Dermal-Epidermal Regeneration Matrix (µDERM) model. The importance of fibroblast-keratinocyte paracrine interactions for epidermal wound healing and for the establishment of *in vitro* skin models has been well established by multiple laboratories (Delaporte *et al.*, 1989; El-Ghalbzouri *et al.*, 2002; El Ghalbzouri *et al.*, 2004; El Ghalbzouri *et al.*, 2005; El Ghalbzouri *et al.*, 2002; El Ghalbzouri and Ponec, 2004; Erdag and Sheridan, 2004; Knighton *et al.*, 1990; Maas-Szabowski *et al.*, 1999; Marionnet *et al.*, 2006; Werner *et al.*, 2007). Therefore, the dermal collagen-GAG sponge analogs of µDERMs were pre-seeded with $2x10^5$ fibroblasts ($8x10^4$ cells/cm^2). Following 48 hours of culture, keratinocytes were seeded on the micropatterned collagen gel and µDERMs were cultured as previously described (Bush and Pins, 2012). We first investigated the effects of fibroblast signaling on epidermal morphology and epidermal thickness by using quantitative

morphometric analysis of hematoxylin and eosin stained histological sections. We found that inclusion of fibroblasts in µDERMs resulted in a better organized epidermal layer characterized by the presence of a defined stratum granulosum and a tightly packed basal layer. The epidermal morphology of µDERMs with fibroblasts more closely resembled keratinocytes seeded on control decellularized dermis (DED) than µDERMs without fibroblasts. Additionally, we showed that fibroblasts increased epidermal thickness on µDERMs both within channels and on adjacent plateaus and flats. These observations are consistent with those in other *in vitro* model systems (El-Ghalbzouri, Gibbs, Lamme, Van Blitterswijk and Ponec, 2002; El Ghalbzouri, Lamme and Ponec, 2002; Maas-Szabowski, Shimotoyodome and Fusenig, 1999; Werner, Krieg and Smola, 2007). Based on these findings, we hypothesize that fibroblast inclusion in the µDERM model in order to fully evaluate the effect of topography on keratinocyte function.

After demonstrating that fibroblast inclusion positively regulates epidermal thickness and epidermal morphology, we sought to confirm fibroblast signaling within the co-culture model. Keratinocyte growth factor (KGF; fibroblast growth factor 7), previously identified as a major player in keratinocyte proliferation, is secreted by dermal fibroblasts in response to keratinocyte signaling (Maas-Szabowski, Shimotoyodome and Fusenig, 1999). Immunohistochemical staining of µDERMs showed an increase in KGF in grafts incorporating fibroblasts. In conjunction with the increased epidermal thickness and enhanced epidermal organization of µDERMs cultured with fibroblasts, these results suggest active paracrine signaling and provide support for nutrient diffusion through the dense collagen gel layer.

After validating the importance of fibroblast co-culture in out µDERM system, we continued to investigate the role of topographic cues in directing cellular function and epidermal regeneration. Previous analysis of epidermal morphogenesis, cellular proliferation and stem cell localization on µDERMs were performed in fibroblast free culture. However, since the absence of fibroblast paracrine signals may result in a more quiescent phenotype, analyses done on µDERM containing fibroblasts may provide more robust and clinically relevant results. Therefore, using our new co-cultured µDERMs, we systematically analyzed the relationship between microtopographic

dimensions and epidermal morphology, epidermal thickness, keratinocyte proliferation, keratinocyte differentiation, basement membrane deposition (laminin 332) and keratinocyte stem cell clustering. µDERMs cultured with fibroblasts and keratinocytes for 7 days at the A/L interface were fixed and processed for H&E or immunohistochemical staining. Similar to the keratinocyte-only model system, we showed increased epidermal thickness in narrow 50 µm and 100 µm channels compared to wider channels. Additionally, we found that epidermal thickness was increased on plateaus adjacent to narrow channels compared to flat regions and plateaus adjacent to wide channels. These differences in epidermal thickness were statistically significant. Additionally, epidermal organization was further enhanced by the presence of microtopography. In particular, the stratum granulosum and basal layers were more pronounced in µDERM containing microchannels than in flat regions.

After demonstrating changes in epidermal thickness in response topography, we further investigated the underlying mechanism by examining keratinocyte proliferation. Based on the absence of significant difference in the density of ki67+ keratinocytes in channels of varying widths on µDERM lacking fibroblasts, we previously hypothesized a space filling mechanism by which the smaller void volume of the narrow channels filled more quickly during the initial proliferative burst resulting in a thicker epidermal layer. Interestingly, in the presence of fibroblasts we noted a statistically significant increase in the linear density of ki67+ keratinocytes per graft length (in 50 µm channels) and per DEJ length (in 100µm channels) compared to wider channels and flat regions. This suggests that the mechanism driving the increased epidermal thickness is not only space-filling but also a result of narrow cellular microniches supporting a proliferative phenotype. Additionally, we examined laminin-332 synthesis on µDERMs containing fibroblasts. We noted statistically higher laminin 332 deposition in wide (200 µm and 400 µm) channels compared with narrow channels and flat controls. Importantly, both keratinocyte proliferation and laminin-332 synthesis are regulated by KGF. The absence of statistically significant differences in proliferation in the absence of KGF secreting fibroblasts suggests that KGF may play a role in regulating keratinocyte responses to their microenvironment. We hypothesize that the collagen gel topography may create differences in nutrient diffusion within

the gel, possible resulting in differential concentrations of KGF. Although our current staining methods are not sensitive enough to observe any differences.

Finally, we looked at keratinocyte differentiation and clustering of $\beta_1^{bri}p63^+$ keratinocytes on µDERMs containing fibroblasts. We showed involucrin expression in the upper strata of the epidermal layers for all channel dimensions. The thickness of the involucrin positive layers was increased in narrow channels and highly correlated to the thickness of the overall epidermal layer. This suggests that keratinocytes are undergoing terminal differentiation following detachment from the basal layer similar to other *in vitro* models (Adams and Watt, 1990; Hotchin *et al.*, 1995; Hotchin and Watt, 1992; Levy *et al.*, 2000; Watt, 1988; Watt *et al.*, 1993). To examine the effect of microtopography on keratinocyte stem cell clustering, we identified the location of $\beta_1^{bri}p63^+$ keratinocytes within our model system. We observed these cells primarily in the bottoms of narrow channels and in the corners at the base of wider channels. This is consistent with our previous results that demonstrated β_1^{bri} keratinocyte clustering in these regions. While keratinocyte stem cells are preferentially located at the tips of dermal papillae or the bases of rete ridges in native skin (Lavker and Sun, 1982, 1983; Watt, 1998, 2001, 2002), in currently used flat *in vitro* skin substituted models stem cells are randomly distributed. Previous studies have demonstrated the importance of maintaining attachment to the basement membrane for the maintenance of keratinocyte stemness (Hotchin, Gandarillas and Watt, 1995; Li *et al.*, 1996). In fact, suspension culture is a accepted method of keratinocyte differentiation (Rheinwald, 1980). The increase in substrate surface area may play a role in regulating keratinocyte attachment and stem cell clustering. We have demonstrated that µDERMs can be used to recreate stem cell patterning *in vitro*, making them an important platform for future studies of epidermal morphogenesis and epidermal pathologies.

In conclusion of Part I: Identification of Microchannel Niche Dimensions that Regulate Cell Function on Bilayered Skin Analogs Containing Fibroblast Paracrine Signaling Cues of this thesis, we demonstrated that microtopography creates distinct keratinocyte niches by regulating cellular functions such as proliferation and protein synthesis. After enhancing the physiological relevance

of our µDERM model through the incorporation of fibroblasts in the dermal sponge layer, we established the existence of three keratinocyte niches: the proliferative niche, the synthetic niche and the stem cell niche. The proliferative niche is located in the narrow 50 µm and 100 µm channels and is characterized by a thicker epidermal layer and an increased density of ki67^{+} keratinocytes. The synthetic niche is located in the wide 200 µm and 400 µm channels and is characterized by increased laminin 332 synthesis. Finally, we demonstrated clustering of $\beta_1^{bri}p63^{+}$ keratinocytes in the narrow microchannels and the basal corners of wide channels, which define the keratinocyte stem cell niche. These findings create a platform for developing the next generation of skin substitute for clinical use and in vitro study of disease pathogenesis and epidermal wound healing.

7.2.2 Part 2: Evaluation of keratinocyte attachment and stem cell localization on dermal papillae analogs.

In this section of this thesis, we incorporated the findings from Part I: Identification of Microchannel Niche Dimensions that Regulate Cell Function on Bilayered Skin Analogs Containing Fibroblast Paracrine Signaling Cues, into a three dimensional dermal papillae analog for whole mount analysis. Specifically, in order to better mimic the native DEJ microenvironment, we designed dermal papillae analogs that contained both proliferative and synthetic niches while maximizing the number of basal corners to create stem cell niches. In order to facilitate rapid whole mount analysis, we eliminated the dermal sponge component from our µDERM model. Using the same photolithography techniques described in Part I, we created a micropatterned collagen gel substrate that contained both large (400 µm diameter) and small (54 µm diameter) hexagonal post papillae separated by wide (200 µm) and narrow (50 µm) channels. We seeded these analogs with keratinocytes and following culture at the A/L interface analyzed them in whole mount for initial cell seeding and β_1 and p63 expression.

To analyze keratinocyte seeding, cultured DEJ analogs were incubated with Hoechst to stain cell nuclei. Constructs were imaged using an inverted confocal microscope. We found that upon seeding keratinocytes formed a confluent monolayer conforming to the topography of the analog. Significantly, keratinocytes were attached the vertical sides of the papillae and wells in

addition to the tops of the papillae and bottoms of the wells and channels. This observation was consistent on substrates with varying topographies. By 3 days, we noted multiple keratinocyte cell layers on plateaus and within wells and channels. Interestingly, this supports our previous assertion that increased epidermal thickness within channels is a response to topography and not simply as a result of initial cell deposition due to gravity.

Additionally, analogs were immunostained for β_1 integrin. In order to successfully stain through the multiple cell layers, following formalin fixation constructs were permeabilized with HEPES containing 0.25% gelatin from cold water fish skin, 0.5% skim milk, and 0.5% Triton X-100 according to a protocol established by Jensen *et al* (Jensen *et al.*, 1999). Incubation with primary and secondary antibodies was performed overnight at room temperature with a minimum of 4 hours of rinsing in between. Following incubation with the secondary antibody, DEJ analogs were rinsed overnight while shaking. Confocal analysis of keratinocytes seeded on DEJ analogs containing hexagonal wells following 24 hours of culture at the A/L interface showed that β_1 integrin expression was confined to cells in the basal layer. Additionally, a larger percentage of β_1^{bri} keratinocytes were observed in or near the hexagonal wells. Analysis of keratinocytes seeded on DEJ analogs with multi-scale hexagonal papillae following 3 days of A/L interface culture also revealed that β_1 integrin expression was found solely in the basal layer. In these constructs, β_1^{bri} keratinocytes were preferentially located in narrow channels and at the bases of hexagonal papillae in wide channels. This supports both our previously published results with µDERMs lacking fibroblasts (Bush and Pins, 2012) and our results from Part I with µDERMs containing fibroblasts (Clement *et al.*, 2013). Additionally, the stem cell patterning observed on these DEJ analogs with whole mount imaging closely mimics the patterning observed in native skin (Jensen, Lowell and Watt, 1999). Interestingly, β_1^{bri} keratinocyte clustering was more pronounced on the hexagonal papillae DEJ analogs cultured for 3 days at A/L than on the hexagonal well DEJ analogs cultured for only 24 hours at A/L. This suggests that keratinocyte stem cell clustering in response to topographic cues is not simply due to topographically regulated cellular segregation upon initial seeding. Rather clustering may be driven by cellular migration to preferential locations, a phenotypic switch based on location or another unknown mechanism. Future studies will focus

on establishing the temporal component of keratinocyte stem cell localization on micropatterned substrates and elucidating the mechanism responsible for stem cell clustering.

Finally, we examined p63 expression on DEJ analogs containing multi-scale hexagonal papillae. P63 staining was performed similarly to β_1 integrin staining. Like β_1 integrin expression, p63 expression was confined to basal keratinocytes. However, the majority of basal cells stained positive for p63 and no clustering was observed. This is in conflict with our results in Part I which showed $\beta_1^{bri}p63^{+}$ keratinocyte localization in narrow channels and corners of wide channels in cross-sections of µDERMs cultured for 7 days at the A/L interface. This may indicate that the basal layer is still in a state of activated wound healing and has not yet reached a mature steady state. In fact our previous studies in µDERMs lacking fibroblasts suggest a proliferative burst around 3 days (Bush and Pins, 2012).

In conclusion of Part II: : Evaluation of Keratinocyte Attachment and Stem Cell Localization on Dermal Papillae Analogs in this thesis, we developed a method for whole mount analysis of micropatterned dermal-epidermal junction analogs and created new analogs that more closely mimic the 3D papillary structure of the dermis. Additionally, we demonstrated clustering of β_1^{bri} *keratinocytes in narrow channels and corners, in agreement with our previous cross-sectional analyses. We also showed p63 expression in the basal compartment which we hypothesize indicates an immature basal layer.*

7.2.3 Part 3: Assessment of µDERM graft integration *in vivo*

In the final section of this thesis, we evaluated µDERMs *in vivo* to test our hypothesis that incorporation of microtopography in skin grafts create cellular niches that promote epidermal wound healing. Full thickness wounds were created on the dorsum of athymic nude (*Foxn1*^{nu}*)* mice, an established skin wound healing model (Eming and Morgan, 1997; Medalie and Morgan, 1999). µDERMs with microchannel topography, µDERMs with flat topography and decellularized dermis (fabricated as described in Part I and crosslinked with either 5 mM or 60 mM EDC) were implanted into the defects. µDERM were irrigated with keratinocyte medium immediately

following bandaging and every day thereafter to prevent dehydration of the graft during integration.

We observed a higher than expected mortality rate. Interestingly, all of the mice implanted with 5 mM EDC crosslinked µDERMs survived to 7 days while none of the mice implanted with 60 mM EDC crosslinked µDERMs survived beyond 4 days. The majority of mice implanted with DED survived and the only fatality was the result of a bandaging failure. At 7 days following implantation, DED implants appeared well integrated, exhibiting signs of re-epithelialization at the wound margins. Histological assessment confirmed re-epithelialization and showed a robust epidermal layer and stratum corneum. These results are consistent with positive outcomes in other studies and validate our surgical implantation model (Powell and Boyce, 2007). Similarly, µDERM implant crosslinked with 5 mM EDC were well integrated by 7 days. Additionally, the graft showed signs of vascularization. Histological evaluation showed an epidermal layer, although the epidermal organization was limited. Significantly, we were unable to find evidence of micropatterning on µDERMs crosslinked with 5 mM EDC following implantation.

Although no animals implanted with µDERMs crosslinked with 60 mM EDC survived to 7 days, we analyzed a graft at 2 days after implantation. At this early time point, there were no signs of graft integration or significant re-vascularization. Histological assessment revealed the persistence of the micropattern on the collagen gel and the cultured epidermal layer. However, the epidermal layer shows signs of disorganization possibly caused by poor nutrient diffusion. Although infiltration of the dermal sponge is apparent, there is no indication of infiltration of the gel layer.

Together, these results suggest that a high degree of cross-linking inhibits graft integration while a low degree of cross-linking is insufficient for maintaining topography *in vivo*. Therefore, we analyzed at the effect of EDC concentration on epidermal morphology and epidermal thickness on µDERMs *in vitro.* Interestingly, we found that epidermal thickness was increased on flat regions of 5 mM EDC crosslinked µDERMs compared to flat regions of 60 mM EDC crosslinked µDERMs. In contrast, epidermal thickness was increased in microchannels of 60 mM EDC crosslinked µDERMs compared to in microchannels of 60 mM EDC crosslinked µDERMs. These

seemingly contradictory results can be explained by the observation that the measured well depth on 60 mM EDC crosslinked µDERMs was significantly greater than on µDERMs crosslinked with 5 mM EDC. In Part I we demonstrated that microtopography increases epidermal thickness and previous studies have shown that epidermal thickness is increased in high aspect ratio (deep) wells (Bush and Pins, 2012; Clement, Moutinho and Pins, 2013; Downing *et al.*, 2005). Therefore, we hypothesize that while EDC has a negative effect on keratinocyte proliferation and epidermal thickness, the enhanced microtopography of the collagen gel due to the high concentration of EDC promotes proliferation and increased epidermal thickness. Future studies will include determining the optimal crosslinking protocol to maximize maintenance of gel microtopography while minimizing the negative effects of EDC on cellular function.

In conclusion of Part III: : Assessment of µDERM Graft Integration In Vivo in this thesis, we implanted µDERMs into an athymic mouse model and demonstrated integration of µDERMs crosslinked with 5 mM EDC with the surrounding tissue. Additionally, these preliminary results suggest that a high degree of cross-linking (60 mM EDC) inhibits graft integration and may be associated with animal morbidity and mortality. These results suggest that further development of the µDERM skin graft is necessary to improve clinical outcomes.

7.3 Future Work

7.3.1 Developing Advanced *in vitro* Model Systems

We have developed a toolbox of 3D *in vitro* skin models that allow for the analysis of cellular responses to topography both in cross-section (µDERMs) and whole mount (micropatterned DEJ analogs). These models advance the current state of research by incorporating three dimensional architectural cues as well as biochemical cues. Additionally, the unique design of µDERM allows for co-culture with a mesenchymal cell and the fabrication method allows for facile protein conjugation at the DEJ. In addition to utilizing these models to elucidate the role of the physical microenvironment in regulating cell fate and function, we expect that both the µDERM model and the micropatterned DEJ model can be used as *in vitro* models of wound healing and disease pathogenesis, particularly for pathologies such as psoriasis and basal cell carcinoma which may

have a topographic component to the etiology. Finally, these tools provide a platform for investigating the role of topography in other epithelial tissues.

7.3.1.1 Psoriasis Models

Psoriasis is a chronic inflammatory skin disease that is characterized by hyperproliferative keratinocytes that result in the formation of red, scaly plaques (Rook and Burns, 2010). In addition to the physical symptoms, psoriasis is associated with psychological and social problems. Estimated to affect 2% of the population in the US, psoriasis has been shown to negatively impact health-related quality of life (a measure of physical and emotional well being established by patient self-evaluation) as much as major chronic conditions such as cancer, diabetes and arthritis (Rapp *et al.*, 1999). Histopathologically, in addition to abnormal keratinization, psoriatic skin exhibits elongated rete ridges and correspondingly elongated dermal papillae (Murphy *et al.*, 2007). Currently, *in vitro* psoriasis models utilize keratinocytes cultured on flat substrates or on DED from non-psoriatic patients; varying strategies are employed to establish the psoriatic phenotype including the use of keratinocytes harvested from psoriatic lesions, co-culture of normal keratinocytes with fibroblasts harvested from psoriatic lesions and the addition of cytokines such as IL-20, IL-22 or oncostatin-M (Barker *et al.*, 2004; Danilenko, 2008; Saiag *et al.*, 1985; Tjabringa *et al.*, 2008). Although these models are useful for investigating the psoriatic keratinocyte phenotype and identifying signaling pathways involved in psoriasis, they lack the topographic cues necessary to fully recreate the psoriatic microenvironment. µDERMS provide an *in vitro* platform for investigating the role of topography in psoriatic pathogenesis. Computational modeling of the changes in psoriatic DEJ architecture with respect to keratinocyte proliferation suggest that hyperproliferation is strongly correlated with DEJ elongation, leading to the mechanistic hypothesis that the decreased turnover time leads to an expansion of the basal proliferative compartment and consequently the increase in DEJ surface area (Iizuka *et al.*, 1997, 1999; Iizuka *et al.*, 2004). However, based on our results that demonstrate an increase in proliferation in deep, narrow channels the hyperproliferation exhibited by psoriatic keratinocytes may be stimulated by the topographical changes. This suggests that a positive feedback mechanism may be partially responsible for development of psoriatic lesions. Accordingly, using

a psoriatic µDERM model to gain a better understanding of the psoriatic microtopographic environment may lead to new strategies for promoting plaque resolution.

7.3.1.2 Epithelial Cancer Models

Skin cancer is the most common type of cancer, affecting an estimated 20% of Americans over the course of their lives (Robinson, 2005; Stern, 2010). Non-melanoma cancers including basal cell carcinomas and cutaneous squamous cell carcinomas comprise the majority of skin cancers and have a low mortality rate. However, melanoma, which accounts for less than 2% of skin cancers despite being responsible for the majority of deaths, is expected to claim nearly 10,000 lives in 2014 (American Cancer Association, 2014). Both 2D and 3D *in vitro* models of skin cancer have been used for drug screening and to study disease pathogenesis/carcinogenesis (Borchers *et al.*, 1997; Commandeur *et al.*, 2009; Eves *et al.*, 2000; Obrigkeit *et al.*, 2009). Like other *in vitro* models of skin, these lack defined topography at the DEJ. Research has shown that skin cancer cells cultured *in vitro* respond differently to treatment in 3D compared to 2D (Smalley *et al.*, 2006; Vorsmann *et al.*, 2013).

Further, research into other types of cancer suggest a role of topography in epithelial tumor development. For example, models of breast cancer suggest an important role of the tumor microenvironment in tumorogenesis (Bissell *et al.*, 2002; Gudjonsson *et al.*, 2003; Weaver *et al.*, 1996; Weigelt and Bissell, 2008). Additionally, in colon cancer the underlying matrix topography is altered, with a loss of the characteristic crypt organization in areas with poorly differentiated tumors (Anderson *et al.*, 2006; Rapier *et al.*, 2010). Therefore, we propose that the introduction of microtopography into an epidermal cancer model will not only allow us to investigate the role of microtopography in tumorogenesis, but also create a more physiologically relevant cancer model with high utility for drug screening.

7.3.1.3 Wound healing models

Chronic wounds represent a growing problem as the global population ages with an estimated 14 million venous and diabetic ulcers and 5.2 million pressure sores treated annually worldwide (MedMarket, 2007). Current 3D *in vitro* cutaneous wound healing models rely on flat substrates

or DED with undefined surface topography. Although these models provide valuable insight into re-epithelialization and the mechanisms of wound healing, there are currently no model systems that allow for the investigation of the role of topographical cues in wound healing. Here we have demonstrated that microtopography regulates cellular functions such as proliferation and basement membrane protein deposition which are critical to wound healing. In order to determine the role of DEJ architecture in guiding wound healing, we propose using µDERMs as a platform for a wound healing model. Previously, several different methods have been utilized to create an *in vitro* cutaneous wound including cryoburn (El Ghalbzouri, Hensbergen, Gibbs, Kempenaar, van der Schors and Ponec, 2004; Han *et al.*, 2005), scratch assay (Kandyba et al., 2010), and incisional wounding (Garlick and Taichman, 1994a, b). In our laboratory, we have developed a device for creating reproducible cryoburns on *in vitro* skin grafts (Figure 7.1). In future studies, we will use this technique to create cryoburns on µDERMs in order to determine the role of microtopography in regulating keratinocyte migration and re-epithelialization.

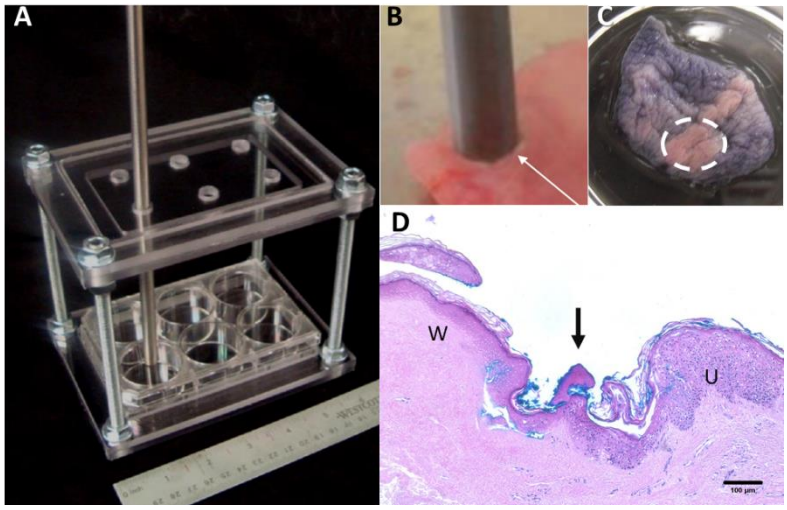

Figure 7.1 Cryoburn device for creating repeatable burn on the surface of skin. Photos show (A) polycarbonate frame with guide plates used to direct frozen stainless steel rod onto the surface of the tissue (B). Gross morphologic observation (C) of MTT stained, cryoburned tissue highlights damaged tissue (white circle) and H&E stained cross-section of tissue (D) shows a clearly defined wound margin (arrow) between wounded (W) and unwounded (U) tissue. Images courtesy of 2009-2010 WPI Major Qualifying Project Team (Jason Forte, Kathleen Most, Jennifer Sansom, and Ishita Tyagi)

7.3.1.4 Models for intestinal epithelium

Like skin, intestinal epithelium is characterized by micron-scale topography of the underlying basement membrane. The topography of the intestine includes fingerlike projections (villi) interspersed with deep invaginations (crypts) (Barrett and Rabould, 2008). Similar to the dermal papillae and rete ridges of the skin, these topographic features define microenvironments for the

intestinal epithelium with Lgr5^{+} intestinal stem cells localizing to the bottoms of crypts (Barker *et al.*, 2009; Samuel *et al.*, 2009; Sato *et al.*, 2009). Researchers have developed novel 3D substrates to investigate the role of topography in the intestine. Wang *et al* has used a micropatterned PDMS substrate to recreate the crypt topography using circular microwells of similar size scale to our µDERMs (Wang *et al.*, 2009). They found that particularly on their smaller (50 µm and 100 µm diameter, 120µm deep) micropatterned surfaces, Caco-2 cell differentiation was decreased while cellular metabolism was increased, supporting the hypothesis that topography can regulate cell fate. This model differs from ours in that the PDMS substrate significantly limits nutrient diffusion, which may additionally affect cellular function. Another topographic model of the intestinal epithelium using micropatterned collagen gels was developed Yu *et al* (Yu et al., 2012). Focused on creating a model for testing drug permeability, they found that the permeability coefficients of their 3D scaffolds containing synthetic villi more closely approximated the permeability of native intestine than flat controls. This study highlights the need to consider topographical structure in the development of *in vitro* model systems.

7.3.1.5 Further characterization of the epidermal morphology and tissue architecture on µDERMs

Here we have characterized the overall epidermal morphology of keratinocytes cultured on µDERMs. In order to validate µDERMs as an *in vitro* model system, the physical and biochemical composition of µDERMs should be further evaluated and compared to native skin. For example, in this thesis, we examined the deposition of the basement membrane protein, laminin 332. However, the presence of basement membrane proteins alone does not demonstrate the formation of an organized basement membrane (Bohnert *et al.*, 1986). Future studies utilizing transmission electron microscopy to examine the ultrastructure of the µDERM DEJ are necessary to confirm the formation of a mature basement membrane.

Additionally, here we presented histological and immunohistochemical evaluation of cultured µDERMs. However, there are additional markers that we should evaluate to establish that the epidermis formed on µDERMs is fully formed and mature. For example, spatially regulated E-cadherin expression is necessary for normal tissue architecture in human skin (Koizumi *et al.*, 2005; Wakita *et al.*, 1998). Upregulation of E-cadherin expression is also characteristic of

keratinocytes that have detached from the basement membrane and committed to differentiation (Moles and Watt, 1997). Immunohistochemical analysis of E-cadherin expression in µDERM would complement out involucrin, $\beta_1$integrin and p63 staining and help us better elucidate the patterns of keratinocyte stem cell clustering and terminal differentiation within µDERMs.

7.3.1.6 High throughput evaluation of keratinocyte niche dimensions on DEJ analogs

Our cross-sectional analysis of our µDERM model allows for evaluation of multiple channel dimensions on a single graft. While our current DEJ analog model features a series of wide and narrow channels, these our interspersed making an thorough analysis of the effect of topographic feature dimension on cellular function and localization difficult. Therefore, we have developed a new topographic pattern to allow for the high throughput evaluation of different keratinocyte niche dimensions (Figure 7.2).

Specifically, we have created a single pattern of hexagonal posts which varies both hexagon diameter (10 µm, 50 µm, 100 µm 200 µm and 400 µm) and channel width (10 µm, 50 µm, 100 µm 200 µm and 400 µm) in a series of twenty five test squares. In future studies, we will create DEJ analogs with this topography and evaluate keratinocyte function in response to topographic cues, which will allow for evaluation of multiple channel dimensions on a single graft. Additionally, each combination of post and channel dimension is designed to fill a 4 mm by 4 mm square. This allows for the DEJ analogs to be dissected into individual test squares for bulk cellular analysis while controlling for the initial cell population.

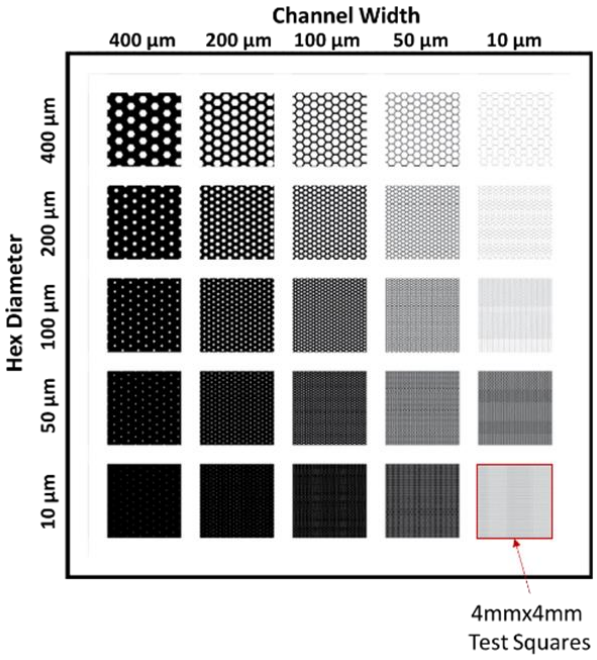

Figure 7.4 New pattern for high throughput evaluation of the effect of topographic dimensions on keratinocyte function

7.3.2 Creating Robust Bioengineered Skin Substitutes for Traumatic and Chronic Wounds

The next generation skin substitute must be a robust graft that promotes the prompt re-establishment of the epidermal barrier, supports angiogenesis and rapidly integrates with the surrounding tissue. It is clear that the ideal skin substitute will replace both the dermal and epidermal components (Sheridan and Tompkins, 1999; Shevchenko *et al.*, 2010). Current composite skin substitutes lack the topography of the native DEJ. The increased surface area created by the series of dermal papillae found that the DEJ is thought to increase the stability of the dermal epidermal junction. Additionally, in this thesis we have demonstrated that incorporation of microtopography into skin substitutes results in increased epidermal thickness and superior epidermal morphology. Further, we have shown that topographic cues create distinct cellular microniches that differentially promote keratinocyte proliferation and basement membrane protein synthesis. Based on these results, we hypothesize that incorporation of microtopography into the next generation skin substitutes will improve clinical outcomes. While our µDERM model represents a step towards an advanced clinical therapy, our preliminary *in vivo* results clearly indicate that the system needs to be refined to promote graft integration. We hypothesize that the high concentration of EDC crosslinking used to maintain high fidelity micropatterning results in a stiff, non-degradable graft that does not integrate with the surrounding tissue. Therefore, future studies must determine the minimum concentration of EDC necessary to recreate patterning or investigate other methods of creating micropatterns that replicate the topography of the DEJ. Finally, an advantage of the µDERM model is that the dermal sponge allows for easy incorporation of a mesenchymal cell type. Here we demonstrated that incorporation of fibroblasts into the dermal sponge resulted in increased epidermal thickness and superior epidermal morphology. However, previous studies have shown that there is a dose dependent response to the inclusion of fibroblasts and that at high fibroblast densities keratinocytes do not differentiate appropriately (Erdag and Sheridan, 2004). Although our fibroblast density was selected based on previous results, it is necessary to optimize the fibroblast density for our model system. Additionally, we can use the µDERM model to investigate keratinocyte responses to other mesenchymal cells such as dermal papillae cells and mesenchymal stem cells or genetically modified cells.

Finally, following optimization µDERMs could be used to improve the clinical treatment of traumatic wounds when used as a full-thickness skin replacement or in conjunction with other therapies. Although our preliminary *in vivo* studies demonstrated sub-optimal outcomes with highly crosslinked µDERMs, results with 5 mM EDC crosslinked µDERMs demonstrated good re-epithelialization and graft integration at early (7 day) time points. However, µDERMs still require extensive time in culture prior to implantation, which may limit their use as a trauma therapy. An alternative therapeutic strategy could be to use unseeded µDERMs, together with the application of "spray skin" as a replacement for a meshed split thickness autograft. A major benefit of ReCell Spray-On Skin is that the keratinocytes are harvested at the time of surgery and do not require time consuming *in vitro* expansion, however ReCell healing outcomes are dramatically improved when used in conjunction with a split-thickness autograft or alternative dermal substitute (Gravante *et al.*, 2007; Tenenhaus and Rennekampff, 2012). Our *in vitro* studies demonstrate that microtopography increases epidermal thickness and enhances epidermal morphology, especially at early time points, suggesting that the unique microtopgraphic interface may help promote the rapid formation of a robust epidermal barrier layer. This combination of an off-the shelf scaffold that provides biochemical and topographic cues with a readily available, autologous cell source in the surgical suite would address the concerns with the long lead time required for tissue engineered grafts as well as minimize the risk of secondary site morbidity. Accordingly, future *in vivo* studies to assess the ability of µDERMs to serve as a template for autologous skin regeneration are essential.

7.4 Final Conclusions

In this thesis, we redesigned our previous µDERM model by minimizing the thickness of the collagen gel layer and incorporating fibroblasts into the dermal sponge component to create a model system that allows for the evaluation of topographic cues in conjunction with paracrine signaling cues. We investigated the role of physical topographic cues in promoting epidermal morphogenesis and mediating cellular functions such as proliferation, differentiation and basement membrane protein synthesis. Importantly, we demonstrated that the use of a micropatterned substrate resulted in a robust epidermal layer with morphology and epidermal

thickness approaching that seen in the epidermal layers of cultured DED and on native skin. We found that the dimensions of topographic features defined different keratinocyte functional niches with small niches (50 μm and 100 μm) supporting a proliferative phenotype and wider niches (200 μm and 400 μm) supporting a synthetic phenotype. Additionally, we characterized the locations of $\beta_1^{bri}p63^+$ keratinocytes, putative keratinocyte stem cells, within cultured μDERMs. We showed that these cells were preferentially located in the bottoms of narrow channels and the bottom corners of wide channels. Future work should be done to elucidate the mechanisms responsible for the differential cell functional responses to topography and the mechanisms that drive stem cell localization.

We hypothesize that this model system represents an important advancement for *in vitro* study of disease pathologies and wound healing. Future studies will involve the development of *in vitro* models for the study of psoriasis and skin cancer. Additionally, we will build on previous work to establish a cryoburn model to assess epidermal wound healing mechanisms in response to topography. Further, optimization of the scaffold for implantation through changes to the crosslinking protocol will enable future *in vivo* studies and represent the next step towards the development of the next generation clinical skin substitute.

7.5 References

Adams JC and Watt FM (1990) Changes in Keratinocyte Adhesion During Terminal Differentiation: Reduction in Fibronectin Binding Precedes Alpha 5 Beta 1 Integrin Loss from the Cell Surface. *Cell* 63:425-35.

American Cancer Association (2014) Cancer Facts & Figures 2014. Atlanta.

Anderson R, Anderson E, Shakir L and Glover S (2006) Image Analysis of Extracellular Matrix Topography of Colon Cancer Cells. *Microscopy and Analysis* 20:5-7.

Barker CL, McHale MT, Gillies AK, Waller J, Pearce DM, Osborne J, Hutchinson PE, Smith GM and Pringle JH (2004) The Development and Characterization of an in Vitro Model of Psoriasis. *J Invest Dermatol* 123:892-901.

Barker N, Ridgway RA, van Es JH, van de Wetering M, Begthel H, van den Born M, Danenberg E, Clarke AR, Sansom OJ and Clevers H (2009) Crypt Stem Cells as the Cells-of-Origin of Intestinal Cancer. *Nature* 457:608-11.

Barrett K and Rabould H (2008) Functional Anatomy and General Principles of Regulation in the Gastrointestinal Tract. In: *Berne and Levy Physiology* (Koeppen B, Stanton B, eds), Philadelphia, PA: Elsevier, 487-95.

Bissell MJ, Radisky DC, Rizki A, Weaver VM and Petersen OW (2002) The Organizing Principle: Microenvironmental Influences in the Normal and Malignant Breast. *Differentiation* 70:537-46.

Bohnert A, Hornung J, Mackenzie IC and Fusenig NE (1986) Epithelial-Mesenchymal Interactions Control Basement Membrane Production and Differentiation in Cultured and Transplanted Mouse Keratinocytes. *Cell Tissue Res* 244:413-29.

Borchers AH, Steinbauer H, Schafer BS, Kramer M, Bowden GT and Fusenig NE (1997) Fibroblast-Directed Expression and Localization of 92-Kda Type Iv Collagenase Along the Tumor-Stroma Interface in an in Vitro Three-Dimensional Model of Human Squamous Cell Carcinoma. *Mol Carcinog* 19:258-66.

Bush K and Pins G (2012) Development of Microfabricated Dermal Epidermal Regenerative Matrices to Evaluate the Role of Cellular Microenvironments on Epidermal Morphogenesis. *Tissue Eng Part A* 18:2343-53.

Clement AL, Moutinho T and Pins GD (2013) Micropatterned Dermal-Epidermal Regeneration Matrices Create Functional Niches That Enhance Epidermal Morphogenesis. *Acta Biomater* 9:9474-84.

Commandeur S, de Gruijl FR, Willemze R, Tensen CP and El Ghalbzouri A (2009) An in Vitro Three-Dimensional Model of Primary Human Cutaneous Squamous Cell Carcinoma. *Exp Dermatol* 18:849-56.

Danilenko DM (2008) Review Paper: Preclinical Models of Psoriasis. *Vet Pathol* 45:563-75.

Delaporte E, Croute F, Vincent C, Bonnefoy JY, Robert J, Thivolet J and Nicolas JF (1989) [Keratinocyte-Fibroblast Interactions: I. Production by the Keratinocytes of Soluble Factors Stimulating the Proliferation of Normal Human Skin Fibroblasts]. *Pathologie-biologie* 37:875-80.

Downing BR, Cornwell K, Toner M and Pins GD (2005) The Influence of Microtextured Basal Lamina Analog Topography on Keratinocyte Function and Epidermal Organization. *J Biomed Mater Res A* 72:47-56.

El-Ghalbzouri A, Gibbs S, Lamme E, Van Blitterswijk CA and Ponec M (2002) Effect of Fibroblasts on Epidermal Regeneration. *Br J Dermatol* 147:230-43.

El Ghalbzouri A, Hensbergen P, Gibbs S, Kempenaar J, van der Schors R and Ponec M (2004) Fibroblasts Facilitate Re-Epithelialization in Wounded Human Skin Equivalents. *Lab Invest* 84:102-12.

El Ghalbzouri A, Jonkman MF, Dijkman R and Ponec M (2005) Basement Membrane Reconstruction in Human Skin Equivalents Is Regulated by Fibroblasts and/or Exogenously Activated Keratinocytes. *J Invest Dermatol* 124:79-86.

El Ghalbzouri A, Lamme E and Ponec M (2002) Crucial Role of Fibroblasts in Regulating Epidermal Morphogenesis. *Cell Tissue Res* 310:189-99.

El Ghalbzouri A and Ponec M (2004) Diffusible Factors Released by Fibroblasts Support Epidermal Morphogenesis and Deposition of Basement Membrane Components. *Wound Repair Regen* 12:359-67.

Eming S and Morgan J (1997) Methods for the Use of Genetically Modified Keratinocytes in Gene Therapy. In: *Gene Therapy Protocols* (Robbins P, ed) Vol. 7: Humana Press, 265-79.

Erdag G and Sheridan RL (2004) Fibroblasts Improve Performance of Cultured Composite Skin Substitutes on Athymic Mice. *Burns* 30:322-8.

Eves P, Layton C, Hedley S, Dawson RA, Wagner M, Morandini R, Ghanem G and Mac Neil S (2000) Characterization of an in Vitro Model of Human Melanoma Invasion Based on Reconstructed Human Skin. *Br J Dermatol* 142:210-22.

Garlick JA and Taichman LB (1994a) Effect of Tgf-Beta 1 on Re-Epithelialization of Human Keratinocytes in Vitro: An Organotypic Model. *J Invest Dermatol* 103:554-9.

Garlick JA and Taichman LB (1994b) Fate of Human Keratinocytes During Reepithelialization in an Organotypic Culture Model. *Lab Invest* 70:916-24.

Gravante G, Di Fede MC, Araco A, Grimaldi M, De Angelis B, Arpino A, Cervelli V and Montone A (2007) A Randomized Trial Comparing Recell System of Epidermal Cells Delivery Versus Classic Skin Grafts for the Treatment of Deep Partial Thickness Burns. *Burns* 33:966-72.

Gudjonsson T, Ronnov-Jessen L, Villadsen R, Bissell MJ and Petersen OW (2003) To Create the Correct Microenvironment: Three-Dimensional Heterotypic Collagen Assays for Human Breast Epithelial Morphogenesis and Neoplasia. *Methods* 30:247-55.

Han B, Grassl ED, Barocas VH, Coad JE and Bischof JC (2005) A Cryoinjury Model Using Engineered Tissue Equivalents for Cryosurgical Applications. *Ann Biomed Eng* 33:972-82.

Hotchin NA, Gandarillas A and Watt FM (1995) Regulation of Cell Surface Beta 1 Integrin Levels During Keratinocyte Terminal Differentiation. *J Cell Biol* 128:1209-19.

Hotchin NA and Watt FM (1992) Transcriptional and Post-Translational Regulation of Beta 1 Integrin Expression During Keratinocyte Terminal Differentiation. *J Biol Chem* 267:14852-8.

Iizuka H, Honda H and Ishida-Yamamoto A (1997) Epidermal Remodeling in Psoriasis (Ii): A Quantitative Analysis of the Epidermal Architecture. *J Invest Dermatol* 109:806-10.

Iizuka H, Honda H and Ishida-Yamamoto A (1999) Epidermal Remodelling in Psoriasis (Iii): A Hexagonally-Arranged Cylindrical Papilla Model Reveals the Nature of Psoriatic Architecture. *J Dermatol Sci* 21:105-12.

Iizuka H, Takahashi H and Ishida-Yamamoto A (2004) Psoriatic Architecture Constructed by Epidermal Remodeling. *J Dermatol Sci* 35:93-9.

Jensen UB, Lowell S and Watt FM (1999) The Spatial Relationship between Stem Cells and Their Progeny in the Basal Layer of Human Epidermis: A New View Based on Whole-Mount Labelling and Lineage Analysis. *Development* 126:2409-18.

Kandyba E, Hodgins M and Martin P (2010) A Versatile Murine 3d Organotypic Model to Evaluate Aspects of Wound Healing and Epidermal Organization. *Methods Mol Biol* 585:303-12.

Knighton DR, Phillips GD and Fiegel VD (1990) Wound Healing Angiogenesis: Indirect Stimulation by Basic Fibroblast Growth Factor. *J Traum* 30:S134-44.

Koizumi M, Matsuzaki T and Ihara S (2005) Expression of P-Cadherin Distinct from That of E-Cadherin in Re-Epithelialization in Neonatal Rat Skin. *Development, growth & differentiation* 47:75-85.

Lavker RM and Sun TT (1982) Heterogeneity in Epidermal Basal Keratinocytes: Morphological and Functional Correlations. *Science* 215:1239-41.

Lavker RM and Sun TT (1983) Epidermal Stem Cells. *J Invest Dermatol* 81:121s-7s.

Levy L, Broad S, Diekmann D, Evans RD and Watt FM (2000) Beta1 Integrins Regulate Keratinocyte Adhesion and Differentiation by Distinct Mechanisms. *Mol Biol Cell* 11:453-66.

Li L, Tennenbaum T and Yuspa SH (1996) Suspension-Induced Murine Keratinocyte Differentiation Is Mediated by Calcium. *J Invest Dermatol* 106:254-60.

Maas-Szabowski N, Shimotoyodome A and Fusenig NE (1999) Keratinocyte Growth Regulation in Fibroblast Cocultures Via a Double Paracrine Mechanism. *J Cell Sci* 112 (Pt 12):1843-53.

Marionnet C, Pierrard C, Vioux-Chagnoleau C, Sok J, Asselineau D and Bernerd F (2006) Interactions between Fibroblasts and Keratinocytes in Morphogenesis of Dermal Epidermal Junction in a Model of Reconstructed Skin. *J Invest Dermatol* 126:971-9.

Medalie D and Morgan J (1999) Preparation and Transplantation of a Composite Graft of Epidermal Keratinocytes on Acellular Dermis. In: *Tissue Engineering Methods and Protocols* (Morgan J, Yarmush M, eds) Vol. 18: Humana Press, 407-21.

MedMarket (2007) Worldwide Wound Management, 2007-2016. Report no. #S245.

Moles JP and Watt FM (1997) The Epidermal Stem Cell Compartment: Variation in Expression Levels of E-Cadherin and Catenins within the Basal Layer of Human Epidermis. *The journal of histochemistry and cytochemistry : official journal of the Histochemistry Society* 45:867-74.

Murphy M, Kerr P and Grant-Kels JM (2007) The Histopathologic Spectrum of Psoriasis. *Clin Dermatol* 25:524-8.

Obrigkeit DH, Jugert FK, Beermann T, Baron JM, Frank J, Merk HF, Bickers DR and Abuzahra F (2009) Effects of Photodynamic Therapy Evaluated in a Novel Three-Dimensional Squamous Cell Carcinoma Organ Construct of the Skin. *Photochem Photobiol* 85:272-8.

Powell HM and Boyce ST (2007) Wound Closure with Edc Cross-Linked Cultured Skin Substitutes Grafted to Athymic Mice. *Biomaterials* 28:1084-92.

Rapier R, Huq J, Vishnubhotla R, Bulic M, Perrault CM, Metlushko V, Cho M, Tay RT and Glover SC (2010) The Extracellular Matrix Microtopography Drives Critical Changes in Cellular Motility and Rho a Activity in Colon Cancer Cells. *Cancer Cell Int* 10:24.

Rapp SR, Feldman SR, Exum ML, Fleischer AB, Jr. and Reboussin DM (1999) Psoriasis Causes as Much Disability as Other Major Medical Diseases. *J Am Acad Dermatol* 41:401-7.

Rheinwald JG (1980) Chapter 15 Serial Cultivation of Normal Human Epidermal Keratinocytes. In: *Methods in Cell Biology* (Curtis C. Harris BFT, Gary DS, eds) Vol. Volume 21: Academic Press, 229-54.

Robinson JK (2005) Sun Exposure, Sun Protection, and Vitamin D. *JAMA* 294:1541-3.

Rook A and Burns T (2010) Rook's Textbook of Dermatology. (Wiley-Blackwell: Chichester, West Sussex, UK ; Hoboken, NJ.

Saiag P, Coulomb B, Lebreton C, Bell E and Dubertret L (1985) Psoriatic Fibroblasts Induce Hyperproliferation of Normal Keratinocytes in a Skin Equivalent Model in Vitro. *Science* 230:669-72.

Samuel S, Walsh R, Webb J, Robins A, Potten C and Mahida YR (2009) Characterization of Putative Stem Cells in Isolated Human Colonic Crypt Epithelial Cells and Their Interactions with Myofibroblasts. *Am J Physiol Cell Physiol* 296:C296-305.

Sato T, Vries RG, Snippert HJ, van de Wetering M, Barker N, Stange DE, van Es JH, Abo A, Kujala P, Peters PJ and Clevers H (2009) Single Lgr5 Stem Cells Build Crypt-Villus Structures in Vitro without a Mesenchymal Niche. *Nature* 459:262-5.

Sheridan RL and Tompkins RG (1999) Skin Substitutes in Burns. *Burns* 25:97-103.

Shevchenko RV, James SL and James SE (2010) A Review of Tissue-Engineered Skin Bioconstructs Available for Skin Reconstruction. *J R Soc Interface* 7:229-58.

Smalley KS, Lioni M and Herlyn M (2006) Life Isn't Flat: Taking Cancer Biology to the Next Dimension. *In Vitro Cell Dev Biol Anim* 42:242-7.

Stern RS (2010) Prevalence of a History of Skin Cancer in 2007: Results of an Incidence-Based Model. *Arch Dermatol* 146:279-82.

Tenenhaus M and Rennekampff HO (2012) Surgical Advances in Burn and Reconstructive Plastic Surgery: New and Emerging Technologies. *Clin Plast Surg* 39:435-43.

Tjabringa G, Bergers M, van Rens D, de Boer R, Lamme E and Schalkwijk J (2008) Development and Validation of Human Psoriatic Skin Equivalents. *Am J Pathol* 173:815-23.

Vorsmann H, Groeber F, Walles H, Busch S, Beissert S, Walczak H and Kulms D (2013) Development of a Human Three-Dimensional Organotypic Skin-Melanoma Spheroid Model for in Vitro Drug Testing. *Cell Death Dis* 4:e719.

Wakita H, Shirahama S and Furukawa F (1998) Distinct P-Cadherin Expression in Cultured Normal Human Keratinocytes and Squamous Cell Carcinoma Cell Lines. *Microsc Res Tech* 43:218-23.

Wang L, Murthy SK, Fowle WH, Barabino GA and Carrier RL (2009) Influence of Micro-Well Biomimetic Topography on Intestinal Epithelial Caco-2 Cell Phenotype. *Biomaterials* 30:6825-34.

Watt FM (1988) Keratinocyte Cultures: An Experimental Model for Studying How Proliferation and Terminal Differentiation Are Co-Ordinated in the Epidermis. *J Cell Sci* 90 (Pt 4):525-9.

Watt FM (1998) Epidermal Stem Cells: Markers, Patterning and the Control of Stem Cell Fate. *Philos Trans R Soc Lond B Biol Sci* 353:831-7.

Watt FM (2001) Stem Cell Fate and Patterning in Mammalian Epidermis. *Curr Opin Genet Dev* 11:410-7.

Watt FM (2002) The Stem Cell Compartment in Human Interfollicular Epidermis. *J Dermatol Sci* 28:173-80.

Watt FM, Kubler MD, Hotchin NA, Nicholson LJ and Adams JC (1993) Regulation of Keratinocyte Terminal Differentiation by Integrin-Extracellular Matrix Interactions. *J Cell Sci* 106 (Pt 1):175-82.

Weaver VM, Fischer AH, Peterson OW and Bissell MJ (1996) The Importance of the Microenvironment in Breast Cancer Progression: Recapitulation of Mammary Tumorigenesis Using a Unique Human Mammary Epithelial Cell Model and a Three-Dimensional Culture Assay. *Biochem Cell Biol* 74:833-51.

Weigelt B and Bissell MJ (2008) Unraveling the Microenvironmental Influences on the Normal Mammary Gland and Breast Cancer. *Semin Cancer Biol* 18:311-21.

Werner S, Krieg T and Smola H (2007) Keratinocyte-Fibroblast Interactions in Wound Healing. *J Invest Dermatol* 127:998-1008.

Yu J, Peng S, Luo D and March JC (2012) In Vitro 3d Human Small Intestinal Villous Model for Drug Permeability Determination. *Biotechnol Bioeng* 109:2173-8.